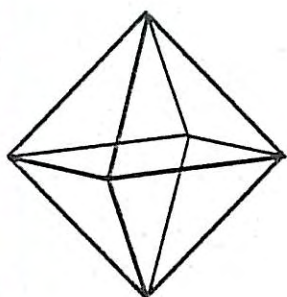


Appendix B

Hydrologic and Geochemical Mass Balance Modeling Report

Report



Kennecott

Eagle Minerals

Humboldt Tailings Disposal Facility Hydrologic and Geochemical Mass Balance Model Report

Project I.D.: 06W003

**Kennecott Eagle Minerals Company
Marquette, Michigan**

November 2007



Humboldt Tailings Disposal Facility Hydrologic and Geochemical Mass Balance Model Report

Project ID: 06W003

Prepared for
Kennecott Eagle Minerals Company
ISO 14001:2004 Registered System

Prepared by
Foth Infrastructure & Environment, LLC

November 2007

Addendum

This addendum addresses a minor change to an important attribute of the Humboldt Tailings Disposal Facility (HTDF). The watershed boundary described in Section 2.2 was adjusted to coincide with elevation contours developed from the same aerial survey. A revised estimate for the total HTDF basin area is 907,319 m² (224 Ac), an increase of 5.8% over the prior estimate. The estimated area of the HTDF water surface remained unchanged. The proportional drainage area to the northern HTDF decreased slightly from 14.4 percent to 14.3 percent of the total watershed. This change is insignificant. The revised estimate for the total watershed area is consistent with the boundaries and area table shown in Figure 2.

For purposes of water balance calculations and mass balance modeling presented here, the prior estimate for the watershed area (212 Ac) was applied. The revised area estimate was available only after extensive modeling had been completed and summarized. Several checks were made to show that, while the average annual outflow from the HTDF would increase by roughly 12 gpm as a result of applying the revised area estimate, the effect on the mass balance model results was negligible. For instance, changes to nickel concentrations at the expected HTDF outlet (and all main model compartments) were less than 0.1 ug/L for the 14 year period of simulation.

Humboldt Tailings Disposal Facility

Hydrologic and Geochemical Mass Balance Model Report

Contents

	Page
Executive Summary	vi
List of Abbreviations, Acronyms, and Symbols	ix
1 Purpose and Scope	1
2 Summary of HTDF Hydrology	2
2.1 Summary of Monthly Climate	2
2.2 Watershed Drainage and Groundwater	2
2.3 Geological Conditions	3
2.4 HTDF Water Balance and Bathymetric Characteristics	4
3 HTDF and Mill Water Budget	5
3.1 HTDF Water Balance on Annual Basis	5
3.1.1 Estimated HTDF Outflows on Annual Basis without Proposed Mill Operation	5
3.1.2 Estimated HTDF Outflows on Annual Basis with Proposed Mill Operation	5
3.2 HTDF Water Balance on Monthly Basis	6
3.2.1 Estimated Monthly HTDF Outflows without Proposed Mill Operation	6
3.2.2 Estimated Monthly HTDF Outflows with Proposed Mill Operation	6
3.3 Scheduling of Tailings Loadings to HTDF	7
4 HTDF Physical and Chemical Limnology	10
4.1 Stratification of HTDF	10
4.1.1 HTDF Thermocline and Chemocline	10
4.1.2 HTDF Field Parameters May 2007	11
4.1.3 Seasonal Persistence of HTDF Thermocline	12
4.2 HTDF Depth Profiles of Dissolved Constituents	13
4.3 HTDF Chemical Limnology	14
4.3.1 Background	14
4.3.1.1 Acid-Base and Redox Chemistry	15
4.3.1.2 Complexation and Precipitation Chemistry	16
4.3.2 Major and Minor Chemical Species in the HTDF	16
4.3.2.1 Alkalinity and Carbon Chemistry	18
4.3.3 Dissolved Oxygen and Primary Productivity	18
4.3.4 HTDF Oxidation-Reduction Chemistry	20
4.3.4.1 Sulfide Mineral Chemistry	23
4.3.5 Iron Cycling and Metal Scavenging	24
5 Complete Mixing Model of the HTDF	28
5.1 Fully-Mixed Model Predictions and Historical Washout	29
6 Multi-Compartment Model of the HTDF	30
6.1 Motivation for HTDF Multi-compartment Model	31
6.2 Compartmentalization of the HTDF Model	32
6.2.1 Upper HTDF Volume Changes Due to Storage	33
6.2.2 Lower HTDF Volume Changes Due to Tailings Loadings	34
6.2.3 General Approach for Mass, Heat and Flow Balances	34
6.2.4 Diffusion from Active Bed Tailings and Burial of Inactive Tails	35

Contents (*continued*)

	Page
6.3 Flows in Multi-compartment Model	35
6.3.1 Formation of Discharge Plume	36
6.3.2 Distribution of Discharge Plume and Density-Dependent Mixing	36
6.3.3 Density-Dependent Mixing and Inter-compartmental Flows	37
6.4 Parallel Model Components and Simulation of HTDF Chemistry	38
6.4.1 Surface Heat Flows	38
6.4.1.1 Considerations for Ice Formation and Melting	39
6.4.1.2 Considerations of Surface and Groundwater Flows	40
6.4.2 Considerations of Heating from Mill Discharge	40
6.5 Flow and Water Level Dynamics	41
6.6 Dissolved Oxygen and Iron Chemistry Dynamics	41
6.6.1 Alkalinity Effects	42
6.6.2 Metal Scavenging by Iron Hydroxides	43
6.7 HTDF Simulation Results for Complexed Metals	44
6.7.1 Nickel	44
6.7.2 Copper	44
6.7.3 Mercury	45
6.7.4 Other Complexed Metals	45
6.8 HTDF Simulation Results for Non-Complexed Species	46
6.8.1 Tracer Simulation	46
6.8.2 Selenium	46
6.8.3 Nitrate and Ammonia Nitrogen	47
6.9 Further Discussion of HTDF Simulation Results	47
7 Conclusions	50
7.1 Recommendations	51
8 References	53

Tables

(Tables located after Tables tab)

Table 1	Expected Climate at Humboldt Mill
Table 2	Expected Mill Tailings Production Schedule for Purposes of HTDF Mass Balance Model
Table 3	Initial and Weighted Average Concentrations of Chemical Constituents in HTDF and Expected Mill Discharge
Table 4	Expected Concentrations of Chemical Constituents in HTDF Outlet after 1, 3, 7, 10 and 14 Years of Operation, with Complete Mixing
Table 5	Expected Concentrations of Chemical Constituents in HTDF Outlet after 1, 3, 7, 10 and 14 Years of Operation, with Multi-Compartment Model

Figures

Contents (*continued*)

Figure 1	Normal Monthly Climate for HTDF
Figure 2	Humboldt Mill Expected HTDF Drainage Basin for Mass Balance Modeling
Figure 3	Net Precipitation and HTDF Basin Discharge – Existing Conditions
Figure 4	HTDF Existing Bathymetry and Volumetric Relationships
Figure 5	Water Balance – HTDF Average Annual Precipitation Humboldt Mill Project
Figure 6	Water Balance – HTDF Maximum Annual Precipitation Humboldt Mill Project
Figure 7	HTDF Vertical Profile – Selected Field Parameters
Figure 8	HTDF Vertical Profile – Thermocline and Chemocline
Figure 9	HTDF Vertical Profile – Selected Chemical Constituents
Figure 10	HTDF Vertical Profile – Multiple Chemical Constituents
Figure 11	HTDF Major Element Concentrations
Figure 12	HTDF Minor Element Concentrations
Figure 13	HTDF Dissolved Oxygen
Figure 14	HTDF Redox Chemistry
Figure 15	Aquatic Iron Cycling
Figure 16	Observed Decrease in HTDF Nickel Concentrations
Figure 17	Parallel Model Components and Interdependencies
Figure 18	HTDF Model Compartment Dimensions Upon Loading
Figure 19	Fluid Flow Balance for HTDF Mass Balance Model
Figure 20	HTDF Model Mass and Heat Balances for Initiation of Discharge Plume
Figure 21	Derivation of Mixing Flow from Differences in Density
Figure 22	Modeled Trends in Temperature Density, and Flow
Figure 23	HTDF Model Depth Profiles for System Variables
Figure 24	Dissolved Oxygen, Iron, and Alkalinity Model Dynamics
Figure 25	HTDF Model Depth Profiles for Selected Metals
Figure 26	HTDF Model – Simulated Trends for Nickel, Copper, and Mercury
Figure 27	HTDF Model – Simulated Trends for Tracer Input Case

Appendices

Appendix A	Gradation and Specific Gravity Measurements for Representative Tailings
Appendix B	Cyanamid Report
Appendix C	Montgomery Watson Memoranda
Appendix D	Results of Bench Scale Lock Cycle Testing of Mill Tailings
Appendix E	Calculation of Preliminary Effluent Limits for Wetland EE
Appendix F	Multi-Compartment Model: Definition of Flows, Variables, and Compartment Mass Balances

Humboldt Tailings Disposal Facility

Hydrologic and Geochemical Mass Balance Model Report

Executive Summary

Kennecott Eagle Minerals Company (KEMC) is proposing to rehabilitate the existing Humboldt Mill facilities located in Humboldt Township, Marquette County, Michigan, for processing nickel and copper ore. The proposed milling operations are expected to produce tailings, and the proposed plan calls for the residual tailings to be placed in the Humboldt Tailings Disposal Facility (HTDF).

The HTDF is a former mine excavation adjacent to the mill, formed from iron mining and associated dewatering operations at the Humboldt Mine. The mine was developed in 1954, operated until about 1970, and then the excavation was allowed to fill with water to a water depth of approximately 350 ft (107 m). Tailings from on site milling of ore from the Ropes Gold Mine, operated by Callahan Mining Company and located 10 miles east of the Humboldt Mill, were placed in the HTDF from 1985 until 1989. The water depth decreased to roughly 190 ft (58 m). While the water quality is still impaired at depth within the HTDF, water quality has improved significantly since 1990. Monitoring data and the dynamics of the recovery of the water quality since the Ropes operation serve as a major data source for projecting the HTDF behavior upon additional loadings.

This report describes the proposed sub-aqueous placement of tailings, initial conditions in and surrounding the HTDF, and the expected response of the HTDF to the tailings discharge. The purpose of this report is to assess the water chemistry characteristics during active milling and tailings placement operations at the site and to assess post operations water chemistry and related post closure care needs. The report also provides a detailed description of the current state of water chemistry, bathymetry, climatology, and flows associated with the HTDF.

Recent field measurements indicate that the HTDF exhibits seasonal stratification with respect to temperature and, because stratification is very stable, complete mixing of the HTDF is not evident. Historical data shows that the original mine excavation pit was once completely oxygenated, but recent oxygen profiles show a persistent oxygen chemocline located at mid-depth in the HTDF, well beneath the thermocline. Diurnal oxygen measurements indicate essentially no primary productivity in the HTDF. The appearance of anoxic conditions in the bottom waters of the HTDF coincides with the placement of tailings from on site milling of ore from Ropes mine. Oxidation reduction potential measurements, as well as very low levels of organic carbon in the water column, strongly suggest that the existing sulfide tailings help to maintain anoxic conditions. The anoxia will be further enforced by the proposed placement of fresh sulfide tailings and slow rate of oxygen mass transfer to sediments, thus creating a persistent reducing environment near the tailings. Measured depth profiles of metals in the water of the HTDF show that, for most metals, highest concentrations occur in the bottom waters, and concentrations decrease, often to less than twenty percent of maximum concentrations, above the oxygen chemocline. This behavior is attributed to an ongoing iron cycle operating near the oxic-anoxic boundary, creating iron particles that scavenge other metals from the water column and deliver them to the bottom of the HTDF. Thus, extensive chemical characterization of the HTDF

reveals the presence of a system that prevents oxygen from reaching deep water, while also greatly limiting the transport of metals to surface waters.

Particular attention within the report is drawn to a detailed, multi-component, multi-compartment mass and heat balance model which was developed to prepare predictions of HTDF water quality and other conditions in the HTDF that are expected to change during and after the placement of tailings. The numerical model addresses heat and mass balances, density-dependent mixing between different strata or compartments of the HTDF, allowance for variable water storage to accommodate an even influent flow to the WWTP, and several key chemical processes. The tailings are planned to be delivered to the HTDF as a high density slurry at depth. The dynamics of heat and mass transfer at the point of discharge are included in the model. Modeled chemical processes include dissolved oxygen mass transfer and depletion, dynamics of oxygen-demanding chemicals, formation and settling of ferric hydroxide, scavenging of metals by ferric hydroxide, and alkalinity effects from the discharge and oxidation-reduction reactions. Various calibration measures were taken to provide reasonable estimates for seasonal runoff, ice conditions, temperature profiles within the HTDF, volume change and water elevation estimation, and outflows.

Given the complexity and scope of processes simulated by the model, this report also provides a detailed assessment of the water chemistry and hydrology of the HTDF as it relates to implications for tailings placement and subsequent changes in water chemistry. This includes an assessment of the range of potential water chemistry conditions during operations and after closure of the mill.

A key outcome of the multi-compartment mass balance model was that, during and after the period of the placement of mill tailings, the stratified behavior of the HTDF would likely be sustained. This is a particularly important and reasonable conclusion, but one which follows from the nature of the placement of the tailings, internal processes which tend to reinforce stability, and conditions regarding the natural flows and bathymetry of the HTDF.

The placement of tails at a high slurry density and the preservation of a stratified HTDF generally leads to low surface concentrations at the HTDF surface. Shallow surface water represents the source of water that will be pumped to the wastewater treatment facility during operations. Shallow surface water also represents the source of water at the outlet that will be allowed to naturally drain after closure of the mill. Modeling included simulation of a conservative tracer test, which showed that the HTDF outlet concentrations would peak at roughly 3% of the discharge concentration, but only after a long loading period of 7 years.

For metals that undergo complexation and precipitation reactions, such as nickel, copper, mercury, and other metals, the concentrations at the HTDF outlet and within the HTDF are expected to be greatly reduced due to complexation, precipitation, and scavenging by iron hydroxide. In addition, the levels for these constituents within the HTDF drop significantly after the period of tailings placement.

With current estimates of the Preliminary Effluent Limits (PELs) available for the constituents from the multi-component model, none of the modeled constituent concentrations for the HTDF outlet exceeded the PEL. For nickel, copper, mercury, and selenium, the outlet concentrations were all well beneath the PEL, and generally by an order of magnitude or greater. The main

conclusion of this report is that the mass balance model predicts that the HTDF will remain stratified during and after the proposed placement of mill tailings, and the constituent concentrations at the HTDF outlet are expected to never exceed the associated PEL.

A fully-mixed model was also developed to estimate maximum HTDF outflow concentrations. It is important to note that this model represents a highly unlikely scenario, given the known stratification of the HTDF, the nature of placement, and chemical processes, such as metals scavenging, that tend to remove metals from the water column in the HTDF. The washout mechanism inherent in the fully-mixed model was tested using historical measurements of nickel, and was found to greatly over-predict outflow concentrations. The level of over-prediction is expected to be higher for the period of tailings loadings, since the fully-mixed model also assumes that the pore water associated with the tailings would also be fully mixed within the HTDF. Nevertheless, the fully-mixed model predicted that water from the HTDF would require treatment to comply with standards for copper, mercury, and nickel, and possibly selenium. Under the fully mixed condition, treatment for these constituents would be required for at least seven years after mill production ceases.

Several recommendations are issued within the report. While the fully-mixed case is likely unrealistic, the model outcomes may be referenced as a worst-case for the proposed wastewater treatment plant (WWTP). Treatment should be provided to meet the expected wastewater treatment discharge limits for nickel, copper, and mercury. A management plan for the HTDF should provide routine monitoring of the mill tailings carriage water, the HTDF bathymetry, and water quality within the HTDF. Finally, with respect to contingency plans for the HTDF, it is recommended that the plans include options such as treatment with coagulants (such as ferric salt or alum) to remove suspended solids and metals within the HTDF by adsorption, coagulation, and flocculation. Although high concentrations are not unexpected, elevated HTDF concentrations of metals and other constituents from the tailings discharge could be effectively removed from the water column (within the HTDF) in order to meet and sustain constituent concentrations below discharge standards after closure.

This report has identified the use of the multi-compartment model, largely to provide estimates of the expected concentrations at the HTDF outlet. However, the model may also be used as a way to track the progress and state of the HTDF during loading. The modeling could be refined from regular calibration to observed conditions during loading, then used to refine projections for future performance.

Humboldt Tailings Disposal Facility

Hydrologic and Geochemical Mass Balance Model Report

List of Abbreviations, Acronyms, and Symbols

ac	acre
°C	Celsius
cm	centimeter
d	day
DEM	digital elevation model
DO	dissolved oxygen
E _H	Standard Hydrogen Potential
EQL	Estimated Quantitation Limits
°F	Fahrenheit
ft	feet
Foth	Foth Infrastructure & Environment, LLC
GJ	giga-Joules
gpm	gallons per minute
hr	hour
HTDF	Humboldt Tailings Disposal Facility
in.	inches
J	Joules
°K	Kelvin
KEMC	Kennecott Eagle Minerals Company
kg	kilograms
K _s	Solubility Product
L	liter
m	meters
m ²	square meters
m ³	cubic meters
MDL	Method Detection Limit
mg	milligrams
mm	millimeters
mV	millivolts
mol	mole
N	Nitrogen
NCDC	National Climatic Data Center
ng	nanogram
ORP	oxidation reduction potential
%	percent
pcf	pounds per cubic foot
pE	- Log [E]
PEL	Preliminary Effluent Limit
pH	- Log [H ⁺]
s	second
TDS	total dissolved solids
tonnes	metric tonnes (1.102 tonnes per ton)
ug	microgram

List of Abbreviations (*con't*)

V	volts
WWTP	wastewater treatment plant
yr	year

1 Purpose and Scope

The purpose of this report is to assess the water chemistry characteristics of the Humboldt Tailings Disposal Facility (HTDF) during proposed milling and tailings placement operations at the site and to assess post operations water chemistry and related post closure care needs. The scope of the report includes a summary of the hydrogeology of the HTDF and its sources of water and point where water exits the system to a regulated environment, and a water budget for the integrated operations of the mill and existing HTDF including its watershed and outlet.

A numerical model has been created to simulate the behavior of the HTDF during and after proposed tailings placement. The model addresses heat and mass balances, density-dependent mixing between different strata or compartments of the HTDF, allowance for variable water storage to accommodate an even influent flow to the wastewater treatment plant (WWTP), and several key chemical processes. The tailings are expected to be delivered to the HTDF as a high density slurry at depth. The dynamics of heat and mass transfer at the point of discharge are included in the model. Modeled chemical processes include dissolved oxygen (DO) mass transfer and depletion, dynamics of oxygen-demanding chemicals, formation and settling of ferric hydroxide, scavenging of metals by ferric hydroxide, and alkalinity effects from the discharge and oxidation-reduction reactions.

Given the complexity and scope of processes simulated by the model, this report also provides an assessment of the water chemistry and hydrology of the HTDF as it relates to implications for proposed tailings placement and subsequent changes in water chemistry. This includes an assessment of the range of potential water chemistry conditions during operations and after closure of the mill.

The proposed strategy for the HTDF includes several controls for water flow and quality. Prior to the placement of tailings, outflows for the HTDF are planned to be contained and controlled by a cut-off wall and surface water control structure (a berm). The berm will allow all HTDF outflows to be sent through a WWTP, from which water will be treated to meet applicable water quality standards prior to surface water discharge. The berm will also allow the build up of water levels within the HTDF, in order to accommodate peak flows during snow melt and storm events. Expected flows and water quality at the influent to the WWTP are addressed in this report.

2 Summary of HTDF Hydrology

The HTDF hydrology is discussed in terms of the monthly climate, watershed drainage subbasins, the lake bathymetry, and the hydrogeology.

2.1 Summary of Monthly Climate

A summary of monthly climate is presented in Table 1 and Figure 1. Climate data are drawn from Champion – Van Riper State Park (NCDC site 201439), a weather station close to the HTDF. Normal annual precipitation is 33.3 inches (846 mm), with extremes of 20.17 inches (low) and 46.94 inches (high). Annual evaporation (Marquette County, Station MI 5178) is estimated as 14.8 inches. Monthly mean temperatures range from 11.3 °F (-11.5 °C) in January to 64.3 °F (17.9 °C) in July. Mean annual snowfall is 132.8 inches, with snow depth highest in February and March (National Climatic Data Center; Natural Resources Conservation Service; Michigan Climatological Resources Program).

2.2 Watershed Drainage and Groundwater

Surface drainage into the HTDF is limited to a small bedrock highland watershed shown in Figure 2. Local relief in the vicinity of the pit is approximately 200 feet (ft). The subbasins and watershed boundary were generated using the watershed delineation tools within ArcGIS, and using a digital elevation model (DEM) based on the aerial survey. The aerial survey data were collected April 27, 2006 by Aero-Metric Engineering (Sheboygan, Wisconsin), and coordinates were reported with reference to the North American Vertical Datum of 1988 and horizontal datum based on NAD 83/96. The estimate for the total HTDF basin area is 857,628 m² (212 Ac), which included the lake area of 269,406 m² (67 Ac) for a water elevation of 468.8 m (1538 ft). The northern HTDF area is somewhat isolated from the main HTDF, and its area is 22,569 m² (5.6 Ac).

The expected discharge flow from the HTDF under normal hydrologic loading conditions was estimated from the simulated net monthly precipitation (adjusted for evaporation, snow storage, and melt) and the basin area. Details of the storage assumptions are shown in Figure 1. The net precipitation and expected monthly discharge from the HTDF under normal, existing conditions is shown in Figure 3. Discharge is limited to the period of March through November. Snow melt effects are most pronounced in April, leading to an average discharge in April of 578 gallons per minute (gpm) (3150 m³/d). The average net annual surface inflow is estimated as 203 gpm (1107 m³/d). Groundwater inputs to the HTDF are estimated to be 43 gpm (234 m³/d). The basis for the groundwater inflow estimate is discussed below. Assuming no change in storage in the HTDF (other than ice and snow storage), the average outflow is equal to the sum of net surface and groundwater inflow; average annual outflow from the HTDF is 246 gpm (1341 m³/day).

The model can accommodate seasonal and monthly flow balances and estimate conditions under dry and wet years. However, for the purposes of mass balance modeling, there is sufficient dampening of flow irregularity by the large volume of the HTDF, and the effects of irregular, extended dry or wet periods, while they will affect outflows, are expected to be relatively small in terms of HTDF mass balance modeling. The HTDF volume is 8.0 million m³, and at an average discharge rate of 246 gpm (1341 m³/d), the fully-mixed hydraulic retention time is roughly 16 years.

Under existing conditions, the outflow is expected to be a combination of groundwater and surface water flow. Surface water migrates by flow through an earthen berm and expressed as seepage entering the wetland to the north. Traverse Engineering (1984) calculated a hydraulic conductivity for the outwash of 27 ft/d (0.0094 cm/s) and indicated that two discharge structures were constructed to regulate the flow out of the HTDF. However, only one of these features has been located. A detailed site survey of the HTDF conducted in April, 2007 by a Foth Infrastructure & Environment, LLC (Foth) geologist concluded there is no evidence of any other surface flow out of the HTDF.

It is important to establish the nature of the groundwater inflow and the combined surface water and groundwater outflow of the HTDF. The recent site survey and subsequent groundwater flow mapping confirmed that the outflow from the HTDF flows toward wetlands to the north of the HTDF (Foth, 2007). Generally, groundwater south of the HTDF flows south and away from the HTDF. However, mining of the original pit has created a cone of depression drawing groundwater from a localized area to the south. Almost all of the groundwater flowing into the HTDF at its southern end is from outside the drainage basin of the HTDF, as the perimeter of the drainage basin falls very close to the HTDF in this location (Figure 2). Therefore, this potential input would be distinct from, and in addition to, the rain input in the drainage basin. Thus, the recent groundwater monitoring strongly indicates that groundwater from a small area south of the HTDF flows into the HTDF, and that a small subsurface flow leaves the HTDF at its northern end.

Groundwater input on the southern end of the HTDF is estimated to average 43 gpm (234 m³/d). The groundwater inflow at the southern end of the HTDF was estimated with Darcy's Law, using a hydraulic conductivity of 5.0×10^{-3} cm/s (14.2 ft/d), and a local hydraulic gradient of 0.12 across a rectangular cross-section of 800 ft (244 m) width by 5.0 ft (1.52 m) thickness. While the resulting flow rate from these inputs is 35 gpm, an investigation using varying input parameters indicated a mid-range estimate of 43 gpm is appropriate.

2.3 Geological Conditions

The Humboldt Pit was developed in a narrow valley, floored by iron-rich rocks, cutting through a ridge of silicified, dense, recrystallized sedimentary and mafic intrusive rocks. The east and west sides of the pit are poorly fractured bedrock overlain by a thin, patchy till, and provides very little observed subsurface inflow into the pit. The predominant groundwater flow into the pit is from the south, through sand and gravel outwash.

The stratigraphy in the vicinity of the HTDF consists of Negaunee Iron formation divided into a thin, upper hematite-rich oxide facies and a lower, thicker cherty silicate iron formation. Both units are generally even bedded, recrystallized and may display a strong foliation. The iron formation is overlain by the Goodrich quartzite, which, in the pit consists predominantly of thick lenses of basal conglomerate. Clasts in the conglomerate range from angular to subrounded iron formation and other sedimentary rocks, along with well rounded pebbles and cobbles of vein quartz. The matrix is completely silicified and is dominated by fine grained quartz with accessory muscovite, hematite and magnetite with little or no feldspar. Both have been intruded by a medium to coarse grained diabase that generally forms concordant masses. All of these rocks were then folded and metamorphosed, and contacts between the intrusive rocks and iron

formation were commonly sheared. The rocks are complexly folded, but generally form an anticline which plunges to the west.

The deformation and foliation of these rocks has served to produce a weakly jointed bedrock surface. Sheared and recrystallized contacts at depth would likely limit joint propagation. In addition, due to the interlocking recrystallized texture, storage would be limited to the joint network. Recrystallized formations without a well developed joint network are very poor groundwater producers. An inspection of the site during spring run off confirmed that this is the case at the HTDF.

The narrow valley represents a post-glacial stream channel that cut through the bedrock ridge. The bedrock is overlain by a complex sequence of till and outwash that is generally thinner over the ridge and thicker where it occurs in the valleys. The outwash on the north end of the pit is capped with a rock and earthen berm constructed by the original operator to regulate flow out of the HTDF.

2.4 HTDF Water Balance and Bathymetric Characteristics

The current estimate for the water balance to the HTDF is based on the net precipitation model expressed above and includes an out-of-basin groundwater input from the southern end. Outflows from the HTDF are expected to report fully as influent to a WWTP. The current, combined surface and groundwater seepage outflow along the northern end of the HTDF will be cut off by construction of a berm and slurry wall. Therefore, all flow out of the HTDF will pass through the WWTP.

The bathymetry and area-depth-volume relationships for the HTDF are shown in Figure 4 and are derived from the baseline hydrogeology study (Foth, 2007). The HTDF covers an area of 269,400 m² (67 Ac) at a normal elevation of 468.8 m (1538 ft), with a total volume of 7,997,000 m³. Depths in the main HTDF area are over 20 m (66 ft) for roughly two-thirds of the main HTDF surface area, and are 58.5 m (192 ft) at the deepest point. Depths in the northern HTDF area are limited to less than 20 m, and less than 7 m at the confluence with the main HTDF area. These bathymetric characteristics influence decisions regarding the compartmentalization of the mass balance model.

3 HTDF and Mill Water Budget

This section provides details of the water balance for the HTDF under several loading conditions. HTDF water balances on an annual basis are detailed in Section 3.1. However, the mass balance model was designed for dynamic simulation in order to better understand the impacts of seasonal flows and a set mill tailings discharge schedule. This required an evaluation of hydrological flows on a monthly basis. Elements of the HTDF water balance to better support the mass balance model are detailed in Section 3.2. Details regarding the scheduling of proposed tailings loadings to the HTDF are presented in Section 3.3. Further details of the dynamic simulation of the water balance for the multi-compartment mass balance model are presented in Section 6.

3.1 HTDF Water Balance on Annual Basis

A summary of the HTDF water balance on an annual basis is presented below.

3.1.1 Estimated HTDF Outflows on Annual Basis without Proposed Mill Operation

Without flows associated with the proposed mill operation considered, the average annual flow into the HTDF is estimated as 246 gpm (1341 m³/d). Of this, 43 gpm is from groundwater inflow and 203 gpm is from precipitation minus evaporation.

Maximum annual precipitation is roughly 1.4 times that of the normal annual precipitation of 33.3 in. (845 mm) and the maximum annual net precipitation (precipitation minus average evaporation) is 1.7 times that of normal (see Table 1).

Under maximum annual precipitation conditions and no mill operation, the average annual outflow is estimated as 395 gpm (2153 m³/d). Dry conditions can be estimated from the minimum annual precipitation of 20.17 inches (Table 1) and normal evaporation of 14.8 inches. Under extremely dry conditions and negligible groundwater inflow, the average annual flow is expected to be only 24% of the normal average, or 59 gpm (323 m³/d). Because the volume of the HTDF is expected to be conserved, the sum of outflows is expected to equal the sum of inflows.

3.1.2 Estimated HTDF Outflows on Annual Basis with Proposed Mill Operation

Under annual average precipitation conditions and during proposed mill and wastewater treatment operation, the sum of inflows to the HTDF is estimated as 640 gpm (3489 m³/d), with the largest inflows from precipitation (365 gpm), groundwater (43 gpm), and the mill discharge of water (142 gpm) and solids (70 gpm). The HTDF outflows are expressed to the WWTP (362 gpm), as reclaim water back to the mill (116 gpm), and evaporation (162 gpm). Details of the flow balance are presented in Figure 5, and calculations used to support the estimate of the proposed mill discharge are discussed in Section 3.3. Under the same conditions, the outflows are equivalent to the inflows.

Under similar conditions but with maximum annual precipitation (see Figure 6), the sum of inflows to the HTDF is estimated as 789 gpm (4301 m³/d). The increase in the sum of inflows is due only to the increase in precipitation (514 gpm versus 365 gpm for the average condition). Similarly, the increase in the sum of the inflow is matched by an equivalent increase in the outflow to the WWTP (511 gpm versus 362 gpm for the average condition).

Because a small portion of the HTDF outflow is recycled to the HTDF, the expected wastewater treatment effluent flow is only 352 gpm for the average annual precipitation case and 501 gpm for the maximum annual precipitation case.

3.2 HTDF Water Balance on Monthly Basis

The mass balance model was designed for dynamic simulation in order to better understand the impacts of seasonal flows and a set mill tailings discharge schedule. This required an evaluation of hydrological flows on a monthly basis. Storm flows with periods on the order of days or less will be handled by storage within the HTDF.

3.2.1 Estimated Monthly HTDF Outflows without Proposed Mill Operation

The highest average monthly surface inflow occurs in April at 578 gpm (3150 m³/d). Details for this calculation are shown in Figure 3. With the normal groundwater inflow of 43 gpm, the inflow estimate for the April average increases to 621 gpm (3385 m³/d). It is important to note that this flow estimate does not consider abnormally high winter snow pack and sudden melt conditions.

Two methods were used to estimate peak monthly flow. One method, based on a peaking factor of 1.5 times the normal April inflow of 621 gpm, yields a peak monthly flow of 932 gpm (5080 m³/d). The other method is based on the same storage method shown in Figure 3, monthly precipitation that is 1.41 times the normal (maximum annual precipitation case), and a normal groundwater inflow of 43 gpm. This method yields a similar estimate for peak monthly flow of 953 gpm (5195 m³/d).

It is important to note that these estimates for flows follow from the assumption of constant storage in the HTDF. In reality, heads are likely to build up in wet years and be drawn down in dry years. Head buildup of 0.305 m (1 ft) over the HTDF area yields additional storage of 82,000 m³, enough for 22 days of storage to handle the a peak monthly rate (932 gpm) with an average outflow rate of 246 gpm. Greater storage is available and outflows are expected to be higher during the peak inflow periods. For example, an additional 1 ft of head buildup fully accommodates the necessary storage for the peak monthly inflow with the average outflow rate.

The HTDF water elevation may also rise during a storm event. The 100 year, 24-hr rainfall event for Marquette County is 4.50 inches. The expected change in elevation can be estimated from the precipitation magnitude, multiplied by the ratio of the area for the watershed over the area of the HTDF (see Section 2.2). Assuming rapid runoff, no evaporative losses and negligible outflow during the storm, the expected increase in HTDF water elevation is 1.21 ft (0.37 m).

3.2.2 Estimated Monthly HTDF Outflows with Proposed Mill Operation

During active tailings loadings of the HTDF at the design rate, the discharge of water and solids from the mill is expected to be 50.5 m³/hr (1213 m³/d or 223 gpm) with a return water flow of 26.7 m³/h (641 m³/d or 118 gpm). (Although Figure 5 shows the return water flow as 116 gpm, the calculated return flow is closer to 118 gpm; the difference is due to rounding of several, balanced flow values). The discharge flow includes a 60% solids discharge of tailings plus 2.3 m³/hr (54.5 m³/d or 10 gpm) of miscellaneous contact water and truck wash water. The net

discharge would be 572 m³/d (105 gpm). Further details about the discharge are discussed below. With an annual average background flow of 246 gpm, the discharge raises the HTDF outlet flow to roughly 351 gpm (1912 m³/d).

A conservative estimate for very wet conditions (without storage), based on the estimate for peak monthly flow without the proposed mill discharge (932 gpm), is 1037 gpm. As mentioned above, additional storage within the HTDF of a foot or more can greatly dampen peak outflows.

Flow rates are important for sizing of the wastewater treatment system, which will treat HTDF water prior to groundwater discharge. The treatment system design relies on storage within the HTDF to adequately handle storms and peak flow periods. The multi-compartment model was used to dynamically simulate the expected heads during normal and peak precipitation cases. Further details are presented in Section 6.

3.3 Scheduling of Tailings Loadings to HTDF

A schedule of tailings loadings to the HTDF, necessary as a model input, was created from available estimates of the total dry tons of tailings expected, nominal loading rates, and the expected period of loading of 7.1 years.

According to M3 Engineering, the design rate for the discharge of tailings is set by the expected milling rate for the ore, 1584 metric tons (tonnes) per day. Assuming an ore moisture content of 6.78% (or 6.35% water per wet weight) and 78.13% tailings produced from dry ore, the dry tailings processing rate is 1159 tonnes per day (48.3 tonnes/h). The total quantity of ore to be processed is expected to be 3,419,430 tonnes (wet). The total production of tailings by the proposed mill is expected to be 2,501,969 tonnes (dry).

The discharge of tailings would be taken from the thickener underflow at 60% solids. The basis for volumes and densities, unless otherwise specified, is for 25° C (standard conditions). The density of water (γ_w) at 25° C with zero salinity is 997.3 kg/m³ (62.261 pcf). The main solids relationships describing the placement of the tailings are the volume, percent solids by weight, P (or gravimetric water content, w), and specific gravity, G_s . A common assumption is 100% saturation ($S_r = 1$). Key relationships are:

$$\% \text{ solids } P \text{ and moisture content } w: \quad P = \frac{100\%}{1 + w} \quad (1)$$

$$\text{Dry density:} \quad \gamma_d = \frac{\gamma_w}{\frac{1}{G_s} + \frac{w}{S_r}} = \frac{997.3 \text{ kg/m}^3}{\frac{1}{G_s} + \frac{w}{(1)}} \quad (2)$$

$$\text{Bulk (wet) density:} \quad \gamma = \frac{\gamma_w(1 + w)}{\frac{1}{G_s} + \frac{w}{S_r}} = \gamma_d(1 + w) = \frac{\gamma_d}{P/100\%} \quad (3)$$

With a specific gravity of 3.03 and water density of 997.3 kg/m^3 , the dry density of the tailings slurry is 1000.6 kg/m^3 . Lab sheets for gradation and specific gravity measurements on representative mill tailings are presented in Appendix A. For the design dry processing rate of tailings at 1159.0 tonnes/d (dry) and 60% solids, the expected volumetric flow for the tailings slurry is $1158.3 \text{ m}^3/\text{d}$ (212.5 gpm). Additional water discharges, from miscellaneous sources, are expected to add 10 gpm ($54.5 \text{ m}^3/\text{d}$) to the flow, so the total discharge flow is expected to be $1212.8 \text{ m}^3/\text{d}$ (222.5 gpm).

The water balance design for the proposed mill also includes a reclaim water stream from the HTDF back to the mill. This flow was provided by M3 Engineering as 118 gpm ($640.5 \text{ m}^3/\text{d}$).

For the purposes of mass balance modeling, the proposed milling process is assumed to be continuous, with operation 24 hours per day, 7 days a week, 320 days a year, for approximately 7.1 years. The milling rates were matched to meet a schedule detailed in Table 2 and the total dry tonnes of tails and ore that are expected to be processed. Table 2 shows a reduced milling rate in the first calendar year, a constant mill processing rate of 1159 dry tonnes/d of tails in operating years 2 through 7, and a reduced rate in the last year of mill operation to yield a total project duration of 7.1 years.

As a simplifying measure, flows for the wastewater treatment operation were considered constant for the full period of simulation. However, there is ample opportunity for greater flexibility in the scheduling of flows at the wastewater treatment facility. The proposed wastewater treatment facility will have a treatment capacity to handle peak flow periods and may be shut down during winter months. Since the residence time of water in the HTDF is on the order of years and there is significant storage in the HTDF, shut-down periods of several months for the wastewater treatment facility can be handled by increasing flows during active operation, without significant implications to water quality or water levels within the HTDF. Similarly, wastewater treatment flows may be adjusted seasonally to handle the higher expected HTDF input flows in the spring and fall.

The volume change to the HTDF as a result of the proposed placement of tails was estimated from an assumption of the percent solids of the tails deposit after placement and consolidation. Further consolidation of the tails placed by the previous operator was assumed to be negligible. If the percent solids of the new tails deposit is estimated as 72% ($w = 0.389$) after placement and consolidation, the dry density is found (Eqn. 2) as 1387.3 kg/m^3 (86.6 pcf). For the processing rate of 1159.0 tonnes/d, the change in the HTDF volume from the proposed tails loading would be $835.5 \text{ m}^3/\text{d}$. For the purposes of mass balance modeling, the volume of HTDF water is reduced to adjust to the expected tails mass loading and density. The total proposed tailings loading is expected to reduce the volume of the HTDF by approximately 1.8 million m^3 , or 22.5%.

Although the water balance diagram (Figure 5 and Figure 6) shows a 10 gpm flow of treatment solids from the proposed wastewater treatment facility to the HTDF, this stream was not incorporated to the mass balance model. When compared to the main HTDF input stream from the mill, the expected impacts from the treatment solids stream to flow, water quality, and solids loadings to the HTDF were considered negligible.

As mentioned above, the schedule of tailings loadings (shown in Table 2) will affect other processing rates. Loading and flow rates associated with the mass balance model were set by the expected schedule of dry tails loadings.

4 HTDF Physical and Chemical Limnology

4.1 Stratification of HTDF

The mass balance model for the HTDF was formed using ModelMaker™ (Version 4.0, Cherwell Scientific, 2000, Oxford, United Kingdom). The concept for the model was developed as a multi-compartment model, with variable volumes, loading rates, and flow rates. Flow rates vary to adjust to the dry tails loading schedule, mill downtime, and variations in the flows expected from the watershed.

Compartmentalization of the HTDF is based on measured stratification of temperature and water quality of the HTDF, as presented by Foth, 2007. In addition, compartmentalization of the northern HTDF area is supported by bathymetric characteristics.

4.1.1 HTDF Thermocline and Chemocline

A compartmentalization of water bodies occurs when a thermocline is created. As springtime air temperatures increase and the water body warms from the surface downward, the surface water will be warmer than the deep water. It is possible, due to specifics of thermal transfer in a particular water body, that the warm surface water becomes thermally separated from deep cold water, creating two stable compartments. The stability of the two compartments is a result of the density differences between the water in each compartment, with lower density warm water floating on top of denser cold water. The boundary between these compartments is known as the thermocline and is characterized by an extreme vertical temperature gradient relative to temperature gradients in each compartment. Mixing between compartments is reduced when a thermocline is present. However, as annual air temperatures cool, the thermocline may abruptly collapse and the two compartments can then mix vigorously, often greatly changing the chemistry in each compartment. The water body is said to “turnover” during this time.

The presence of a thermocline during a portion of the year does not imply that the water body will fully mix when the thermocline disappears. If sufficient turbulence is not present, a slowly mixing single compartment is briefly created and the possibility of large changes in chemistry is decreased. Also, as water has a maximum density at about 4° C, a stable surface compartment can reform as the water temperature in this compartment falls below this temperature.

A second important compartmentalization of a water body can occur when dissolved substances enter from sources located at either the surface or the bottom of the water body. A decreasing chemical concentration gradient away from the source will then be present. As with temperature, a single gradient may form, or a very sharp gradient may develop between two compartments, each with their own chemical gradient, and each with a unique concentration of the substance. When two chemically distinct compartments form, they are separated by a chemocline.

It is important to note that the presence of a thermocline, and the limited mixing that follows, will often be sufficient to create two chemically distinct compartments. Conversely, a chemocline may form in the absence of thermal stratification. Regardless of how they form, the presence of a thermocline and or a chemocline in a water body requires additional consideration of the water body structure, particularly with respect to mixing.

The presence or absence of any thermocline or chemocline must be known to construct an adequately detailed model of the HTDF. Such a model should have sufficient predictive capabilities to reliably predict outcomes from the dominant processes and inputs. To more adequately define the thermal and chemical structure of the HTDF, Foth conducted a water profiling regime with three-foot resolution at seven locations within the HTDF during May, 2007. Five sample locations are roughly equally spaced along a line parallel to the long axis of the HTDF (HPL-001 through HPL-005), with two more locations (HPL-006 and HPL-007) located on either side of HPL-003. The sample locations are shown in Figure 2. The profiling includes measurements of temperature, as well as DO, pH, and specific conductance. The results of this sampling are summarized below and are derived from the baseline hydrogeology study prepared by Foth (Foth, 2007).

4.1.2 HTDF Field Parameters May 2007

Temperature—Temperature measurements are presented as depth profiles in Figure 7. Temperature measurements vary somewhat in the surface water at each station, but all stations show a constant low temperature in deep water. A well-developed thermocline is clearly present at each station, and the shape of the thermocline does not vary among stations. Temperature stratification begins sharply at approximately 20 ft below the surface and is complete by the 50 foot depth.

Dissolved Oxygen—As shown in Figure 7, DO concentrations vary little among stations (mostly due to instrument noise) but change dramatically over the depth of the water column. The HTDF exhibits a very pronounced oxygen chemocline, with maximum concentration holding steady over the uppermost 80 ft of water, and then disappearing almost completely between 80 and 120 ft deep. The chemocline divides the HTDF into two distinct compartments: a well-oxygenated upper compartment and an anoxic lower compartment.

pH—Hydrogen ion concentration (pH) does not change greatly in the HTDF, remaining relatively constant both laterally and vertically, as seen in Figure 7. Vertical variation is greater than lateral variation, and there is a distinct vertical structure: maximum pH at the water surface, minimum values at approximately 100 ft deep, and intermediate pH values in the deep water.

Specific Conductance—Specific conductance (Figure 7) provides a general measurement of the concentration of dissolved ions in water. Values of this parameter vary little among sampling locations, but the HTDF may be divided into two distinct vertical compartments based on specific conductance measurements. While not as extreme as temperature and oxygen, specific conductance (and thus, dissolved ions) changes rapidly from lower values in the upper waters to higher values in the bottom waters, with the change occurring at about 100 ft deep.

The various elements of the vertical structure present in the HTDF water column, suggested by the individual field parameter depth profiles, are more apparent when all four profiles are displayed in a single figure; Figure 8 shows this comparison. Because units and scaling differ among the profiles, each profile is plotted in Figure 8 relative to its maximum value. Thus, the temperature falls to about 40% (value of 0.4) of its maximum value deep in the HTDF, relative to its maximum surface temperature.

Figure 8 shows that the HTDF cannot be adequately modeled as a single compartment. Instead, an appropriate model consists of five contiguous compartments, with the boundaries of each compartment defined by the vertical structure of the individual field parameters, as well as the water surface and HTDF sediment floor. The necessary model compartments are

1) surface water	0-6 ft
2) start of the thermocline	6-24 ft
3) below the thermocline, above the oxygen chemocline	24-96 ft
4) below the oxygen chemocline	96-144 ft
5) deep water	144-192 ft

The actual boundaries are less important than the mid-depths of each compartment, and chemical data representative of each compartment was collected at the compartment mid-depth. Finally, it is important to note that three field parameters change abruptly at about 95 ft deep. This depth is at the mid-point of the major change in DO concentration and specific conductance, and the minimum pH occurs here. This result strongly suggests that the water chemistry is different in the top and bottom waters of the HTDF.

4.1.3 Seasonal Persistence of HTDF Thermocline

Temperature field measurements shown above (from May, 2007), as well as additional field and chemistry data from August and October, 2006, indicate the presence of a thermocline in the HTDF during these times of the year. As surface water temperatures cool in the late autumn, water temperatures (and densities) will momentarily become the same between top and bottom water, until surface water cools below 4° C and again becomes less dense than bottom water. During this time, the HTDF may theoretically mix completely. However, momentary loss of temperature (density) stratification alone will not bring about complete mixing; sufficient turbulence must also be present.

Thermal stability of a body of water may be quantified by the densimetric Froude number (Tchobanoglous and Schroeder, 1987), a dimensionless ratio comparing inertial and gravitational forces acting on the body of water:

$$N_{DF} = \frac{Q/(b \times d)}{\sqrt{(\Delta\rho / \rho) \times g \times d}} \quad (4)$$

where

N_{DF} = Densimetric Froude Number
 Q = Volume flow
 b = Average width
 d = Average depth
 $\Delta\rho$ = Top and bottom water density difference
 ρ = Depth-average water density
 g = Gravity constant

Values of N_{DF} greater than one indicate that turbulent mixing prevents thermal stratification, while values less than one indicate that thermal stratification will remain despite small levels of mixing.

Representative values used to calculate N_{DF} for the HTDF were obtained from recently acquired data, as presented above. Direct measurement of aerial photography was used to estimate the length to width ratio for the facility (3.33:1). This ratio was then used with the known surface area to determine the average width of the facility.

From equation 4, the HTDF has a $N_{DF} = 0.0000054$ and is very strongly stratified. Moreover, because of the very small flow out of the facility compared to the cross-sectional area, the difference in density between the upper and lower zones must be less than about 10^{-14} before the Froude number approaches unity. This suggests that it is unlikely that the HTDF will mix completely.

4.2 HTDF Depth Profiles of Dissolved Constituents

As presented in Foth, 2007, measurements of the chemical concentrations of many dissolved constituents in the HTDF have been completed. These measurements are fundamental inputs for any model describing the evolution of the HTDF as new mine tailings are added to the facility.

Water samples were collected from five depths defined by the vertical structure of the HTDF, as discussed above. These depths are 3, 15, 60, 120, and 175 ft deep. Sampling at each depth was done at two locations (HPL-003 and HPL-004) to assess horizontal variability in the HTDF. The data from a given depth varied little between these two locations, and results presented here are from HPL-003, located in the center of the HTDF.

All water samples were analyzed for a suite of chemicals. Twenty-two chemicals (including related parameters such as hardness, turbidity and alkalinity) were successfully quantified (reported values were greater than the Estimated Quantitation Limit [EQL], also known as the Limit of Quantitation) at all five depths at each sampling station. In addition, ammonia was quantified at the two deepest depths (120 and 175 ft). To facilitate comparisons among the chemicals, and to examine the vertical structure displayed by each chemical (if any), data presented here are in the form of depth profiles for each chemical. Representative results for four metals found in the HTDF are shown in Figure 9.

The constituents measured in HTDF water vary in concentration over five orders of magnitude. Despite this range, three general patterns with respect to depth are observed in the data. Some constituents, for example nickel, are present at low concentrations in surface water, but increase to high levels with increasing depth; other constituents, like copper, increase from intermediate to high values with increasing depth; finally, another set of constituents, represented here by calcium, are nearly constant with depth.

The fourth depth profile shown in Figure 9 displays measured concentrations of iron. The shape of this profile is unique and points to the importance of iron in the HTDF as a mediator of surface concentrations of a number of metals. The mechanism involves the reduction-oxidation coupling of Fe^{+2} and Fe^{+3} below and above the oxygen chemocline, and formation of iron precipitates in the upper regions of the HTDF. A complete model of HTDF mixing will include this aspect of HTDF chemistry.

The patterns present in the individual depth profiles are compared in Figure 10 by plotting all profiles together using relative values, as was done above with field parameters. Three of these field parameters are also included in Figure 10.

Although Figure 10 is complex, several general patterns are present. Almost all of the chemical constituents in the HTDF are present at highest concentration at the very bottom of the HTDF. This result strongly suggests that the sediments (old tailings) are the predominant source of these constituents. As noted above, almost all of these chemicals then decrease to varying degree at shallower depths. The greatest decrease occurs for nickel, manganese, molybdenum, cobalt, and antimony; all of these fall to less than 20% of their maximum concentrations. Potassium, sodium, chloride, copper, and boron also decrease, but by only about one-half their maximum levels. Finally, magnesium and calcium change very little with depth, suggesting that the rock that forms the HTDF is the source of these cations. The rock forming the HTDF contains large amounts of iron, so the fact that iron does not behave like calcium and magnesium strongly suggests that iron participates in reactions within the HTDF. And, it is likely that the decrease in other metal concentrations is due to iron chemistry in the HTDF.

4.3 HTDF Chemical Limnology

Understanding the complexity present in Figure 10 requires a more thorough examination of the chemical limnology of the HTDF. While the transport of chemical species from the deep water to the surface water of the HTDF will be primarily controlled by mixing within the facility, mixing alone cannot explain the variation among the relative depth profiles displayed in Figure 10. If the transport was only due to mixing, all relative profiles would be identical and appear as a single profile, because bulk mixing would affect all chemical species equally. The variation observed in relative surface concentrations implies that chemical species are affected to varying degree by chemical processes within the sediments and water column of the HTDF.

4.3.1 Background

All surface water bodies share many common chemical characteristics because of a common bulk solvent (water), and because almost all exist under an atmosphere rich in oxygen with a small, but relatively constant amount of carbon dioxide. Also, a small set of twelve elements, present at relatively high concentrations, dominate the chemistry of surface waters. These major aquatic elements are boron, carbon, nitrogen, oxygen, sodium, magnesium, aluminum, silicon, sulfur, chlorine, potassium and calcium. All of the other elements, while essential in many cases for biochemical reactions and life, are referred to as minor aquatic elements based on their relatively low concentrations.

The chemistry of surface waters is regulated by four types of reactions: acid-base, oxidation-reduction (redox), complexation, and precipitation. The state of a particular body of water with respect to these four types of reactions is assessed with intensity parameters; pH (acid-base reactions) and pE (redox reactions; equal to the negative logarithm of the theoretical electron activity) are common intensity parameters. The chemical state of a body of water, as described by intensity parameters, determines which chemical reactions are most prevalent. The extent of a particular type of reaction required to move a body of water to a new chemical state is quantified by capacity parameters. Alkalinity is the capacity parameter associated with acid-base reactions; similar capacity parameters exist for the other three reaction types, though they are more difficult to quantify.

4.3.1.1 Acid-Base and Redox Chemistry

The most prevalent major aquatic elements (and chemical species formed from these elements) within a body of water control the acid-base and redox chemistry within that body of water, and the intensity and extent of these two types of reactions then regulate the concentration and speciation of both the major and minor elements in the body of water.

In many surface bodies of water, acid-base chemistry (and, therefore, pH) is dominated by the carbonate system, comprised of atmospheric carbon dioxide and calcium carbonate. In bodies of water in contact with calcareous rock, the fixed atmospheric concentration of carbon dioxide and solubility of calcium carbonate set the pH at about eight.

At the air-water interface of a body of water, the redox chemistry (and, therefore, pE) is most influenced by atmospheric oxygen. Oxygen is one of the most potent oxidants, and conditions near the air-water interface are generally very oxidizing. However, the extent to which oxygen influences redox conditions in deeper waters varies greatly, and is affected by both physical and biological processes.

Surface concentrations of oxygen are set, in part, by its solubility in water, which varies inversely with water temperature (oxygen saturation is about 8-9 mg/L at 20° C and increases to 12-13 mg/L at 5° C). Also, oxygen concentrations at increasing depths are affected by the relatively slow diffusion of oxygen downward from the surface. Given the constant atmospheric supply, diffusion of oxygen to deep water is continuous. However, depletion of oxygen with increasing water depth is often observed in bodies of water, as internal chemical processes consume oxygen more rapidly than diffusion can replace it.

The presence of life capable of photosynthesis (predominantly algal cells, and referred to as primary production) near the air-water interface will also affect oxygen concentrations, as well as acid-base (pH) and redox (pE) chemistry in these waters. During daylight hours, ongoing photosynthesis will produce oxygen and consume carbon dioxide, increasing DO, pH, and pE. Conversely, algal respiration during dark hours will consume oxygen and release carbon dioxide, and so, often lower pH and pE.

As noted above, oxygen concentrations in deep waters (greater than about thirty ft) depend on the rate at which oxygen is consumed by various chemical processes. In waters with high primary productivity (eutrophic waters), most oxygen in waters below the surface is rapidly consumed by the decomposition of settling detritus resulting from primary productivity. Although the detrital material may consist of a number of compounds, it is predominantly organic, or reduced, carbon. Often in eutrophic systems, the amount of organic carbon produced greatly exceeds that needed to remove essentially all oxygen from deep waters. In these systems, an oxygen chemocline will develop, the bottom waters will become anoxic, and the excess organic carbon will accumulate in bottom sediments.

Organic carbon is a potent reductant, and in a system like that described above, a redox gradient will be present, with oxidizing conditions in surface waters and reducing conditions in deep water. In fact, the system represented by oxygen reduction and organic carbon oxidation sets the possible redox (pE) range for most bodies of water. With acidic surface water, pE values in

these systems range between almost 20 at the water surface to -10 at (or just under) the sediment surface.

If primary production is very low in a body of water (oligotrophic waters), the extent to which oxygen is depleted in deep water will depend on the amount of reductants present from sources other than the settling detritus of primary production. These may still include organic carbon which enters the water body from outside (allochthonous carbon), but also include reduced nitrogen, manganese, iron, and, importantly, sulfur.

In water bodies where organic carbon is in limited supply, sulfur compounds may become the dominant reductants in sediments. Sulfur compounds are common in most natural systems, and are particularly prevalent in those systems in contact with sulfide minerals.

4.3.1.2 Complexation and Precipitation Chemistry

Once the large-scale chemistry of a water body is established by the major aquatic elements through acid-base and redox reactions, the fate of the minor aquatic elements is largely determined by those complexation and precipitation reactions that are possible under prevailing pH and pE conditions. Minor elements are most often removed from the water column through complexation reactions with the surface of aquatic particles, and subsequent sedimentation of these particles.

Settling particles with suitable complexation sites for minor element binding may come from a variety of sources, including allochthonous organic matter, clay particles, and iron, aluminum and manganese oxide particles. In some water bodies, autochthonous (formed within the water body) colloids form from precipitation of major and minor elements within the water column. The colloid surfaces often contain a large number of complexation sites and are in close proximity to dissolved metal ions in the water body. This combination results in very effective scavenging of the dissolved metals by the colloids. Subsequent coagulation of these colloids produces settling particles. This completely internal mechanism effectively reduces surface concentrations of a number of metals by transporting them to deep waters.

4.3.2 Major and Minor Chemical Species in the HTDF

Table 3 lists the concentrations of all quantified chemical species in each of the five compartments of the HTDF, as well as the volume-weighted average for each species. As described previously, only chemical species at concentrations above EQL are considered in detail in this report, as other species were reported to be either below the EQL or below EQL and Method Detection Limit (MDL). Four elements within this unquantifiable group of chemicals are mentioned here, because while they could not be quantified, they were often observed above the MDL, and so must be considered present in the HTDF. The four elements are arsenic, lead, zinc, and mercury, and EQLs for these elements are (ug/L) 1, 1, 10, and (ng/L) 0.5, respectively. These elements are present in the HTDF at levels below their respective EQL. Arsenic and mercury were observed in all five compartments, zinc was present in the bottom three compartments, and lead was only observed in the bottom compartment. In addition, mercury was quantified at levels just above its EQL at two depths at station HPL-004 (15 ft, 0.63 ng/L; 60 ft, 0.55 ng/L). Measurements at these depths at station HPL-003 were below EQL. Therefore, given that eight out of ten (two stations, five depths) mercury measurements were below EQL, mercury is best described as present in the HTDF at levels below its EQL.

Concentrations of quantified species in Table 3 are reported in common units of mass per volume (ug/L). To assess the chemistry that can occur within the group of chemical species shown in Table 3, it is necessary to convert all concentrations to a mole per liter (molar, M) basis so that direct comparisons of amounts are possible, and so that possible stoichiometric relationships are apparent. Molar concentrations of major aquatic species are displayed on the graph in Figure 11. Concentrations of minor aquatic species are shown in Figure 12.

Nine of the twelve major aquatic elements described above are found in the HTDF as major chemical species, and are shown in Figure 11 (oxygen is shown in the table below the graph). Boron is present but at reduced concentration (shown on the top graph in Figure 12); aluminum was sought as an analyte but was never detected above its MDL; and silicon was not an analyte.

Figure 11 shows that sulfur, in the form of sulfate, is the most abundant species measured in the HTDF. Concentrations of sulfate decrease with distance from the bottom, suggesting that sediments (tailings) are the source of the sulfur in the sulfate.

Calcium and magnesium are also abundant and present, particularly in the bottom two compartments, in roughly equal proportions. This is most likely due to the presence of dolomite in the previously placed tails. This possibility is confirmed by an earlier analysis (Cyanamid, 1986, Appendix B) of the tailings generated by the Ropes Mine, which stated that ferroan dolomite, as well as calcite and talc, were common in the tailings from this mine.

Ammonium and nitrate concentrations are inversely related in the bottom two compartments. Ammonium decreases while nitrate increases with distance from the bottom, such that concentrations are approximately equal in compartment four. This oxidative transformation of nitrogen away from the bottom shows that waters are most reducing near the sediments.

A summary table listing average compartment values of pH, pE, ionic strength, DO and temperature in the HTDF is also shown in Figure 11. Values in the table summarize a second field sampling effort conducted in July, 2007 (Foth, 2007). The values for these parameters, measured in July, confirm earlier observations from May (discussed above; redox potential was not measured in May). Redox potentials (pE) and DO are discussed later in this report.

As in May, pH is relatively constant in the HTDF. Maximum pH (8.30) occurs at the surface of the HTDF, and a minimum (7.28) is found in the fourth compartment. Overall, the pH profile is consistent with a system buffered by a carbonate system, with a small acidic influence deep in the water column.

Water column temperatures are similar to those in May, although surface temperatures are higher. As before, a sharply defined thermocline is present.

Ionic strength, a parameter describing the change in aquatic chemistry due to the presence of charged species, is shown for each HTDF compartment, and a volume weighted average is also provided. Ionic strength values are relatively low (about eighty times lower than seawater, for example) in each compartment.

Molar concentrations of the minor aquatic species measured in the HTDF are shown in two graphs in Figure 12. It is apparent from these two graphs that, despite over two orders of magnitude difference in concentrations, the behavior of many of the minor species is very similar. Manganese, nickel, antimony, cobalt, and molybdenum are all present at much higher concentrations in the deep water relative to the surface water of the HTDF.

4.3.2.1 Alkalinity and Carbon Chemistry

A second table in Figure 11 shows the calculation of total alkalinity in the HTDF, based on a carbonate dominated system. Bicarbonate is by far the dominant inorganic carbon species at pH values found in the HTDF, and measured values are comparable to those for sulfate, calcium and magnesium (see graph, Figure 11). Based on measured values of bicarbonate, there are over 900 tonnes (CaCO_3 equivalent) of alkalinity in the water column of the HTDF. Also, given that carbonates are present (Cyanamid, 1986; Appendix B) in the almost 2 million tons of tailings from the Ropes mine (Montgomery Watson, 1993, Appendix C), a significant reserve of alkalinity is present in the sediments of the HTDF.

Historical measurements (Traverse Engineering, 1984) indicate that sources of alkalinity other than Ropes tailings contribute alkalinity to the HTDF. Alkalinity was measured at 90 mg/L in both surface water and at 200 ft below the surface in October, 1984. These values are less than current values by about 20% and do not show the increase with depth apparent in the current values. This information indicates that both allochthonous sources and Ropes tailings contribute to the alkalinity in the HTDF.

Organic carbon measurements were obtained as a part of the May, 2007 field sampling (Foth, 2007). Samples were analyzed both for total and dissolved organic carbon (MDL 1.4 mg/L, EQL 2.0 mg/L for both sample types). In total, twenty samples were analyzed for organic carbon (two sampling stations, dissolved and total samples, at five depths). Of these, four were less than MDL, and seven were less than, and two equal to, EQL. The seven quantified samples have an average value of 2.39 mg/L and standard deviation of 0.28 mg/L. The measurements did not agree well between the two stations and no consistent trends were observed with depth or type of sample.

Dissolved organic carbon is much more prevalent than particulate organic carbon in surface bodies of water, often accounting for more than 90% of total organic carbon. Total organic carbon ranges between about 0.7 mg/L (ground water) and 33 mg/L (bog water), with oligotrophic waters averaging 2.2 mg/L and eutrophic waters at about 12 mg/L (Wetzel, 2001). Based on total organic carbon, the HTDF would be classified as, at most, an oligotrophic system. This may be misleading, however, as the number of values below the 2.0 mg/L EQL and the lack of structure suggest that even less organic carbon is autochthonous than in an oligotrophic system. It is likely that the small amount of organic carbon present in the HTDF is predominantly allochthonous.

4.3.3 Dissolved Oxygen and Primary Productivity

Graph A in Figure 13 displays measurements of DO measured in the HTDF during July, 2007. The values are displayed as a depth profile and are very similar to those shown in Figure 7, based on sampling done in May 2007. Oxygen was measured using a different methodology in May and July. May measurements were made using a colorimetric method, whereas measurements in

July used an electronic probe with approximately ten times the resolution of the colorimetric method. Despite this difference, the two profiles are essentially identical, with the exception of the top of the profiles. While both profiles show DO values of about 8 mg/L from the surface to a depth of about twenty feet, the July measurements capture an increase in DO that occurs between twenty feet and about forty feet. At this depth, oxygen reaches a maximum of about 10.5 mg/L. The increase is due to the greater solubility of oxygen in cold water, and the oxygen trend mirrors the water temperature profile shown in Graph B, Figure 13.

The oxygen chemocline observed in the May profile is clearly present in the July profile. The loss of oxygen occurs at the same depths in both profiles, with anoxic water below 100 ft in both cases. Thus, oxygen dynamics are very stable over at least months of time, and show no seasonality between spring and summer.

Also shown in Graph A, Figure 13 is a depth profile of measurements of DO collected in 1984 in the Humboldt Pit (now known as the HTDF) (Traverse Engineering, 1984). In 1984, before Ropes mine tailings were placed, the pit was about 300 ft deep, and the historical measurements show that the entire water column was oxygenated, with DO concentrations at the bottom equal to about 75% of surface values.

Comparison of the historical and contemporary oxygen profiles shows that, in the surface waters of the HTDF, little has changed with oxygen dynamics over about twenty three years. The profiles show very similar surface concentrations, and each profile captures the increased oxygen due to decreasing water temperature.

However, below about 75 ft the two profiles are very different. In 1984, the entire pit was oxygenated, whereas currently the HTDF is anoxic below about 100 ft. Given that atmospheric oxygen levels and rates of oxygen diffusion through water have not changed over the past twenty years, the difference in bottom water oxygen over this time is most likely due to an increase in oxygen demand, that is, an increase in chemical reductants, in the bottom of the HTDF during this time.

An increase in reductants at the bottom of a body of water most often occurs as a result of increased primary productivity in the surface waters. Also, an increase in input of allochthonous carbon might occur. In either case, more organic (reduced) carbon would reach the sediments, leading to an increase in oxygen consumption, and oxygen depletion in bottom waters.

Aerial photography shows that land usage has not changed greatly around the HTDF in the last several decades, so allochthonous carbon loading to the HTDF has likely been relatively constant during this time. Also, dissolved organic carbon levels are typical of a system with low primary productivity. The extent of primary production may also be assessed by examining DO.

Two sets of DO measurements are shown in Graph B, Figure 13. These measurements were taken on the same July day as the measurements shown in Graph A, but at different times. The first set shown in Graph B was obtained at about 5:00 AM, while the second set was measured at about 4:00 PM. As explained above, photosynthesizing algal cells would release a pulse of oxygen during the day and consume oxygen at night, resulting in very different DO levels early and late in the day. The fact that the oxygen profiles in Graph B are almost identical strongly

indicates that photosynthesis, and therefore, primary production, is essentially not occurring in the HTDF.

Measurements of organic carbon and DO show no evidence of high levels of organic carbon production in the water column of the HTDF, and so, little organic carbon is expected in the sediments. The depletion of oxygen in the bottom waters must then be due, at least in part, to the presence of other reductants capable of consuming oxygen.

The change in oxygen dynamics between 1984 and present, visible in Graph A, Figure 13, and the fact that the Ropes tailings were placed during this interval suggests that the tails are helping to maintain anoxic conditions in the HTDF. In this scenario, oxygen continually diffuses into the waters of the HTDF, past depths where primary production would otherwise begin to consume it. At deeper depths, oxygen encounters in situ reductants, including small amounts of predominantly allochthonous organic carbon, and is at least partially consumed by these reductants. Any oxygen that remains at deeper depths eventually reacts with reduced sulfur from mine tailings. Thus, the large mass of sulfidic mine tailings is self-stabilizing, in that variations in amounts of other reductants, principally organic carbon, cannot lead to a build up of oxygen near the tailings.

4.3.4 HTDF Oxidation-Reduction Chemistry

The chemistry of the HTDF was further investigated by measuring the oxidation-reduction potential (ORP [oxidation reduction potential], or redox potential) in July, 2007.

Measurements were taken at three foot intervals using a platinum electrode and an Ag/AgCl reference electrode. These measurements were then converted to Standard Hydrogen Potentials (E_H) using a ZoBell calibration measurement obtained in the field (+231 mV) and the standard conversion equation (American Public Health Association, 1998b)

$$E_{H, System} = E_{Observed} + E_{H, ZoBell-Reference} - E_{H, ZoBell-Observed} \quad (5)$$

where

$E_{H, System}$ = E_H of the sample

$E_{Observed}$ = measured field value

$E_{H, ZoBell-Reference}$ = reference value of ZoBell's solution and Ag/AgCl electrode = +428 mV

$E_{H, ZoBell-Observed}$ = field calibration value of ZoBell's solution

Field measurements were also converted to pE values to facilitate comparison with literature values,

$$pE = E_H \times \frac{F}{2.3 \times R \times T} \quad (6)$$

where

pE = $-\log\{e\}$; e represents electron

F = Faraday constant = 96,485 Coulombs/mol

R = Gas Constant = 8.314 V Coulombs/mol °K

T = Absolute temperature (298 K, 25° C reference temperature)

The redox potential profile for the HTDF, expressed as E_H and pE is shown, along with temperature and DO, in Figure 14.

The redox potential profile is useful for evaluating the redox conditions within a body of water, as indicated by the associated intensity parameter, pE. Evaluation of a redox profile is based on comparisons with laboratory measurements of ideal systems consisting of well-defined chemical solutions, often containing only one redox couple (a single element present in both oxidized and reduced form, as in an electrochemical cell). Actual environmental systems (bodies of water) are complex, contain many chemical species and several redox couples. Because of this, redox profiles should be interpreted with caution and cannot be expected to predict individual chemistries. However, field measurements are very useful in understanding relative conditions within a body of water, and may provide chemical information when compared to literature values of redox potentials.

It is also important, when interpreting redox profiles, to recognize that the presence of a spatial gradient implies that the system is not at equilibrium, much as an electrical battery is far from equilibrium until it is completely discharged. Thus, kinetics is as important as thermodynamics in determining the type and amount of chemical species present at any given time.

Redox information describing a body of water may also be obtained if it is possible to simultaneously measure the concentrations of both species in a redox couple. The observed concentrations, as well as the standard potential for the redox couple, are combined with the Nernst equation to calculate the redox potential of the aquatic system containing the couple. The Nernst equation, in pE units, is

$$pE = pE^\circ + \frac{1}{n} \log \frac{\prod_i \{ox\}^{n_i}}{\prod_j \{red\}^{n_j}} \quad (7)$$

where

pE° = standard potential as pE
 n = number of electrons transferred
 ox = activities of oxidized species
 red = activities of reduced species

Ammonium and nitrate were both present and quantified at depths of 120 and 175 ft in the HTDF. This redox couple is related by the reduction half-reaction and associated standard pE value, pE° (the value of pE when the reaction occurs under standard conditions) shown below:



Because of low ionic strength and the single charge on each species, measured concentrations may be used to approximate activities in the Nernst equation. Inserting these values, and pH at each depth (175 ft, pH=7.4; 120 ft, pH=7.2), the pE at 140 and 175 ft in the HTDF is calculated as 5.89 and 5.59, respectively. These values are shown on the graph in Figure 14. The

calculated values are in good agreement with the measured profile, suggesting relatively stable chemistry at these depths.

As with most bodies of water, the redox profile for the HTDF displays a reduction gradient with increasing water depth; waters are most oxidizing at the surface and are most reducing in the bottom waters. The profile is erratic in the oxygenated top waters, but much more stable in the anoxic bottom waters.

Although a gradient is present, the range of pE values is small, varying between about 7 at the surface and 5.5 near the bottom; as mentioned previously, bodies of water may vary by as much as +20 at the surface and -10 at bottom sediments. The first value in the redox profile is at a depth of three feet below the surface. It is likely that water just below the surface would have higher pE values, perhaps approaching the theoretical maximum for oxygen of 13.75 at pH=7.

Common redox reactions are shown in Figure 14. Each reaction has a $pE^\circ(W)$ value. This is the standard pE° when pH=7. These values allow direct comparison of redox half-reactions under conditions similar to those often found in aquatic environments. The reactions are in order of decreasing $pE^\circ(W)$. It is thermodynamically possible for the oxidant in a reaction with a higher $pE^\circ(W)$ to oxidize a reductant at a lower $pE^\circ(W)$. Whether or not this occurs depends on the concentration of each species in the reaction.

While specific chemistries cannot be known based on the redox profile alone, several inferences can be made. A simple linear gradient connects the top two pE values with values below 100 ft. This indicates that oxygen (the most potent oxidant in the reactions shown in Figure 14) is controlling the redox conditions in the water above about 100 ft but is encountering several reductants at various depths in the top waters. These reductants are oxidized by the oxygen and pull pE values lower until they are consumed. Narrow bands where this occurs are referred to as redox boundaries, and several major and minor boundaries are visible in the profile.

One of the reductants present in the top waters of the HTDF is organic carbon, particularly from allochthonous sources. The carbon redox couple is shown as the last reaction listed in Figure 14 (the six-carbon sugar glucose is a model organic carbon). The large difference in $pE^\circ(W)$ values between the oxygen and carbon redox reactions implies that oxidation of reduced carbon by oxygen will essentially go to completion, such that the reactant present in excess will completely consume the other reactant. As mentioned previously, in eutrophic systems excess carbon eventually consumes all oxygen deep in the water column and accumulates in bottom sediments. If this were the case in the HTDF, the bottom waters would be expected to have a lower pE than that observed in the profile, given the negative $pE^\circ(W)$ associated with the carbon couple.

Other possible oxygen-consuming reductants are shown in the reactions listed in Figure 14. Thus, oxidation of nitrogen compounds, and the formation of oxidized solid phases of manganese and iron from their reduced, dissolved metal ions can all contribute to oxygen consumption within the HTDF.

4.3.4.1 Sulfide Mineral Chemistry

As is the case with many other minerals, the elemental constituents of sulfide minerals enter aquatic solutions through dissolution reactions (a dissolution reaction may be viewed as the opposite of precipitation), as shown in reaction 9, where Me represents a metal ion:



Univalent metals will produce two moles of ions for every mole of sulfur.

Sulfide ions (S^{2-}) are very basic and react strongly with hydrogen ions to produce bisulfide (HS^-) and, at lower pH (less than about seven), hydrogen sulfide



Reactions 10 and 11 are common in water bodies with anoxic bottom waters, particularly within sediments and at the sediment-water interface. Both of these reactions may lead to the production of more oxidized forms of sulfur, including elemental sulfur (S_8), thiosulfate ($\text{S}_2\text{O}_3^{2-}$) and sulfate (SO_4^{2-}). Oxidation of sulfide can follow a number of pathways and can be a complex process (Morin, 1993). However, it is likely that the high concentration in the HTDF of sulfate is due to sulfide oxidation via several pathways.

Because of the very basic nature of sulfide, a more representative dissolution reaction for a metal sulfide under environmental conditions is given by the sum of Reactions 9 and 10



The solubility of a metal sulfide can be defined as equal to the metal concentration on the right side of Reaction 12 when the reaction has reached equilibrium. The solubilities of metal sulfides can be quantified by determining the equilibrium constant for Reaction 12; this value is referred to as a conditional solubility product, $^*\text{K}_s$, for metal sulfides (conditional because of its dependence on hydrogen ion concentration).

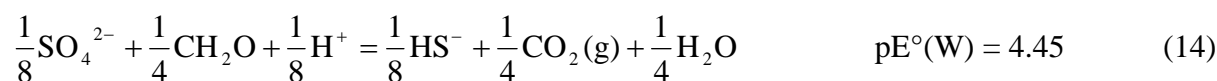
Tabulated values of $^*\text{K}_s$ are available (Stumm and Morgan, 1996). Metal sulfide solubilities vary greatly, depending on the specific metal and the mineral phase. Qualitatively, with the exception of manganese sulfide, metal sulfides have low to extremely low solubilities, with $\log ^*\text{K}_s$ values ranging between about -3 and -40.

Solubilities of iron sulfides are variable and relatively high to intermediate, with $\log ^*\text{K}_s$ values such as -2.95 (amorphous), -5.1 (pyrrhotite) and -16.4 (pyrite). Sulfides of nickel and cobalt have intermediate solubilities, with $\log ^*\text{K}_s$ ranging between about -6 and -13. Mercury sulfides are among the least soluble of the metal sulfides; $\log ^*\text{K}_s$ values are almost -40.

Concentrations of several metals have been measured in the bottom water of the HTDF (Figure 12), and a qualitative ranking of these concentrations is similar to a ranking of the observed $^*\text{K}_s$ values discussed above. It is likely that a limited dissolution of sulfide tailings helps to maintain

the low metal concentrations observed in the bottom water of the HTDF. This process will also increase the concentration of reduced sulfur, present as bisulfide, in the tailings porewater and near the sediment-water interface.

Given the high sulfur content of the in-place tailings, and the prevalence of sulfate, another relevant reaction is the oxidation of reduced carbon by sulfate. This reaction is not uncommon in bodies of water. The reaction thermodynamics may be estimated by summing the sulfur reaction shown in Figure 14 with the carbon couple reaction shown below (a simple carbohydrate is used as a model of reduced carbon). The sum is performed by reversing the carbon reaction (carbon is being oxidized) and subtracting the $pE^\circ(W)$ of the oxidized couple from that of the reduced couple.



The positive $pE^\circ(W)$ value associated with Reaction 14 indicates that, under standard conditions of unit concentrations and $\text{pH}=7$, the reaction will go to the right.

In the HTDF, sulfate concentrations are high, particularly in the bottom waters, and pH is about 7. Thus, under existing conditions, Reaction 14 may go to the right and consume any remaining organic carbon present at the bottom of the HTDF. In the process, bisulfide is produced. Bisulfide is also a product of any dissolution of metal sulfide tailings. Production of bisulfide by oxidation of organic carbon would therefore be expected to limit dissolution of tailings and as the case with DO, the sulfide tailings would be self-stabilizing under the redox conditions in the HTDF.

As with oxygen at the surface, the presence of bisulfide at or just in the sediments (tailings) suggests that the actual pE at the very bottom of the HTDF is lower than measured values indicate, and may approach the theoretical maximum for sulfur of around -3 at $\text{pH}=7$. Thus, the actual shape of the redox profile may be sigmoid, with a central linear portion resembling the measured profile and long tails at each end very near the air-water and water-sediment interfaces.

In summary, a profile of redox measurements in the HTDF shows that reducing conditions increase with depth, but only by a small amount in the water column. The range of observed pE values suggests that sulfur may be more important than organic carbon with respect to establishing the redox range. If oxygen and sulfur redox couples are assumed to be the end members of the redox profile, the actual range will be larger than that suggested by the measured profile. Reductants other than reduced carbon are available to consume oxygen. And, the large excess of sulfate, due in part to limited dissolution of sulfide tailings, may ultimately limit this process through oxidation of small amounts of residual organic carbon.

4.3.5 Iron Cycling and Metal Scavenging

As discussed above, major aquatic elements establish the fundamental chemical conditions within the water column of the HTDF. Specifically, carbon in the form of carbon dioxide and

calcium carbonate maintain the pH near 8. Oxygen and sulfur, with some carbon, allow the pE to range between values somewhat greater than 7 and somewhat less than 5 in most of the water column, but approach values nearer to 13 at the air-water interface and nearer to -3 at the water-sediment interface. Redox reactions in the HTDF also involve the major element nitrogen, as well as the minor elements iron and manganese. With dominant chemistry established, it is possible to consider complexation and precipitation in the HTDF, and how these reaction types control the fate of the minor aquatic elements.

Complexation refers to the formation of complexes and complex ions, that is, species that result when complexants form coordination bonds with metal atoms or ions in solution. Once formed, coordination bonds are no different than covalent bonds. Unlike covalent bonds (formed when each of two atoms donates one electron to form a bond), coordination bonds form using an electron pair from one atom and an open orbital on the other atom. The electron pair comes from the complexant and the open orbital is present around the metal atom or ion. If the resulting species (consisting of the central metal atom and bonded complexants, referred to as ligands) carries no charge, it is a complex; if charged, it is a complex ion. Coordination chemistry, named for the bonds that form complexes and complex ions, is the dominant chemistry of metals, and greatly affects the fate and transport of metals in the environment.

Precipitation reactions occur when several dissolved chemical species that are capable of reacting to form solids are present in solution at concentrations that exceed solubility limits. The dissolved constituents may then combine to form new molecules. If present in sufficient quantity, the molecules will coalesce into a solid phase, often initially as colloids. If conditions of pH and pE are favorable, the colloids will coagulate to form particles of sufficient mass such that settling may occur. Precipitation reactions affect the fate of minor aquatic elements because the surfaces of precipitated particles often contain very high numbers of molecular sites that act as complexants in the presence of metal ions. The resulting complexes, consisting of metal ions and surface sites on settling particles, represent a very effective mechanism for scavenging dissolved metals from the water column and transporting them to the bottom of the water body.

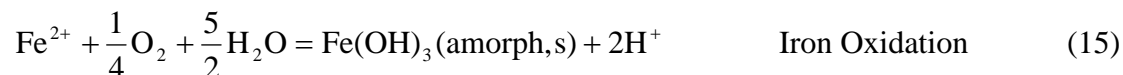
There are many possible aquatic complexants, and they may be grouped into three types (Buffle and De Vitre, 1994):

- ♦ Small ligands, including hydroxide, chloride, carbonate and amino acids
- ♦ Macromolecules, such as proteins, polysaccharides, fulvic and humic acids
- ♦ Colloids and particles like iron and manganese oxides, and clay particles

Any and all of these complexants may be present in the HTDF and affect the fate of the minor elements shown in Figure 12. Many of these complexants are capable of scavenging the minor elements from the HTDF. This report will focus on one representative, and very common scavenging mechanism in bodies of water: the reduced-oxidized iron cycle, or simply, the iron cycle. Scavenging by this system is a component of the multi-compartment model of the HTDF.

The iron cycle has long been recognized as an important mechanism in water bodies for the regulation of a number of species, for example, bioavailable phosphorus and other trace nutrients. The essential aspects of the mediation of these species by the iron cycle are identical to the mechanism by which minor elements are scavenged from the water column.

The relationship between reduced and oxidized iron is of primary importance in the iron cycle, as is the fact that iron changes oxidation state when transported between oxic and anoxic portions of the water column. The main chemical reaction describing this relationship is shown below



It is important to note that Reaction 15 affects alkalinity. In oxic waters, iron is oxidized and hydrogen ions are released, thereby reducing alkalinity.

The above reaction is a redox reaction and involves release of hydrogen ions. Therefore, the direction of the reaction not only depends on the presence of oxygen, but also on pE and pH. Also, iron undergoes a phase change from reduced dissolved to oxidized solid. Several other reactions involving the iron couple in water, and various dissolved and solid phases, are possible. To understand the iron cycle, and if and when it may occur in a water body, it is necessary to describe these various states of iron and to know which state will be dominant under different pE and pH conditions. A useful tool for this type of analysis is the pE-pH diagram.

The construction of a pE-pH diagram for any species begins by creating functional relationships between pE, pH and all possible species for the chemical components under consideration. The iron diagram might begin with the reduction of oxidized iron



combining this reaction with the Nernst equation

$$\text{pE} = 13 + \log \frac{\{\text{Fe}^{3+}\}}{\{\text{Fe}^{2+}\}} \quad (17)$$

At the boundary between conditions of pE where the dominant form of dissolved iron changes between oxidized and reduced, the concentrations of both species will be equal, and the functional relationship describing this boundary reduces to

$$\text{pE} = 13 \quad (18)$$

By considering all other possible reactions between water and reduced and oxidized iron, as well as equilibrium constants like pE° for each reaction, functional relationships can be developed that predict the dominant species for any pE and pH value. Some of these relationships will also depend on total dissolved iron concentrations, so each pE-pH diagram will be unique to a specific concentration of total iron.

A pE-pH diagram has been constructed for the HTDF and is shown at the top of Figure 15. This diagram includes bicarbonate as a component, so it is a pE-pH diagram for the Iron-Carbon Dioxide-Water system in the HTDF, and the associated concentrations of total dissolved iron and bicarbonate are listed at the top of the diagram.

The diagram displays regions bounded by lines within which a particular form of iron is the dominant species. The axes show the values of pE and pH so that for any set of pE-pH values, the dominant species can be found. Note that the example functional relationship presented above appears as the short horizontal line in the upper left of the diagram, and separates dissolved reduced iron from dissolved oxidized iron. The other lines are representations of the other functional relationships for each of the species in this system. The red dashed lines on the diagram indicate the stability zone for water.

The dominant iron species in the HTDF can be found by reading the diagram. pH in the HTDF ranges between 7 and 8, and pE values over the entire water column, including estimates near the air and sediment interfaces, range between -3 and about 12. By examining the area on the diagram enclosed by these pE-pH ranges, it is found that amorphous iron (III) hydroxide solid and dissolved iron (II) are the dominant iron species in the HTDF. These two iron species form the iron cycle in water bodies, so it is very likely that this cycle is operating in the HTDF.

The iron cycle is displayed in the lower diagram in Figure 15. Dissolved iron (II) enters the water column by diffusion upward from the sediments. This is common in water bodies with anoxic bottom waters, and very likely in the HTDF, given the iron pyrite tailings (Cyanamid, 1986) that form the sediments. As the upward diffusing iron (II) encounters oxygen diffusing downward from above, the iron is oxidized, producing amorphous solid iron (III) oxide, initially as colloids. The colloid surfaces provide many complexation sites, and various dissolved minor aquatic metals react with these sites to form surface-bound complex ions (this process is also known as adsorption). As the oxidized iron oxide colloids and associated metals coagulate, larger particles form and begin to settle back to low pE, anoxic conditions. Some of the particles begin to undergo reductive dissolution, while other, larger particles deposit in the sediments. As the cycle continues, some of the iron (III) oxides on the sediment surface are reductively dissolved. This provides more iron (II) for the cycle, while also releasing minor metals. The released metals may diffuse upward, but they are prevented from moving beyond the bottom waters by the iron cycle. In this way, high concentrations of dissolved minor metals may appear in the deep waters, but these metals cannot reach the surface water.

The cycle is strengthened by allochthonous iron entering from above and settling toward the bottom, adding to the pool of available iron. Ground water near the south end of the HTDF has high dissolved iron (Foth, 2007). Additional iron, both reduced and oxidized may enter the HTDF at the south end and help sustain the iron cycle, and so help retain dissolved metals deep in the HTDF.

The unusual relative depth profile for iron (Figure 10), compared to the depth profiles for other chemical species in the HTDF, may now be explained as a consequence of the iron cycle within the HTDF, and inflowing iron at the surface of the HTDF. Iron concentrations are elevated in the surface waters due to allochthonous iron input at the surface. Iron concentrations decrease below the oxygen chemocline as oxidized iron particles settle rapidly from this depth. And, iron concentrations increase near the sediments as settling iron oxides undergo reductive dissolution.

5 Complete Mixing Model of the HTDF

The previous discussion has established that the HTDF has a well defined vertical structure with respect to field parameters and chemical constituents and reactions. An appropriate model of this system will consist of five discrete compartments. However, it is important to examine the HTDF under the assumption that all vertical structure decays and the HTDF becomes completely mixed. A fully mixed model was developed and run during and after a simulated mill operation to estimate HTDF effluent concentrations during these periods.

A fully mixed system will have much higher surface water concentrations of many constituents, compared to the stratified HTDF, and, as such, represents a “worst-case” scenario under the planned loading conditions with respect to the concentrations of chemical constituents in the water that enters the WWTP. The model is presented here to aid in the design of the WWTP. In addition, because analytical solutions are available for the fully mixed case, the simulations can be easily checked.

Model parameterization of the fully mixed HTDF was done by calculating daily loadings for all constituents quantified in bench scale process water. Laboratory reports describing the process water testing are included as Appendix D. Measured concentrations from three tests were averaged to create a solution representing mill effluent into the HTDF, and daily loadings were calculated by multiplying these concentrations by the daily volume of carriage water necessary to convey a slurry containing 60% mine tailings by weight. The masses of metals and other constituents calculated in this way were added to the previous daily totals in the HTDF. The total mass of each constituent was then divided by the total volume of the HTDF water (decreased daily by the volume occupied by the tailings as a 72% weight percent sediment) to calculate the daily concentration of each constituent in the HTDF.

Each day, a mass of each constituent was removed by flow out of the HTDF, equal to the annual flow divided by 365 days, plus the water displaced that day by the tailings, and the difference between water from, and back to, the mill. The actual mass removed was equal to the product of the concentration from the previous day and the daily flow. Initial conditions in the HTDF were set by calculating the mass of all constituents in the HTDF, based on measured concentrations in each of the five identified model compartments. These masses were divided by the initial volume of water in the HTDF to determine initial concentrations of constituents in the HTDF under the assumption of complete mixing. The iterative process of adding the current day loadings to the current mass in the HTDF, dividing by the current HTDF water volume, and exporting mass proportional to concentrations from the previous day was run for 2555 days, equivalent to seven years of mill operation. Then, the loading term was removed, and the model was run for an additional 2555 days. Under these conditions, the volume of the HTDF remains constant at that reached on day 2555, no new loading occurs, and a daily mass of chemical constituents is exported (just as during the loading phase). Thus, the concentrations of chemical constituents decrease over this second 2555 day period, simulating ongoing washout of the HTDF after loading ceases.

Input concentrations in each of the five HTDF compartments, calculated initial concentrations, and concentrations of chemical species in the mill effluent are shown in Table 3. Model predictions of HTDF concentrations under fully mixed conditions at the end of years one, three, seven, ten and fourteen are shown in Table 4; preliminary effluent limits (PEL, see Appendix E)

are also provided. Note that mill effluent contains several constituents not currently found in the HTDF, but antimony, boron, and lithium are currently in the HTDF (Figure 12) but not in the mill effluent.

Concentrations of constituents that are greater in the mill effluent than initially in the HTDF increase in HTDF water over time (for example, copper, iron and nickel), while those that are initially elevated in HTDF water relative to mill effluent decrease over time as washout removes more than is added (for example, manganese and nitrate). After loading, concentrations decrease as chemical constituents wash out of the HTDF. Thus, all values decrease in years ten and fourteen, relative to maximum values in year seven.

The fully mixed model predicts several metals will enter the WWTP at concentrations that will require treatment to meet regulatory limits. These metals include copper, mercury, nickel, and possibly selenium.

5.1 Fully-Mixed Model Predictions and Historical Washout

The HTDF has been used previously as a tailings disposal facility for tailings from the Ropes mine. This resulted in elevated concentrations of some metals in the HTDF after closure of the Ropes mine, and subsequent monitoring of some metal concentrations. One historical depth profile is available describing nickel concentrations at five depths similar to those used here to describe the five compartments of the HTDF (Montgomery Watson, 1995). Using these historical data and current nickel concentrations (Table 3), it is possible to test the assumption that a simple washout mechanism controls nickel concentrations over time in the HTDF.

The specific calculation used to test this assumption, as well as the results of the calculation, are shown in Figure 16. The washout calculation depends on the volume and the retention time of water in the HTDF. The upper curve on the graph shows how nickel concentrations decrease over time if nickel is only removed by washout. The predicted nickel concentration in 2007, beginning with 1994 concentrations, is about three times higher than that actually measured in 2007. The lower curve on the graph is fitted to the data points, and predicts that flow from the HTDF would have to be almost three times greater (such that retention time is almost three times lower) to remove enough nickel to decrease concentrations from 1994 levels to those measured in 2007.

There is no evidence that flows from the HTDF have changed significantly between 1994 and 2007. Thus, a simple washout model like that presented above for the fully-mixed HTDF will greatly over-predict future metal concentrations in water flowing from the HTDF. And, the over-prediction of future concentrations indicates that mechanisms in addition to mixing (such as particle scavenging) must be actively reducing outflow concentrations from the HTDF. More accurate predictions require a multi-compartment model that includes compartmentalization and chemical reactions within the HTDF.

6 Multi-Compartment Model of the HTDF

The concept for the model was developed with a multi-compartment network, with variable volumes, loading rates, and flow rates. Flow rates vary to adjust to the dry tails loading schedule, mill downtime, and expected variations in the flows from the watershed.

The multi-compartment model of the HTDF addresses dynamic simulation of the following processes:

- ♦ Dynamic Loading and Seasonality
 - Mill tailings loading according to schedule
 - Uses average monthly climate and hydrology
- ♦ Variable Volumes
 - Variable surface water elevation
 - Accounting for mill tailings loading and associated pore volume
 - Dynamic updating of compartment volumes
- ♦ Flow Balance
 - Seasonal surface precipitation minus evaporation in watershed
 - Steady groundwater flow input
 - Steady water outflow from surface compartments to WWTP
 - Mill discharge and reclaim water recycle stream
 - Intercompartment flows balanced to inputs and volume changes
- ♦ Density-Driven Mixing and Plume Distribution
 - Density calculated from temperature and total dissolved solids
 - Intercompartment mixing affected by density differences
 - Distribution of mill discharge plume affected by density of compartments and plume
- ♦ Heat Balance
 - Surface heating from solar and atmospheric radiation
 - Surface heat exchange from back radiation, conduction, convection, evaporation
 - Predictions of ice formation and melting
 - Heating from mill discharge of tailings
 - Accounting of all compartment inflows and outflows
 - Heat transfer from tailings bed
 - Temperatures of discharge plume and all compartments tracked
- ♦ Mass Balances
 - Background concentrations in runoff
 - Initial concentrations from profile sampling of HTDF
 - Estimated loading from mill tailings porewater
 - Total dissolved solids modeled as conservative component.
 - Chemically active components include DO, oxygen demand, oxidized iron, alkalinity, and metals.
 - DO dynamics from surface water exchange and reaction with oxygen demand
 - Oxygen reaction rates and saturation affected by temperature

- Oxidized iron formation from conversion of oxygen demand
- Alkalinity effects from oxidation-reduction chemistry
- Metals scavenging from complexation and settling of oxidized iron
- Alkalinity dependence on settling of oxidized iron
- Bed diffusion from tailings bed porewater

The model is carried out using seven parallel components, each having the same general flow and mixing dynamics for inputs, outputs, and between compartments. These main components and their interdependencies within the model are shown in Figure 17. The mass balance model for the HTDF was fully implemented using ModelMaker™ (Version 4.0, Cherwell Scientific, 2000, Oxford, United Kingdom). Further details regarding the motivation and methods for modeling are presented below. A model definition and parameter listing is presented in Appendix F.

6.1 Motivation for HTDF Multi-compartment Model

The need for a multi-compartment model for the HTDF was to allow the simulation of stratification identified as five vertical compartments, while also allowing the disruption of the natural stratification by continuous, inter-compartmental mixing. Since the proposed mill discharge will be placed at depth, and the influent to the water treatment facility will be drawn from the HTDF near the surface, assessing stratification of the HTDF during mill operation is necessary.

The stability of stratified compartments is established by the trend of increasing water density with depth. If this general trend in water density is maintained during and after proposed loading, the compartments should remain stratified. Conversely, if the density of a lower compartment decreases relative to the adjacent upper column, the instability can be modeled as a relatively high inter-compartment flow. If the instability is maintained over time, the two compartments will mix to a high degree, effectively destroying the stratification. Stratification is affected by surface heating and cooling, as well as dissolved solids in the water. Stratification in the upper layers is also affected by wind-generated currents.

It is important to note that the model is based on the assumption that the individual compartments are completely mixed, a generally conservative assumption. A water parcel from the discharge, entering the lower compartment, may quickly come into contact with the interface of the next compartment. Once regular flow and inter-compartment mixing flow brings that parcel into the above compartment, a portion of that parcel is immediately available to flow to the next compartment.

Another reason for a multi-compartment model was to simulate tailings loading to the bed. As intended, the mill discharge is to be more dense and thermally stable relative to the bottom HTDF compartment, and the discharged tailings slurry should be delivered at a relatively high percent solids to the bed and the lower compartment. A large portion of the discharged pore water from the slurry would be delivered to the freshly placed sediment bed, although bed compression and diffusion would lead to a steady bed flux of the chemical constituents to the lower compartment. This placement strategy for the mill tailings is preferred, because it reduces HTDF mixing and will lead to lower metals loadings to the upper HTDF compartments.

Conversely, if the mill discharge water is less dense than the surrounding water or placed with a high rate of flow, the slurry would mix more completely at the point of discharge and a significant portion of the fluid flow may be expected to rise to the surface. Negative chemical consequences would compound the other disadvantages of a high-rate or low-density mill discharge. Although the tailings would settle to an anoxic sediment bed, metals and other compounds from the mill discharge pore water would mix with water from the upper compartments. DO from the HTDF surface waters, mixed into the upper compartments, would react quickly with the reduced sulfur species and reduced iron in the discharged water, producing sulfate, oxidized iron, a loss of alkalinity, and higher dissolved metals concentrations. For these reasons, the placement of mill tailings in the HTDF at high rate and low density is to be avoided.

Chemical processes internal to the HTDF are expected to remove metals and other chemical constituents from the water column. Under suitable pH and alkalinity conditions, oxidized iron will form ferric hydroxide and other iron precipitates, which will complex with dissolved metals and settle to the lower compartments. Removal of metals by complexation and settling of ferric hydroxide is referred to as metals scavenging. The chemistry of other metal precipitates, such as metal hydroxides, manganese carbonate, and calcium carbonates, are not modeled directly. The multi-compartment model tracks oxygen demand, DO, oxidized iron, alkalinity, and provides simulation of metals scavenging.

Since the tailings loading will significantly reduce the volume of the HTDF, the multi-compartment model must accommodate compression of the compartments. Volume changes in the upper HTDF compartments will also vary with seasonal surface water runoff from the HTDF watershed and a steady outflow to the water treatment facility.

6.2 Compartmentalization of the HTDF Model

Compartmentalization of the HTDF was based on measured stratification of temperature and water quality of the HTDF, as determined from Foth surveys in Fall 2006 through Summer 2007. In addition, compartmentalization of the northern HTDF area was suggested by bathymetric characteristics.

The multi-compartment model was developed as is shown in Figure 17. For the stratified HTDF, Compartment 1 corresponds to the surface samples, compartment 2 corresponds to samples immediately above the thermocline, compartment 3 corresponds to the region between the thermocline and the chemocline, compartment 4 corresponds to the regions immediately below the chemocline, and compartment 5 corresponds to the near-bed region. The top 2 compartments (1 and 2) are assumed to be relatively fixed in volume, changing only with changes in the surface elevation. Compartment 1 represents the normal water depth interval of 0-6 ft (0-1.83 m), and compartment 2 represents the water depth interval of 6 – 24 ft (1.83 – 7.32 m). The bottom elevation of compartment 2 is assumed fixed, at 1514 ft (461.5 m), and the volume fraction of compartment 1 ($VF_1 = Vol_1 / (Vol_1 + Vol_2)$) is held fixed at 0.26. The lower compartments (3-5) are initially assumed to cover the water depth intervals of 24-96 ft, 96-144 ft, and 144 – 192 ft, respectively. Expected volumes and depth range information for the compartments are shown in Figure 18.

6.2.1 Upper HTDF Volume Changes Due to Storage

A polynomial regression model of bathymetric data provided the following relationships between the volume of the HTDF and the surface water elevation. The upper storage volume in main HTDF is presented as:

$$V_{US} = V_1 + V_2 = V_M \{elev\} - V_M \{1514.ft\} \quad (19)$$

where $V_M \{elev\}$ is the main HTDF volume prior to new tailings loadings, but subject to changes in surface elevation and $V_M \{1514.ft\}$ is a reference volume of 6,094,897 m³ for the elevation of 1514 ft (461.467 m). Fitting bathymetric data over the elevation range of 461-470 m leads to the following relationship:

$$V_M \{elev\} = a_M (elev)^2 + b_M (elev) + c_M \quad (20)$$

where $a_M = 2098.946$ m, $b_M = -1,717,071$ m², and $c_M = 352.131 \times 10^6$ m³. A similar fitting process was used develop equations with the same form for the northern HTDF and the full HTDF volume. For the northern HTDF, $a_N = 809.614$ m, $b_N = -735809$ m², and $c_N = 167.216 \times 10^6$ m³. For the full HTDF, $a_F = 2905.56$ m, $b_F = -2,452,880$ m², and $c_F = 519.347 \times 10^6$ m³.

Changes in the volumes can be related to changes in elevation, by differentiation. For the main HTDF (and upper storage volume), the change in volume is

$$\dot{V}_{US} = \dot{V}_M = (2a_M (elev) + b_M) \frac{\partial elev}{\partial t} \quad (21)$$

Similarly, the change in the full HTDF volume is

$$\dot{V}_F = (2a_F (elev) + b_F) \frac{\partial elev}{\partial t} \quad (22)$$

From the flow balance, the change in volume in the full HTDF is also

$$\dot{V}_F = Q_D - Q_R + Q_{nat} + Q_{gw2} - Q_{T,out} \quad (23)$$

Where Q_D is the total discharge flow (mill to HTDF), Q_R is the reclaim flow (HTDF to mill), Q_{nat} is the net natural surface flows to the HTDF (see Figure 3), Q_{gw2} is the groundwater inflow (43 gpm, delivered to compartment 2), and $Q_{T,out}$ is the total outflow that is set by the WWTP design. Setting the last two equations equal yields the following model equation for rate of the change in the elevation (elevRate):

$$\frac{\partial elev}{\partial t} = \frac{Q_D - Q_R + Q_{nat} + Q_{gw2} - Q_{T,out}}{2a_F (elev) + b_F} \quad (24)$$

Using a starting elevation of 1538 ft (468.782 m), the model keeps track of the flows and integrates this equation to provide the surface elevation at all times. With the elevation, the elevation rate, and fixed volume fractions of compartments 1 and 2 known, the change in the volumes of these two compartments can be expressed. For compartment 1, the expression for the volume rate (VolRate1), is

$$\dot{V}_1 = VF_1 \dot{V}_{US} = 0.26(2a_M(elev) + b_M) \frac{\partial elev}{\partial t} \quad (25)$$

The expression for the rate of change in the compartment 2 volume has the same form, but the volume fraction VF_2 is 0.74. For the northern HTDF, the coefficients a_N and b_N (presented above) are used, and the volume fraction is 1.0.

6.2.2 Lower HTDF Volume Changes Due to Tailings Loadings

As the lower HTDF volume is occupied by the discharged mill tailings, the volume associated with these compartments decreases. The volumes of the compartments 3-5 were adjusted so that they represented the same proportional volume to the total remaining volume in the lower HTDF (sum of water volumes above placed tails, or sum of Vol_3 , Vol_4 , and Vol_5). If VRL is the volume remaining in the lower HTDF (sum of volumes 3-5), Vol_3 was adjusted to 0.60 times VRL, Vol_4 was adjusted to 0.24 times VRL, and Vol_5 was adjusted to 0.16 times VRL. Bathymetric relationships (shown in Figure 4) were used to estimate available water depth after uniform placement of tails.

The volume rate of tails loading (VolRateTails) is found from the dry tailings loading rate and the expected dry density

$$VolRateTails = \dot{V}_{TB} = \frac{\dot{M}_{DT}}{\gamma_d} \quad (26)$$

At 72% solids, the dry density of the new tails deposit is 1387.3 kg/m^3 (86.6 pcf). For the dry tails processing rate of 1159.0 tonnes/d, VolRateTails would be $835.5 \text{ m}^3/\text{d}$. The decrease in the volume remaining in the lower HTDF is VolRateTails. Therefore, the changes in the lower compartment volumes are found as:

$$\dot{V}_3 = -0.60 \dot{V}_{TB} \quad (27)$$

$$\dot{V}_4 = -0.24 \dot{V}_{TB} \quad (28)$$

$$\dot{V}_5 = -0.16 \dot{V}_{TB} \quad (29)$$

Volume change information for the compartments is needed for establishing compartmental mass and heat balances, as well as to establish inter-compartmental flows.

6.2.3 General Approach for Mass, Heat and Flow Balances

The mathematical approach for mass, heat, and flow balances is based on completely-mixed compartments that may have a variable volume. As an example, consider one compartment with a known inflow Q_{in} , a known volume change, and an unknown outflow Q_{out} . The flow balance would be written as:

$$Q_{out} = Q_{in} - \dot{V} \quad (30)$$

If the volume change is negative (compartment compresses), the outflow would have to be higher than the inflow for the flow balance to be satisfied. If the concentration in the compartment is C and the input concentration is C_{in} , the mass balance would be constructed as:

$$\frac{d(VC)}{dt} = \dot{V} C + V \frac{dC}{dt} = C_{in} Q_{in} - C Q_{out} \quad (31)$$

For a well-mixed compartment, the concentration of the outflow has to be equal to C , the concentration within the compartment. Rearranging, the expression for the change in concentration is:

$$\frac{dC}{dt} = \frac{C_{in} Q_{in} - C(Q_{out} + \dot{V})}{V} \quad (32)$$

Similarly, the heat balance would be

$$\frac{dT}{dt} = \frac{T_{in} Q_{in} \rho_w C_p + \dot{H}_{in} - T(Q_{out} + \dot{V}) \rho_w C_p}{V \rho_w C_p} \quad (33)$$

where T is the temperature, \dot{H}_{in} is the net heat input into the compartment (other than from fluid flow), ρ_w is the water density, and C_p is the heat capacity.

6.2.4 Diffusion from Active Bed Tailings and Burial of Inactive Tails

The model allows diffusion and heat transfer from active bed tailings to compartment 5. Heat and mass balances for the active bed tailings compartment are tracked normally, although there is some additional complexity regarding the pore volume and combined heat capacity of tailings and porewater. In particular, the model keeps track of the tailings bed area for all loadings. Details are provided in the model definition and parameter files presented in Appendix F.

All simulations discussed in this report were run with an active bed tailings layer thickness of 0.50 m (1.64 ft), a diffusion mass transfer coefficient of 4.0×10^{-4} m/d, and a bed heat transfer coefficient of 0.05 GJ/m²-d. Because the active bed is assumed to be completely mixed, the effective bed diffusion and heat transfer rates should be considered to be conservative (favoring mass and heat flows back to compartment 5).

Once the tailings bed thickness exceeds the active bed thickness of 0.5 m, the mass and heat associated with the overflow volume is reported to a buried tails compartment. Once buried, there are no mechanisms within the model for mass or heat return to the HTDF. However, the heat and mass delivered to the buried tails are tracked for purposes of checking model mass and heat balances.

6.3 Flows in Multi-compartment Model

The flow balance for the HTDF mass balance model is presented in Figure 19. The compartments are set up in a straightforward network, with introduction of tails at compartment 5, upward flow at the discharge flow rate through compartment 4 to compartment 3, return flow to the mill at compartment 3, and the remainder of the forward flow through compartment 2 to

the surface compartment 1. In the upper compartments, there are additional flow inputs from groundwater at compartment 2 and to the surface from the watershed. Forward flow exits from compartment 1 and from the northern HTDF to the influent of the WWTP. Under this conceptualization, the northern HTDF is expected to be somewhat segmented from the main processes of the HTDF, since only a very limited portion of the discharge will enter it and normal surface flows will continually flush out this compartment.

6.3.1 Formation of Discharge Plume

The model considers the discharge from the mill to first form a discharge “plume” at a mixing point. This concept is shown in Figure 20, along with the relevant mass and heat balances. Discharge solids (mill tailings) and water are delivered to a plume mixing point, where compartment 5 water is also brought in and the inputs are completely mixed. All the tailings solids are delivered to the tails bed, and the porewater associated with the expected bed porosity is also drawn to the bed. The heat and chemical mass associated with tailings can diffuse back to compartment 5, but the model assumes no additional flow from further compression of the tails.

The resulting flow to the plume comes from a simple flow balance. Commonly, for 40 units of water in the discharge over a set time period, 26.2 units of compartment 5 water is also brought into the mixing point, 23.3 units is delivered to the tails bed porewater, and 42.9 units is brought into the plume.

6.3.2 Distribution of Discharge Plume and Density-Dependent Mixing

Details regarding the distribution of flows from the discharge plume are presented in Figure 19. However, the complexity of the concept requires additional discussion. The flow distribution of the discharge plume is driven by density differences. If the plume is significantly less dense than water in the lower compartments, a greater portion of the discharge plume would be delivered to the upper compartments.

A physical analogy for density-dependent fluid mixing is expressed in Figure 21. While the physical analogy is presented for intercompartment mixing, the same general form is used for the distribution of the plume flow. The physical analogy is a simple pulley system of two weights, where a lighter mass on the bottom M2 will move up and the heavier mass M1 will move down. If the initial potential energy is converted to kinetic energy at the midpoint elevation, this midpoint velocity can be derived. Converting the system to address parcels of water moving across a liquid interface, the physical analogy shows that the velocity should be proportional to the square root of the differences in the densities over the sum of the densities. The mixing function is considered at a maximum flow (simulating complete mixing) if the bottom water is less dense and the density difference is maintained at roughly a 0.08% difference. The formulation allows for some inter-compartment mixing, even if the lower water is denser than the upper water.

For the plume distribution (detailed in Figure 19), the comparison of densities is between the discharge plume and the compartment. The flow is assigned sequentially, from compartment 5, then to compartment 4, then to compartment 3, and so on.

For compartment 5, the mixing function applies to whole discharge plume flow (less what reports to the tails bed). If the density of the plume is greater than that of compartment 5, the

plume is considered stable and 99% of the discharge plume flow is delivered to compartment 5. The remaining 1% of the flow is distributed to the upper compartments, with 0.99% of the discharge plume flow likely to compartment 4.

If the density of the plume is less than that of compartment 5, then the plume is considered unstable and the mixing function is evaluated. To simplify an example, let us assume that the density of compartment 5 water is 1000 kg/m^3 and the density of the discharge plume is 999.6 kg/m^3 . Under the current mixing function settings ($MF_{\min} = 0.03$, $MF_{\max} = 0.99$, $DF = 0.02$), the plot shown on Figure 21 applies, and the mix function would be approximately 0.72. In this case, 72% of the discharge plume flow would report to the upper compartments and only 28% of the discharge plume flow would report to compartment 5. If the density of compartment 4 was also 1000 kg/m^3 , 28% of the remaining flow or 20.2% of the discharge plume would report to compartment 4 ($0.28 \times 0.72 = 0.202$). If the density of compartment 3 was also 1000 kg/m^3 , 28% of the remaining flow or 14.5% of the discharge plume would report to compartment 3 ($0.28 \times 0.72 \times 0.72$). If the density of compartment 2 was lower than the discharge plume, 99% of the remaining discharge flow or 37.0% of the discharge plume would be delivered to compartment 2 ($0.99 \times 0.72 \times 0.72 \times 0.72 = 0.370$). The remaining 0.3% of the discharge flow would be delivered to compartment 1.

If the discharge plume is considerably less dense than water in compartments 2 through 5, more than 96% of the discharge plume could report to compartment 1. The model is therefore sensitive to discharges that are less dense than the lower compartments. In the case of a low-density discharge, a greater portion of the plume flow would simply rise to the surface, effectively bypassing the lower compartments.

It is important to note that the formation of the discharge plume (as shown in Figure 20) is still affected by the temperature and composition of the water from compartment 5. This water is used to exchange some heat and porewater with the incoming tailings before the tails bed is formed. There is some dilution and cooling of the discharge prior to the formation of the discharge plume. Because of heat transfer and chemical diffusion back from the tails bed to compartment 5, the placement of tailings is expected to raise the concentration and heat stored in compartment 5. An increase to total dissolved solids will increase the density of compartment 5, and an increase in temperature will decrease it. The multi-compartment model tracks expected changes to compartment density, and assigns an inter-compartment mixing rate that increases significantly if a lower compartment has a lower density than the compartment above it. Details are discussed below.

6.3.3 Density-Dependent Mixing and Inter-compartmental Flows

Reverse flows in the compartments 1 through 5 are used to provide inter-compartment mixing. Details are described in Figure 19. In this model, this is handled simply as an equal flow (up and down) from adjoining compartments. If the flow rate Q_{21} represents the normal forward flow from compartment 2 to 1 and a backward flow Q_{12} is added to simulate greater mixing, Q_{12} is added to Q_{21} to achieve the same net forward flow. The upper zone mixing flow variable Q_{12} is influenced by a wind-generated mixing flow of $2000 \text{ m}^3/\text{d}$ during the ice-free season and the normal density-driven mixing flow. Density-driven mixing flows can be as high as $15,000 \text{ m}^3/\text{d}$, or roughly 11 times the average natural flow. Typical values for Q_{12} are seasonal, ranging from

2000 m³/d to 7300 m³/d over the ice-free season, but may be only 500 m³/d during the mid winter.

The mixing flow Q_{23} between compartments 2 and 3 is set to the normal density-driven mixing flow, plus one-tenth of the mixing flow Q_{12} . The idea is that forces that mix the upper 20 ft will still have some influence at the next compartmental interface. Typical values for Q_{23} are also seasonal, ranging from 700-1200 m³/d during the ice-free season and 500 m³/d for other periods.

Inter-compartment mixing Q_{1N} between the northern HTDF compartment and compartment 1 is set to a minimum mixing flow of 50 m³/d or 50% of the natural flow to the northern HTDF. Since the natural flow is seasonal, the mixing flow is also, ranging from 50 to 220 m³/d. Flow from both compartments 1 and N are drawn in to form the wastewater influent flow $Q_{T,out}$.

Unless the discharge heats the lower compartments significantly, the inter-compartment mixing in the lower compartments is limited to 500 m³/d. Other factors, such as the compression of compartments, circulation effects of the discharge to compartment 5 and the reclaim water from compartment 3, add additional mixing to the system.

6.4 Parallel Model Components and Simulation of HTDF Chemistry

A range of chemical constituents and heat flow are modeled in parallel, using the same general mixing model to determine inter-compartmental transfers. These parallel components are shown in a diagram in Figure 17. The mill discharge plume and the HTDF are expected to consist of a dissolved metal (C), total alkalinity (Alk), DO, compounds carrying oxygen demand (P), and total dissolved solids (S). In addition, temperatures (T) are tracked and oxidized iron (OxFe) (which is used to track the oxidation of compounds carrying oxygen demand) are also tracked with compartments and inter-compartment flows.

Surface and groundwater flows may carry background concentrations of the constituents and there may be additional fluxes of DO and surface heat at the water surface, without flow. As initial chemical profile data are available, they are used as initial concentrations in the model. Some estimation was required for the constituents P and OxFe.

6.4.1 Surface Heat Flows

Chemical kinetics, DO transfer, ice formation, and water density are sensitive to temperature, and a surface heat balance was considered necessary to properly estimate surface temperatures. Temperature (T) in water is related to heat (H) through the volume, density (ρ_w) and heat capacity (C_p):

$$T = \frac{H}{V\rho_w C_p} \quad (34)$$

While the product of the density and heat capacity does vary with temperature, it ranges from $4.21 \times 10^6 \text{ J/m}^3 \text{ }^\circ\text{C}$ at 0 °C to $4.15 \times 10^6 \text{ J/m}^3 \text{ }^\circ\text{C}$ at 35 °C. For the purposes of HTDF model, the product of the density and heat capacity was referred to as a constant heat factor (HF_w), set at $0.00419 \text{ GJ/ m}^3 \text{ }^\circ\text{C}$, where GJ refers to giga-Joules ($\times 10^9 \text{ J}$). The heat capacity of the dry tailings was set to a value used for common brick, $840 \text{ J/kg }^\circ\text{C}$ or $0.00084 \text{ GJ/ tonne }^\circ\text{C}$.

Chapra (1997) describes the surface heat balance from net absorbed solar and atmospheric radiation, losses by longwave back-radiation and evaporation, changes from conduction and convection, and input/exports from flows. A simplified expression for atmospheric longwave radiation flux was:

$$J_{an} = \left(4.75 \frac{mJ}{m^2 d K^4} \right) (T_{air} + 273)^4 (0.6 + 0.31 \sqrt{e_{air}}) \quad (35)$$

where T_{air} is the air temperature ($^{\circ}C$) and e_{air} is the vapor pressure (mm Hg) that is related to the relative humidity Rh and saturated vapor pressure (e_{sat}):

$$e_{air} = \frac{Rh}{100\%} e_{sat} \quad \text{and} \quad e_{sat} \approx 4.596 \exp\left(\frac{17.27 T_{air}}{237.3 + T}\right) \quad (36)$$

Using monthly normal tabulated values for relative humidity and air temperature at the Champion-Van Riper station, the surface atmospheric radiation flux could be determined. The longwave back-radiation was estimated as:

$$J_{br} = \left(4.75 \frac{mJ}{m^2 d K^4} \right) (T_1 + 273)^4 \quad (37)$$

Where T_1 is the temperature of compartment 1. With assumption of an average wind speed of 7 mph (3.1 m/s), the flux due to conduction/convection was estimated as:

$$J_c = \left(0.55 \times 10^6 \frac{J}{m^2 d ^{\circ}C} \right) (T_1 - T_{air}) \quad (38)$$

The flux due to evaporation was estimated as:

$$J_e = \left(1.17 \times 10^6 \frac{J}{m^2 d mmHg} \right) (e_{sat} - e_{air}) \quad (39)$$

Monthly solar radiation data from the Eagle Project site was presented by Golder (2005). The monthly values starting with June 2004 were 273, 225, 213, 174, 89, 43, 26, 39, 72, 144, 215, and 224 W/m^2 . The values were reduced 10% for losses due to reflection and shading, and converted to units of J/m^2 -d.

6.4.1.1 Considerations for Ice Formation and Melting

When the water temperature was predicted to drop below $0^{\circ}C$, ice was formed from the surface heat imbalance. The surface heat flux was negative, and the balance of other heat flows between the compartments had to be balanced by the formation of ice with a latent heat of 0.334 GJ/tonne and assumed density of 0.916 tonnes/ m^3 . With the surface area known and the total tonnage of ice formed, the thickness of the ice could be estimated.

Without correction to the surface heat fluxes during the ice period, ice formation was very large (3m or more) and the ice period was too long, melting in July. Because the ice and snow cover were expected to provide insulation to the water, the surface heat losses were reduced by a factor that varied exponentially with the ice thickness, and boundary temperature at the air-ice interface

was also adjusted to retain more heat in the system. The simulation led to steady seasonal ice formation and melting, forming in late October or early November, forming a peak ice thickness of approximately 80 cm in mid-February, and melting by mid-April.

6.4.1.2 Considerations of Surface and Groundwater Flows

The water temperature of surface water inputs, including miscellaneous contact water, was assumed to be at the air temperature. Groundwater temperature was assigned a temperature of 15 °C.

6.4.2 Considerations of Heating from Mill Discharge

The temperature of the tailings discharge was modeled as a variable, assuming a constant rate of heat input from dry tailings, use of recycle water at the temperature of compartment 3, and other factors, such as the inclusion of miscellaneous contact water in the discharge. Although an expected discharge temperature of 10 °C has been provided by M3 Engineering, the temperatures modeled for the discharge range from 10.5 °C to 12.6 °C during discharge, with the peak temperature occurring during the summer months.

No additional heating from the tails, such as from exothermic reactions, is expected, since DO and other reactants needed for the exothermic reactions will likely be absent, or at low concentrations.

The heat balance associated with the formation of the discharge plume (see Figure 20) demonstrates that there is some cooling of the discharge prior to full formation of the discharge plume. Some excess heat is stored in the tails bed, but may transfer back to compartment 5. The remaining excess heat is discharged to the compartments. The discharge plume temperatures are expected to be roughly 1.4 °C less than the discharge temperature, or roughly in the range of 9.1 °C to 11.1 °C.

The dynamics of temperature expected in the HTDF during and after loading are shown in Figure 22. The temperature of the bottom HTDF water is initially in the range of 5.0 – 5.6 °C, and the introduction of warmer tails will heat the system over time. The temperature of compartment 5 is expected to increase from 5.6 to 8.2 °C after 7.1 years of loading, declining slowly afterwards. Compartment 4 temperatures are expected to increase from 5.1 to 7.3 °C, without significantly declining after the tails loading. And, compartment 3 temperatures are expected to increase from 5.1 to 6.7 °C during loading, and continue to increase to 7.3 °C seven years after tailings loading ends.

It is important to note that water density was estimated from fitting standard density-temperature tables as well as density-salinity relationships. As an illustration, temperature and density profiles are shown in Figure 23. Temperatures increase during loading from compartments 3 to 5. If the salinity was the same, the higher temperatures at the bottom would be associated with lower densities, and there would be greater mixing. However, the higher salinity (or TDS) in the lower compartments counteracts the temperature effect and density increases with depth. Several years after loading, the temperature profile is relatively flat, but the trend of increasing density with depth appears stable.

Long-term simulations, run for a total of 27 years, showed that the water temperature for the lower HTDF is relatively constant, with compartment 3 showing a slight increase to roughly 8.0 °C at 27 years, and compartments 4 and 5 rising slightly to 7.8 °C at 27 years. No significant changes in the upper HTDF temperatures are expected over the long-term, as compartment 1 and compartment 2 temperatures are controlled by normal seasonal conditions. However, the effect of year-to-year variations in surface heating conditions are not modeled, since the same, normal record for annual climate was used for the simulations.

6.5 Flow and Water Level Dynamics

The record of flows simulated from the model is shown in Figure 22. The irregular natural inflow follows directly from the monthly net precipitation and melt record that is fed into the model. The flow record shows the flows from the mill discharge and the return (reclaim water) flow. The net precipitation to the main HTDF is the same for every year, but the outlet flow (to WWTP) is held constant at 1816 m³/d (333 gpm) during the period of mill discharge and 1340 m³/d (246 gpm) after the tailings loading is completed. Water levels during the loading period range from 468.5 m (1537.2 ft) to 469.1 m (1539.1 ft). This range in elevations is maintained for periods after loading. An alternate model simulation was run, using the net precipitation time-series from the maximum annual precipitation case (see Section 3.2) and an outlet flow to the WWTP at 2627 m³/d (482 gpm) based on a 320 day operating period for the mill. For this simulation, the elevations ranged from 468.5 m (1537.1 ft) to 469.4 m (1540.0 ft). The proposed berm elevation along the northern edge of the HTDF is 470.3 m (1543 ft). Since a 100-yr, 24-hr storm event is expected to raise the water elevation 1.2 ft (see Section 3.2), the maximum HTDF water level should always be less than 470.0 m (1542.0 ft). Since the HTDF volume is large relative to the flows, the hydraulic retention time is also large. The effects of seasonal and year-to-year variations on the mass balance are dampened significantly by the large volume.

As is mentioned in Section 3, flows at the proposed WWTP may be adjusted to handle seasonal variations in flow. Given the significant available storage with the HTDF and low flows during winter months, wastewater treatment operations may be focused during warm weather periods without significant impacts to HTDF water quality and elevations. Based on upon the flow dynamics discussed above and in Section 3.1.2 a WWTP capacity of 510 gpm is appropriate for a mill operations.

6.6 Dissolved Oxygen and Iron Chemistry Dynamics

DO and dissolved components expressing an oxygen demand are modeled to better understand the risks of the oxidation of the placed tailings. The concept for placement of tailings in the HTDF provides two main elements that should greatly limit oxidation:

- ♦ Deep placement of tailings
- ♦ High slurry density

Reducing exposures of the slurry to the overlying water and reducing the amount of water discharged should greatly reduce exposure of the tailings to DO during loading and over the long term.

DO dynamics are modeled by considering aeration of the surface water (compartments 1 and N) during the ice-free season, consumption of oxygen by oxygen depleting chemicals, complete

mixing within compartments, and mass transfer from fluid flow between compartments. Oxygen saturation levels and the rates for reaeration and oxygen depletion are temperature-dependent. Adjustments to oxygen saturation for salinity (as estimated from TDS) were also made. An eight-term polynomial equation was used to relate DO saturation to temperature and salinity (American Public Health Association 1998a, Chapra 1997).

The DO of the background water (from net precipitation, melt, and groundwater input) was modeled to be 3 mg/L below oxygen saturation. However, the surface waters (compartments 1 and N) were well aerated. The Wanninkhof, et al. (1991, as cited by Chapra 1997) estimation for lake reaeration coefficient was used. Although a typical wind speed is 7 mph, a 10 mph wind speed was selected as a conservative measure (more aeration), and the reaeration mass transfer coefficient was estimated as 1.15 m/d. Using a mean depth of compartment 1 of 1.83 m (6 ft) and the surface area, the aeration coefficient at 20 °C was estimated as 156,000 m³/d for compartment 1 and 26,000 m³/d for compartment N. Both rate coefficients were subject to temperature corrections of the form:

$$k_a(T) = k_{a(20^\circ C)} \theta^{T-20} \quad (40)$$

where θ was selected as 1.024. No aeration was allowed during ice seasons.

The interdependencies related to DO dynamics are described in Figure 17 and Figure 24. DO is depleted by oxygen depleting chemicals (P), and the oxidation of P also leads to the formation of oxidized iron (OxFe) and a reduction of alkalinity (Alk). DO, which is abundant at the surface, may be brought into contact with water in the lower layers, from a downward mixing flow, internal recycling associated with the discharge and reclaim streams, or water flow from the lower compartments into the upper compartments. In addition, oxygen depleting chemicals (P) may flow up into compartments with higher levels of DO, and oxidized iron (OxFe) may reduce to form P in compartments with low DO.

The basic rate coefficient for oxygen depletion (k_d) is set to 0.1 m/d. This rate coefficient is corrected by temperature (see Figure 24). The oxygen demand P is assumed to be completely from dissolved ferrous iron. In order to address a model instability at low DO, the oxygen depletion rate is made first-order with respect to DO at DO levels below 1 ppm. This allows fairly rapid numerical integration and a somewhat rapid depletion of DO.

Reduction of oxidized iron (OxFe) to oxygen demand (P) is assumed to occur when the DO is less than 0.5 mg/L. The presence of additional reductants, primarily bisulfide, at low DO levels is expected to convert oxidized iron to reduced iron (or P). However, the reaction rate is first-order with respect to the OxFe concentration and the rate coefficient is assumed to be only 1.5% of k_d , the rate coefficient for oxygen depletion. These settings led to reasonable iron and DO levels for the unloaded model run condition, which was the primary method used for selection of these settings. Expected profiles of DO during and after loading are shown in Figure 23.

6.6.1 Alkalinity Effects

The consumption of DO by oxygen demand (P) is expected to coincide with a decrease in the alkalinity of the water. The oxidation of ferrous iron to ferric iron by DO, followed by the formation of ferric hydroxide, is expected to reduce alkalinity by 12.5 mg as CaCO₃ for 1 mg of

DO consumed. The slower reaction of the reduction of oxidized iron to P is expected to increase alkalinity by 1.68 mg as CaCO₃ for each 1 mg of iron reduced.

While pH is not modeled directly, large decreases in alkalinity would generally indicate more acidic conditions and opportunity for greater leaching from the tailings. There are two main attributes of the loading that provide a significant level of protection against acidic conditions:

- ♦ Discharge is expected to have high alkalinity (900 mg/L as CaCO₃).
- ♦ Deep placement at high percent solids will limit exposure of tailings and chemicals carrying oxygen demand to DO.

In the model, the discharge alkalinity was assigned a value of 860 mg/L as CaCO₃. Using this input and the expected mixing and reaction dynamics of the model, the expected alkalinity profiles for the HTDF during and after loading are shown in Figure 23.

Alkalinity is also expected to affect the settling of ferric hydroxide (see Figure 24). Settling should be more favorable under conditions of higher alkalinity. An empirical alkalinity pivot function was used to scale the settling rate. If the alkalinity of the water was less than 100 mg/L as CaCO₃, the settling rate would be roughly one-tenth of the full rate (8 cm/d) or less. If the alkalinity was 200 mg/L, the settling rate would be roughly one-half the full rate, or 4 cm/d. An alkalinity of 450 mg/L as CaCO₃ would lead to settling at roughly nine-tenths of the full rate.

6.6.2 Metal Scavenging by Iron Hydroxides

Metals, such as nickel, copper and mercury, are expected to complex with ferric hydroxide to form mixed metal complexes. An empirical relationship, shown in Figure 24, was used to simulate the level of complexation, which is sensitive to the level of oxidized iron (OxFe) and adjusted by a complexation coefficient, K_{complex} . Under the formulation, a higher value of the parameter K_{complex} leads to less complexation. Once complexed, the removal of the metal by iron scavenging depends on the settling rate. Therefore, effective removal through scavenging requires favorable complexation and availability of oxidized iron, as well as favorable settling to the lower compartment. As mentioned above, effective settling of iron hydroxides requires that the alkalinity is suitable. For compartment water with a low alkalinity, complexation may be favorable, but losses to scavenging may be small because of the greatly reduced settling rate.

Determining the iron scavenging dynamics of the HTDF is complicated. Fortunately, chemical profile data from 1994 for nickel and copper were available (Montgomery Watson, 1995). The empirical iron scavenging algorithm could be calibrated to fit current (2007) conditions using the earlier 1995 dataset as the initial condition. As shown in Figure 16, the nickel concentration in the HTDF has decreased more than would be predicted from complete mixing and simple washout. Under stratified conditions, the removal from washout is expected to be much less, so internal metals scavenging should be considered to be an important removal mechanism.

A set of nickel scavenging model runs were carried out, using the 1994 initial conditions and without any tailings loading. The initial alkalinity profile was assumed to be 100, 100, 100, 165, and 185 mg/L as CaCO₃, for compartments 1 through 5, respectively. The initial nickel concentrations, estimated from the reported values at 10 m depth intervals (Montgomery Watson 1995), were 520, 510, 910, 990, and 1000 ug/L, respectively (see table, presented in Figure 16).

To be conservative, nickel concentrations in the background were held to 0.0 ug/L. A favorable fit was found with a value for K_{complex} of 0.01. Whereas current (2007) measurements show that the nickel concentration profile is 14, 13, 17, 210, and 280 ug/L for compartments 1 through 5, the modeled concentrations were 13, 27, 113, 174, and 363 ug/L. Since the calibration generally led to higher concentrations than were measured in the 2007 profile, the calibration is considered conservative. In addition, normal model runs conservatively assumed a background concentration for nickel of 5 ug/L, while the calibration case assumed no background.

A similar process was used to find the complexation parameter K_{complex} for copper. The initial copper concentrations, estimated from the reported values at 10 m depth intervals (Montgomery Watson, 1995), were 13, 12, 32, 57, and 70 ug/L, respectively. The background concentration for copper was set to 2.0 ug/L. A favorable fit was found with a value for K_{complex} of 0.05. Whereas current (2007) measurements show that the copper concentration profile is 1.9, 1.8, 1.8, 2.7, and 3.3 ug/L for compartments 1 through 5, the modeled concentrations were 1.5, 2.4, 7.2, 10.8, and 23.8 ug/L.

6.7 HTDF Simulation Results for Complexed Metals

HTDF simulation results for the selected metals of nickel, copper, mercury, and selenium are shown in Figure 25. Trend plots for nickel, copper, and mercury for all major compartments are shown in Figure 26. Model results for concentrations expected at the HTDF outlet, to the WWTP, are presented in Table 5.

6.7.1 Nickel

The concentration of nickel discharge was set to 2230 ug/L. However, with internal mixing and scavenging processes, the simulated peak concentrations in the lower HTDF were always less than 400 ug/L. Even during loading, nickel concentrations increase only slightly or drop significantly because the rate of mass removal due to scavenging is greater than the rate of loading. Scavenging in the lower compartments is particularly strong. The increased alkalinity of the lower compartments (from the discharge) tends to favor more rapid settling. Surface nickel concentrations continue to decrease from the initial value of 14 ug/L to values less than 10 ug/L. At year 10, the surface concentration is expected to be less than 2 ug/L. Due to the assumption of sustained background loadings, the surface concentrations are expected to be stable for a long period after loading, while the concentrations in the lower HTDF compartments 2, 3, and 4 will continue to decline. Because of diffusion from the active bed tailings, the concentration of compartment 5 is relatively constant after year 10 (see Figure 26).

6.7.2 Copper

The concentration of copper discharge was set to 2760 ug/L, with much lower concentrations initially in the HTDF. However, with internal mixing and scavenging processes, the simulated peak concentrations in the lower HTDF were always less than 400 ug/L. During loading, copper concentrations increase significantly in the lower compartments, rising from 3.3 ug/L to roughly 300 ug/L in the first two years of loading, then decreasing to roughly 140 ug/L at the end of loading. Because of stratification and a general delay in the arrival of mass released from the bottom discharge, the surface copper concentrations drop slightly from 1.8 ug/L over the first year of loading, then increase to a peak of roughly 2.6 ug/L at the end of loading. After loading, scavenging is expected to further reduce concentrations throughout the HTDF. At year 10, the

surface concentration is expected to be less than 1 ug/L. Due to the assumption of sustained background loadings, surface concentrations are expected to decline to a level of 0.5 ug/L at year 14, with a much slower rate of decline for periods after year 14. For the 7 year period after loading, copper concentrations in the lower HTDF are expected to decline to 10 ug/L or less. However, diffusion from the active tailings bed porewater will likely lead to copper concentrations in the range of 5 to 10 ug/L to be sustained in compartment 5 for a long period (see Figure 26).

6.7.3 Mercury

Mercury concentrations in the HTDF initially are non-detect, but relatively large in the expected tailings discharge. With a discharge concentration of 200 ng/L, the lower HTDF concentrations increase significantly during loading, from less than 1 ng/L to a peak of roughly 21 ng/L in compartment 5 at the end of the second year of loading. Due to internal scavenging ($K_{\text{complex}} = 0.01$) and some internal mixing of the discharge, the lower HTDF mercury concentrations are expected to decline to roughly 11 ng/L at the end of loading (year 7). After loading is complete, mercury concentrations in the lower HTDF are expected to decrease to less than 1 ng/L.

Even during loading, the surface mercury concentrations continue to decline from the initial setting of 0.5 ng/L. Background concentrations for mercury were set to 0.5 ng/L. However, higher background concentrations of mercury would likely control surface concentrations.

The assumption for assignment of the complexation coefficient of 0.01 is supported by the general chemical behavior of mercury relative to nickel. Mercury is expected to form complexes with iron and other compounds (such as bisulfide) with a higher affinity.

6.7.4 Other Complexed Metals

The model was carried out for several other metals that were expected to be scavenged by complexation and settling with iron hydroxide. Initial concentrations were drawn from Table 3. Background concentrations, estimated from the initial concentrations, are summarized in Table 5.

The set of other metals expected to have iron scavenging complexation coefficients similar to nickel ($k_{\text{complex}} = 0.01$) include aluminum, arsenic, cadmium, chromium, lead, strontium, and zinc. Aluminum, arsenic, chromium, strontium and zinc were not detected above the EQL in the initial profile, but are expected in the mill discharge. For the purposes of modeling, the assumed background and initial concentrations for this set were set to 0.001 ug/L. Of this set, aluminum is expected to have the highest discharge concentration, at 686 ug/L. For the aluminum simulation, the peak concentration in compartment 5 was less than 60 ug/L, and the peak HTDF effluent concentration was less than 0.4 ug/L. It follows that all other metals of this set are expected to have lower concentrations in the profile and at the HTDF outlet.

An additional consideration was made for arsenic. Arsenic would likely be present as the arsenate ion, subject to redox reactions, iron scavenging, and potentially more labile under basic conditions. However, the more complex fate of arsenic species was not modeled. Arsenic was detected in each of the 5 compartments, but reported values were below the EQL of 1 ug/L. Assuming a background concentration of 0.5 ug/L and an upper-bound initial concentration of 1 ug/L in each compartment, the expected arsenic concentration in the HTDF outlet at was 0.5

ug/L at 1 year and drops steadily to roughly 0.2 ug/L at the end of 7 years. At 10 and 14 years, the arsenic concentration at the HTDF outlet is within the range of 0.1-0.2 ug/L. Decreasing the background concentration to 0.1 ug/L resulted in arsenic concentrations at the HTDF outlet of less than 0.1 ug/L after 7 years.

Cobalt, manganese, and molybdenum were modeled with a complexation coefficient of 0.05, the same setting as for copper. Background concentrations were set to match the initial concentrations of the upper compartments. These compounds are expected to be scavenged by iron hydroxides, but not as completely as the other scavenged metals. Although manganese oxides may also participate in metal scavenging and are important in redox reactions, modeled reactions were limited to scavenging with iron.

6.8 HTDF Simulation Results for Non-Complexed Species

The HTDF model was run for a set of compounds not expected to participate in iron complexation. This set included barium, calcium, chloride, fluoride, lithium, nitrate, potassium, selenium, sodium, sulfate, and total dissolved solids (TDS). Although scavenging may be effective for antimony, antimony was also modeled without iron complexation. For each case, the value of K_{complex} was set to 100,000, in order to minimize iron scavenging. Expected concentrations at the HTDF outlet to the WWTP are summarized in Table 5.

6.8.1 Tracer Simulation

An additional HTDF model run was made to simulate a nonreactive tracer. The discharge concentration was set to 1000 ug/L and the initial and background concentrations were set to zero. This run case serves as a useful reference case. For this case, the simulation time was extended to roughly 27 years. A trend plot of the concentrations of the tracer is shown in Figure 27. Concentrations in compartment 5 increase steadily from roughly 110 ug/L after 1 year of loading to a peak of 530 ug/L at the end of loading. After loading the concentration drops steadily to roughly 200 ug/L at year 27. At the HTDF outlet to the WWTP, the concentrations for the same times are 0.0, 0.7, 15.3, 23.0, and 33.3 ug/L. This demonstrates that the peak concentration does not occur at the end of loading, but after loading. During loading the outlet concentrations are generally less than 1.5% of the discharge concentration, and increase to roughly 3% of the discharge at 14 years. After 14 years, there is little decay of the tracer in the HTDF outlet (WWTP influent), due to the inventory in the lower compartments and no scavenging of the tracer within the HTDF.

6.8.2 Selenium

Expected concentration profiles for selenium are presented in Figure 25. Unlike nickel, copper, and mercury, the model was run without any scavenging of selenium by iron hydroxide complexation and settling. The expected discharge concentration was 21 ug/L and the initial and background concentrations were nondetect. The continued loading is expected to lead to a steady increase in the lower HTDF concentrations during loading, increasing the selenium concentration of compartment 5 to approximately 11 ug/L. At year 14, the selenium concentration in the lower HTDF is still somewhat elevated at roughly 7 ug/L. At the surface, the selenium concentration increases to 0.3 ug/L at the end of loading, and continues to increase to roughly 0.7 ug/L at year 14.

6.8.3 Nitrate and Ammonia Nitrogen

The initial concentration profile of nitrate was modeled as the combination of ammonia and nitrate/nitrite nitrogen, with the conservative assumption that the ammonia would eventually convert to nitrate. The initial ammonia nitrogen concentration was 3.0 mg N/L in compartment 4 and 4.5 mg N/L in compartment 5. These levels were added to the measured, initial nitrate levels to yield a modeled, initial nitrate concentration of 5.6 mg N/L in compartment 4 and 6.0 mg N/L in compartment 5. The discharge was expected contain 0.237 mg N/L as nitrate. Using these initial and loading conditions, the model was run without any internal nitrogen reactions. Nitrate concentrations in the HTDF outlet to the WWTP are expected to be only slightly higher than the implied background concentration of 2.0 mg N/L.

Reactions with ammonia nitrogen were not modeled directly. Ammonia may participate in metal complexation in the lower HTDF, leading to elevated dissolved metal concentrations. Ammonia may also be complexed with solid phases, such as with iron hydroxide. Ammonia may also participate in the expression of oxygen demand, provided there are nitrifying organisms active in the HTDF. At the surface, ammonia is currently absent. If detected, the near neutral pH would dictate that it would be in the form of ammonium ion, not as free ammonia. However, the current version of the model did not consider ammonia reactions, other than to adjust the initial profile for modeled nitrate concentrations. While the upper HTDF is well aerated and DO levels remain high during and after loading, it is uncertain whether ammonia in the lower HTDF will migrate to the point of HTDF discharge at trace levels that may require treatment.

In order to address this uncertainty, an upper-bound estimate of ammonia concentration was modeled for the HTDF outlet to the WWTP. The initial profile of ammonia was set to 3 mg N/L at compartment 4 and 4.5 mg N/L in compartment 5, and a washout simulation was performed. This run of the model ignored any other sources of ammonia and no reactive conversion of ammonia. Under this conservative scenario, the ammonia levels in the HTDF outlet increase from zero to roughly 0.4 mg N/L at the end of year 7, with a slow decline to 0.3 mg N/L at the end of year 14. As mentioned above, the ammonia would likely be present as ammonium ion, rather than free ammonia. Since some complexation of ammonium with suspended solids in the lower HTDF is expected, and since conversion of ammonia to nitrate would be expected with the aerobic conditions in the upper HTDF, these modeled ammonia levels conservatively represent an upper bound.

A Preliminary Effluent Limit (PEL) for ammonia was not available (see Table 5). Typically, ammonia levels below 1.0 mg N/L are considered safe to aquatic life for receiving waters with a pH less than 8. Because these conditions are expected to be met prior to wastewater treatment for the HTDF, ammonia is not expected to be present at levels of concern.

6.9 Further Discussion of HTDF Simulation Results

While the level of complexity of the loading condition and chemical trends within the HTDF are relatively high, the HTDF mass and heat balance model has been developed to capture a wide range of processes. Focus was given to what were considered dominant processes, particularly the variable mixing conditions, the heat balance, displacements from the tailings loading on an irregular schedule, oxygen mass transfer and reactions, iron dynamics, and metals scavenging.

While there remains some uncertainty regarding loading conditions and internal chemical processes, the modeling is based on reasonable, empirical measures, fundamental quantities, best estimates for initial and input conditions, and explicit numerical strategies.

An important conclusion of the set of modeling simulations is that the HTDF is expected to remain stratified during and after the period of loading. This is expected for several reasons.

1. The current system is stratified and there are internal chemical mechanisms reinforcing that stratification. Previous tailings loadings, which were more disruptive because tailings were discharged to the surface, were followed by a period of significant restoration of the overall water quality and the stratified conditions that are observed presently.
2. The tailing discharge is expected at a high slurry density, so the level of exchange with the pore water is expected to be minor and a large portion of the inventory is expected to be stored in the tailings bed porewater.
3. Care will be taken to place the mill tailings at the bottom of the HTDF, to minimize exposure with water in the upper compartments of the HTDF.
4. The tailings will be placed at a moderate temperature, to minimize the likelihood of the formation of an unstable, thermal plume that may emerge at the HTDF surface.

The tracer simulations provide a useful mathematical reference for tracking the effects of the discharge on surface concentrations. The tracer simulations showed that, with no initial or background concentration near the HTDF, roughly 3% of the discharge concentration of a non-complexed compound would reach the HTDF outlet to the WWTP. If 1000 ug/L was discharged, the peak concentration occurred at roughly 14 years after loading and was roughly 30 ug/L. Because of the significant mass inventory within the lower HTDF and without any other mechanism to reduce concentrations in the HTDF, this outlet concentration of this ideal compound is expected to be at 20 ug/L at 27 years. Further washout is likely to be slow.

For most of the heavy metals brought in from the mill as tailings are placed in the HTDF, there is good evidence that internal chemical processes, particularly metals scavenging by settling iron hydroxide, will greatly reduce concentrations within the HTDF and at the HTDF outlet. For instance, while nickel is expected to be discharged at a concentration of 2203 ug/L, the concentration at the HTDF outlet is expected to be less than 2 ug/L after 10 years (less than 0.1% of the discharge concentration). Because scavenging causes a reduction of the metals inventory within the HTDF, the concentrations at the HTDF outlet are expected to continue to decline over time.

The model expectation of significant scavenging was supported by an evaluation that compared nickel and copper concentrations in the HTDF profile as measured in 1994 to more detailed measurements from 2007. Simple washout, even with complete mixing, could not explain the significant reductions in the HTDF metals concentrations. Using conservative settings for metals complexation coefficients, the scavenging portion of the model was fit to reproduce the measured decrease in nickel and copper concentrations.

Other chemical processes within the system reinforce the removal of metals and stability of the HTDF system. There is a continuous flow of DO from the surface into the HTDF, and mixing will bring some DO into contact with the lower HTDF compartments. Similarly, there is a

counter-acting flux of oxygen depleting chemicals from the base of the HTDF – and these oxygen depleting chemicals (such as reduced iron and bisulfide) are expected to counterbalance the downward flux of DO. Because the system is adequately buffered with considerable alkalinity from the discharge, the acids produced from the oxidation reactions should be effectively neutralized for a long period. This attribute of the system is particularly important for the sustained scavenging of metals by iron hydroxide within the HTDF.

In Table 5, the HTDF outlet concentrations predicted from the model are compared to PEL for discharge (PEL calculations are provided in Appendix E). None of the modeled outlet concentrations exceed the PEL, and in most cases the concentrations are more than an order of magnitude lower than the PEL.

The range of modeled chemical processes are based on the current understanding of bathymetry, climate, HTDF chemistry, and the estimated properties of the tailings as they are expected to be placed in the HTDF. However, the model may also be used as a way to track the progress and state of the HTDF during loading. At regular intervals during the loading, the modeling could be calibrated to observed conditions before and during loading, then used to refine projections for future performance. This may be particularly valuable during the period of loading, to refine predictions of long-term performance and to better understand loading conditions that tend to reduce long-term impacts.

7 Conclusions

This report presented a detailed assessment of the water chemistry characteristics of the HTDF. The assessment included an evaluation of the drainage basin, the HTDF bathymetry, climate, recent and current water chemistry, detailed evaluations of the thermal stability and stratification of the HTDF, and a detailed mass balance model used to estimate the water chemistry and flows that would be expected at the HTDF outlet to a WWTP.

Field measurements indicated that the HTDF exhibits stratification with respect to temperature, DO concentrations, and almost all dissolved chemical constituents; this is discussed extensively in this report.

An extensive effort was placed on the development and testing of a multi-compartment, heat and mass balance model, which was used to estimate the expected water chemistry and flows at the HTDF outlet to the proposed WWTP. The model included a large set of processes, including dynamic and seasonal loading conditions, variable volumes, density and vertical stability of the discharge plume and HTDF compartments, and a variety of chemical mass balance modeling processes.

Important model outcomes include a predicted average outflow from the proposed WWTP of about 350 gpm during mill operation, with a maximum outflow of about 500 gpm. Volume predictions indicate that the tailings from the proposed mill will occupy about 22.5% of the current HTDF volume, and that water depth after the tailings are placed will be over one hundred feet. With proper control over tailings placement, the bottom waters of the HTDF will remain anoxic, and will continue to be anoxic after placement ceases, and a reserve of alkalinity will be present during and after mill operation.

A key outcome of the multi-compartment mass balance model was that, during and after the period of the placement of mill tailings, the stratified behavior of the HTDF would likely be sustained. This is a particularly important and reasonable conclusion, but one which follows from the nature of the placement of the tailings, internal processes which tend to reinforce stability, and conditions regarding the natural flows and bathymetry of the HTDF.

The placement of tails at a high slurry density and the preservation of a stratified HTDF generally leads to low surface concentrations at the HTDF outlet to a WWTP. Modeling included a conservative tracer test, which showed that the HTDF outlet concentrations would peak at roughly 3% of the discharge concentration, and only after a long loading period of 7 years. However, without internal processes to reduce the concentrations within the HTDF, several decades of washout may be needed to further reduce the concentrations of compounds that behave conservatively in the water column (compounds that are not complexed and not scavenged).

For a set of complexed metals, such as nickel, copper, mercury, and other metals, the concentrations at the HTDF outlet and within the HTDF are expected to be greatly reduced from metals complexation, precipitation, and scavenging by iron hydroxide. In addition, the levels for these constituents within the HTDF drop significantly after the period of tailings placement.

With current estimates of the PEL available for the constituents from the multi-component model, none of the modeled constituent concentrations for the HTDF outlet exceeded the PEL.

For nickel, copper, mercury, and selenium, the outlet concentrations were all well beneath the PEL.

A fully-mixed model was also developed to estimate maximum HTDF outflow concentrations. It is important to note that the fully-mixed case is a highly unlikely scenario, given the known stratification of the HTDF, the nature of placement, and chemical processes, such as metals scavenging, that tend to remove metals from the water column in the HTDF. The washout mechanism inherent in the fully-mixed model was tested using historical measurements of nickel, and was found to greatly over-predict outflow concentrations. The level of over-prediction is expected to be higher for the period of tailings loadings, since the model also assumes that the pore water associated with the tailings would also be fully mixed within the HTDF.

Nevertheless, the fully-mixed model predicted that nickel, copper and mercury will exceed discharge limits in almost all years of mill operation and for at least seven years after mill production ceases. Nickel, copper and mercury concentrations at the HTDF outlet exceeded the PEL, and selenium levels were near the PEL. However, these compounds would be removed by the proposed WWTP.

The dynamic, multi-compartment model was used to evaluate expected changes in HTDF water elevation with a steady flow rate through the proposed wastewater treatment facility. Modeling showed that normal annual variations and peak annual flows can be handled without large variations in the expected water elevation. Simulated water levels for average flow years were always less than 469.1 m (1539.1 ft). An alternative simulation of peak annual flows and steady outflow resulted in simulated water elevations less than 469.4 m (1540.0 ft). Although a 100-yr, 24-hr storm event is expected to raise the water elevation 1.21 ft, the maximum HTDF water level should always be significantly less than proposed berm height of 470.3 m (1543 ft).

Since the capacity of the proposed WWTP will be sized generously, even greater control of water elevations will be available. Periods of high natural inflow during the spring melt or heavier fall rains can be balanced by higher rates of wastewater treatment. In addition, WWTP operations may be scaled back or shut down during winter months, without significant reductions in the expected water quality of the wastewater treatment influent or to the available storage.

7.1 Recommendations

The main conclusion of this report is that the HTDF is expected to remain stratified during and after the proposed placement of mill tailings, and the constituent concentrations at the HTDF outlet are expected to never exceed the associated PEL. The following recommendations are made:

1. Provide wastewater treatment for the outflow of the HTDF in order to handle the metals concentrations under the fully-mixed case. While the fully-mixed case is likely unrealistic, the model outcomes may be referenced as a worst-case for the proposed placement plan. Treatment should be provided to meet the expected wastewater treatment discharge limits for nickel, copper and mercury, in particular. To accommodate maximum annual precipitation conditions, it is recommended that the WWTP be designed for a capacity of 510 gpm.

2. Provide routine monitoring of the mill tailings carriage water, the HTDF bathymetry, and water quality within the HTDF. It is important to note that, due to the large scale of the HTDF and expected continuation of stratification, the time-scale of a response from the point of tailings placement to the proposed wastewater treatment influent is on the order of years. The following basic elements of monitoring plan are recommended:
 - a. Indicators of the composition and density of mill tailings carriage water (such as conductivity and selected metals concentrations) should be sampled routinely, and there should be continuous monitoring of temperature near the point of mill tailings discharge. The sampling frequency for the carriage water composition can be developed according to expected variations in mill operation and ore quality. The main purpose of this monitoring is to develop a controls strategy, which may include regulated placement of mill tailings and associated pore water at or above set densities. Discharges of mill tailings or pore water with densities significantly below the density of the lower HTDF water should be avoided.
 - b. During the period of tailings loading to the HTDF, water quality monitoring should occur at two horizontal locations, with field parameters collected at 5 ft intervals beginning at the surface. Vertical sampling intervals for selected chemical parameters should be set to capture the water composition at the surface, above and below the thermocline and above and below the chemocline. The main purpose of water quality monitoring within the HTDF is to track trends in water quality and to refine projections of expected water quality at the proposed wastewater treatment influent. The frequency of chemical monitoring should be more frequent over the first two years, but may be reduced upon effective demonstration of water quality projections.
 - c. Outflow and water level information within the HTDF should be monitored to support planning for seasonal flows, particularly for the management of spring melt conditions. Basic climatological information such as snow pack, ice thickness, precipitation, and air temperature can be drawn from direct measurements at the HTDF site as well as from the Champion-Van Riper weather station. The frequency of site monitoring may be monthly during the first several years of operation, but may be reduced upon effective demonstration of water level and flow balance predictions.
3. Within contingency plans for the HTDF, include options such as treatment with coagulants (such as ferric salt or alum) to remove suspended solids and metals within the HTDF by adsorption, coagulation, and flocculation. Effective removal of the chemical constituents from the water column may be a cost-effective approach to meeting and sustaining constituent concentrations below discharge standards. Steps such as these are likely to reduce the time required to operate a WWTP for the period following the active placement of mill tailings.

This report has identified the use of the multi-compartment model, largely to provide estimates of the expected concentrations at the HTDF outlet. However, the model may also be used as a way to track the progress and state of the HTDF during loading. The modeling could be refined from regular calibration to observed conditions during loading, then used to refine projections for future performance.

8 References

- American Public Health Association. 1998a, "Method 4500.O C. Azide Modification," in *Standard Methods for the Examination of Water and Wastewater*, 20th Edition, L.S. Clesceri, A.E. Greenburg, and A.D. Eaton, editors.
- American Public Health Association. 1998b, "Method 2580 Oxidation-Reduction Potential (ORP)," in *Standard Methods for the Examination of Water and Wastewater*, 20th Edition, L.S. Clesceri, A.E. Greenburg, and A.D. Eaton, editors.
- Buffle, J. and De Vitre, R.R., 1994. *Chemical and Biological Regulation of Aquatic Systems*, Lewis Publishers
- Chapra, S.C., 1997. *Surface Water-Quality Modeling*. McGraw-Hill.
- Cherwell Scientific, 2000, *ModelMaker User's Manual*, Version 4.0, Cherwell Scientific, Ltd., Oxford, United Kingdom.
- Cyanamid, 1986. Technical Service Report, Project 2551 (provided as Appendix B)
- Foth Infrastructure & Environment, LLC. 2007, *Kennecott Eagle Minerals Company, Humboldt Mill Hydrogeological Report*
- Golder Associates, Inc. 2005, *Report on the Air Quality and Meteorology of the Proposed Kennecott Minerals Company Eagle Project*, Sept. 2005.
- Linacre, E.T. 1994. "Estimating U.S. Class A pan evaporation from few climate data." *Water International*, 19, 5-14.
- Michigan Climatological Resources Program, Michigan State University, Seney Station, <http://climate.geo.msu.edu/Stations/7515/NARRAT.txt>
- Montgomery Watson, 1993. "Humboldt Mill Tailing Pond Sediments Characterization and Evaluation of Metal Leachate Potential." April 2, 1993 Memorandum to Rick Morh, Callahan Mining and Ed Cryer, MW-Boise from Gil Crozes (Provided in Appendix C)
- Montgomery Watson, 1995. "Comparison of Total Phosphorous and Algal Enumeration After Phosphorous Application to Humboldt Pit." August 25, 1995 Letter to Bill Scarffe, Callahan Mining Corporation from Mark Allen (provided in Appendix C).
- Morin, K.A. 1993. "Rates of sulfide oxidation in submerged environments: Implications for subaqueous disposal." In "Proceedings of the 17th Annual Mine Reclamation Symposium, Port Hardy, British Columbia, May 4-7, pp 235-247.
- National Climatic Data Center: US Climate Normals
<http://cdo.ncdc.noaa.gov/cgi-bin/climatenormals/climatenormals.pl>
- Natural Resources Conservation Service-Michigan: Climate Information
<http://www.mi.nrcs.usda.gov/technical/engineering/climate.html>

Stumm, W. and Morgan, J.J., 1996. *Aquatic Chemistry*, 3rd Edition, Wiley Interscience.

Tchobanoglous, G. and Schroeder, E.D., 1987. *Water Quality: Characteristics-Modeling-Modification*. Addison-Wesley.

Traverse Engineering Services, P.C., 1984, *Humboldt Pit Hydrogeological Report*.

Wetzel, R.G., 2001. *Limnology* 3rd Edition, Academic Press, Elsevier.

Tables

Table 1
Expected Climate at Humboldt Mill

Month	Precipitation			Evaporation ³	Temperature Normals ¹		
	Normal ¹	High ²	Low ²		max.	min.	mean
	(in.)	(in.)	(in.)		(°F)	(°F)	(°F)
Jan	1.82	4.74	0.48	0.15	22.4	0.2	11.3
Feb	1.32	3.53	0.24	0.30	28.2	2.1	15.2
Mar	2.32	4.43	0.52	0.89	38.2	11	24.6
Apr	2.42	7.42	0.76	1.33	51.9	23.4	37.7
May	3.10	6.77	0.17	1.63	67.1	35.3	51.2
Jun	3.35	8.54	1.00	2.07	74.6	44.3	59.5
Jul	3.80	7.50	0.90	2.81	78.8	49.7	64.3
Aug	3.74	8.92	0.48	2.66	76.6	48.4	62.5
Sep	3.88	9.89	0.75	1.77	67.1	41.2	54.2
Oct	3.29	6.41	0.77	0.74	55.1	31.8	43.5
Nov	2.44	5.61	0.71	0.30	38.3	20.5	29.4
Dec	1.82	3.38	0.28	0.15	26.3	7.4	16.9
Annual	33.3	46.94	20.17	14.78	52.1	26.3	39.2

Prepared by: GRE
Checked by: CED1

Notes:

1. Precipitation and temperature 1971-2000 NCDC Normals for Station 201439, Champion - Van Riper Park, Michigan. Obtained from Midwest Regional Climate Center.
2. Monthly precipitation extremes, 1949-2001 NCDC Precipitation Extremes for Station 201439, Champion - Van Riper Park, Michigan. Obtained from Midwest Regional Climate Center.
3. From average monthly pan evaporation data for Marquette County, Michigan, National Resources Conservation Service. Multiplied by 0.77 to obtain estimate for actual evaporation.

Table 2
Expected Mill Tailings Production Schedule
for Purposes of HTDF Mass Balance Model

Year	Unit	Year 1	Year 2	Year 3	Year 4	Year 5	Year 6	Year 7	Year 8	Totals
Total Tails (dry)	tonnes	154,000	370,880	370,880	370,880	370,880	370,880	370,880	122,689	2,501,969
Expected Rate	tonnes/d	700	1159	1159	1159	1159	1159	1159	900	
Expected Timing	days	220	320	320	320	320	320	320	136.3	2276.3
	years	0.60	1	1	1	1	1	1	0.37	7.0
Discharge flow	m ³ /d	754.1	1213	1213	1213	1213	1213	1213	953.9	
	gpm	138.3	222.5	222.5	222.5	222.5	222.5	222.5	175.0	
Reclaim flow	m ³ /d	386.8	640.5	640.5	640.5	640.5	640.5	640.5	497.4	
	gpm	71.0	117.5	117.5	117.5	117.5	117.5	117.5	91.2	

Prepared by: GRE
Checked by: JBM

Notes:

1. Total ore production is expected to be 3,419,430 tonnes (wet). Total dry tonnes tails is expected from 6.78% moisture content and tailings content in ore of 78.13% (dry basis).
2. Discharge flow of mill tailings estimated from 60% solids, specific gravity of solids of 3.03, and assumption of complete saturation. Additional mill discharges (added to 60% solids stream) include truck wash and miscellaneous contact water at a flow of 10 gpm. Minor water or solids discharges from WWTP to HTDF were not considered in mass balance model.
3. Reclaim flow is water reclaimed from HTDF, a recycle stream brought back to mill for ore processing.

Table 3

Initial and Weighted Average Concentrations of Chemical Constituents
in HTDF and Expected Mill Discharge

Analyte	HTDF Initial Conditions (ug/L)						Mill Discharge ¹ (ug/L)
	Compartment					Weighted Average	
	1	2	3	4	5		
Aluminum							686
Antimony	8	8	9	35	42	17	-
Arsenic							11
Barium	8	8	8	9	11	9	15
Bicarbonate (CaCO3)	100,000	100,000	100,000	140,000	160,000	114,156	11,000
Boron	85	82	87	130	150	101	-
Cadmium							1
Calcium	47,000	46,000	48,000	49,000	49,000	47,905	114,000
Carbonate (CaCO3)							851,000
Chloride	12,000	12,000	12,000	22,000	26,000	15,432	50,667
Chromium							18
Cobalt	4	4	4	16	21	8	68
Copper	2	2	2	3	3	2	2,760
Fluorine							120
Iron	420	450	390	190	240	347	13,020
Lead							53
Lithium	3	4	3	4	4	3	-
Magnesium	24,000	23,000	24,000	28,000	29,000	25,141	10,010
Manganese	250	250	280	1,300	2,100	665	80
Mercury							0.2
Molybdenum	10	10	11	45	61	23	31
Nickel	14	13	17	210	280	82	2,203
Nitrogen, Ammonia				2,800	4,500		-
Nitrogen, Nitrate (N)	2,000	2,000	2,200	2,600	1,500	2,157	237
Nitrogen, Nitrite (N)							80
Potassium	8,100	7,800	8,200	17,000	20,000	11,091	15,333
Selenium							21
Silicon							18,567
Sodium	13,000	13,000	14,000	27,000	32,000	18,212	542,000
Strontium							96
Sulfate	130,000	130,000	140,000	170,000	180,000	147,803	81,667
Total Alkalinity (CaCO3)	100,000	100,000	100,000	140,000	160,000	114,156	900,000
Total Dissolved Solids	330,000	330,000	340,000	430,000	460,000	367,965	1,146,667
Total Suspended Solids							374,333
Zinc							70

1. Drawn from testing of bench scale process water, see Appendix D.

Prepared by: JBM
Checked by: GRE

Table 4

Expected Concentrations of Chemical Constituents in HTDF Outlet
After 1, 3, 7, 10 and 14 Years of Operation, with Complete Mixing

Analytes	HTDF Concentration at End of Year (ug/L)					Preliminary Effluent Limit (ug/L)
	1	3	7	10	14	
Aluminum	20.2	59.9	135.4	106.8	77.9	NA
Antimony	16.4	14.8	11.9	9.4	6.8	130
Arsenic	0.3	0.9	2.1	1.6	1.2	150
Barium	8.6	8.7	8.8	7.0	5.1	1012
Bicarbonate (CaCO ₃)	109,501	99,728	81,156	64,040	46,700	NA
Boron	96.7	87.5	70.0	55.2	40.3	1900
Cadmium	0.03	0.09	0.19	0.15	0.11	8.4
Calcium	49,053	51,297	55,560	43,842	31,971	NA
Carbonate (CaCO ₃)	25,104	74,374	167,995	132,564	96,670	NA
Chloride	16,282	17,805	20,700	16,334	11,912	NA
Chromium	0.5	1.6	3.6	2.9	2.1	212
Cobalt	9.7	12.9	19.0	15.0	10.9	100
Copper	83.5	243.1	546.3	431.1	314.4	26
Fluoride	3.5	10.5	23.7	18.7	13.6	NA
Iron	715	1437	2809	2217	1617	NA
Lead	1.6	4.6	10.5	8.3	6.0	108
Lithium	3.3	3.0	2.4	1.9	1.4	96
Magnesium	24,306	22,596	19,347	15,266	11,133	NA
Manganese	646	590	482	380	277	3857
Mercury	0.01	0.02	0.04	0.03	0.02	0.0013
Molybdenum	22.8	22.5	22.0	17.4	12.7	3200
Nickel	144	264	492	388	283	111
Nitrogen, Nitrate (N)	2,056	1,874	1,529	1,207	880	NA
Nitrogen, Nitrite (N)	2.4	7.0	15.8	12.5	9.1	NA
Potassium	11,090	10,964	10,723	8,462	6,170	NA
Selenium	0.6	1.9	4.2	3.3	2.4	5
Silicon	548	1,623	3,665	2,892	2,109	NA
Sodium	33,438	63,154	119,619	94,391	68,833	NA
Strontium	2.8	8.4	18.9	14.9	10.9	8300
Sulfate	143,466	134,744	118,171	93,248	68,000	NA
Total Alkalinity (CaCO ₃)	135,726	177,423	256,653	202,523	147,687	NA
Total Dissolved Solids	385,241	418,121	480,597	379,236	276,552	NA
Total Suspended Solids	11,043	32,715	73,897	58,311	42,523	NA
Zinc	2.1	6.2	13.9	11.0	8.0	484

Prepared by: JBM
Checked by: GRE

Notes:

1. PEL calculations are provided in Appendix E

Table 5

Expected Concentrations of Chemical Constituents in HTDF Outlet
After 1, 3, 7, 10 and 14 Years of Operation, with Multi-Compartment
Model

Analytes	Background Concentration (ug/L)	Expected Concentration in HTDF Outlet and Wastewater Treatment Influent at End of Year (ug/L)					Preliminary Effluent Limit (ug/L)
		1	3	7	10	14	
Aluminum	<0.1	<0.1	0.2	0.2	<0.1	<0.1	NA
Ammonia (as N)	<10	<10	<100	<350	<320	<320	NA
Antimony	<0.1	7.7	8.5	10.4	10.0	9.9	130
Arsenic	<0.1	<0.1	<0.1	<0.1	<0.1	<0.1	150
Barium	8	8.0	8.1	8.4	8.5	8.6	1012
Boron	80	83	84	87	86	85	1900
Cadmium	<0.1	<0.1	<0.1	<0.1	<0.1	<0.1	8.4
Calcium	47,000	46,700	47,200	48,900	49,700	50,700	NA
Chloride	12,000	12,000	12,400	13,900	14,100	14,600	NA
Chromium	<0.1	<0.1	<0.1	<0.1	<0.1	<0.1	212
Cobalt	3	2.1	1.8	1.2	1.0	0.7	100
Copper	2.0	1.2	1.5	1.7	0.8	0.5	26
Fluoride	<0.1	<0.1	0.1	1.8	2.8	4.0	NA
Iron	450	390	500	410	290	270	NA
Lead	<0.1	<0.1	<0.1	<0.1	<0.1	<0.1	108
Lithium	3.5	3.5	3.5	3.5	3.5	3.5	96
Magnesium	24,000	23,600	24,000	24,400	24,500	24,500	NA
Manganese	250	155	139	92	79	58	3857
Mercury	0.0005	0.0003	0.0003	0.0002	0.0002	0.0001	0.0013
Molybdenum	10	6.2	5.4	3.6	3.2	2.3	3200
Nickel	5.0	6.6	6.5	5.6	1.8	1.1	111
Nitrogen, Nitrate (N)	2000	2000	2200	2400	2400	2400	NA
Potassium	8100	8020	8390	9310	9320	9460	NA
Selenium	<0.1	<0.1	<0.1	0.3	0.48	0.70	5
Sodium	13,000	13,100	14,100	23,100	27,000	32,500	NA
Strontium	<0.1	<0.1	<0.1	<0.1	<0.1	<0.1	8300
Sulfate	130,000	131,000	134,000	137,000	137,000	137,000	NA
Total Alkalinity (CaCO ₃)	100	100	101	117	124	131	NA
Total Dissolved Solids	200	294	278	288	281	282	NA
Zinc	<0.1	<0.1	<0.1	<0.1	<0.1	<0.1	484

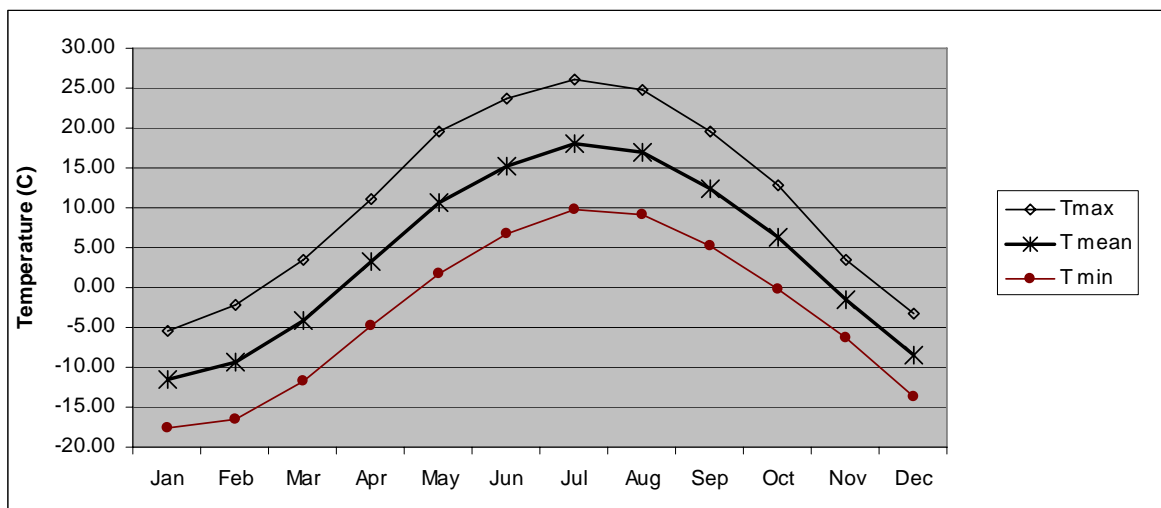
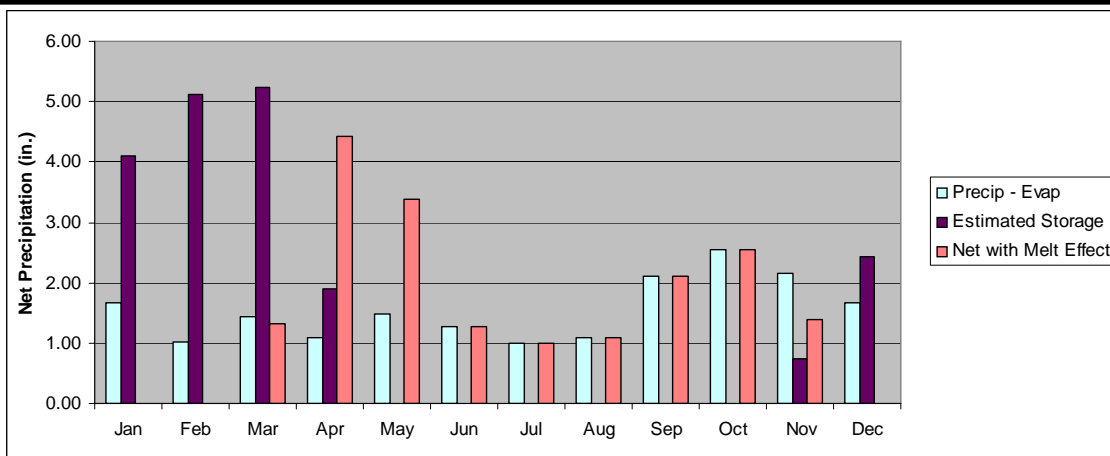
Prepared by: GRE

Checked by: JBM

Notes:

1. PEL calculations are provided in Appendix E

Figures



Month	Precip. (in.)	Evap. (in.)	Precip-Evap (in.)	Percent Storage	Storage (in.)	Net (in.) (mm)	
Jan	1.82	0.15	1.67	100%	4.09	0	0
Feb	1.32	0.30	1.02	100%	5.12	0	0
Mar	2.32	0.89	1.43	80%	5.24	1.31	33.3
Apr	2.42	1.33	1.09	30%	1.90	4.43	112.6
May	3.10	1.63	1.47	0%	0.00	3.37	85.7
Jun	3.35	2.07	1.28	0%	0	1.28	32.5
Jul	3.80	2.81	0.99	0%	0	0.99	25.2
Aug	3.74	2.66	1.08	---	0	1.08	27.4
Sep	3.88	1.77	2.11	0%	0	2.11	53.5
Oct	3.29	0.74	2.55	0%	0	2.55	64.8
Nov	2.44	0.30	2.14	35%	0.75	1.39	35.4
Dec	1.82	0.15	1.67	100%	2.42	0	0
Annual	33.3	14.78	18.52			18.52	470.3


Simulated net precipitation from 1971-2000 NCDC monthly normal precipitation at Champion - Van Riper Park, Michigan and NRCS monthly normal evaporation data from Marquette Co., Michigan. Ice and snowpack storage is estimated based on temperatures and typical seasonal snowpack. Sublimation ignored.

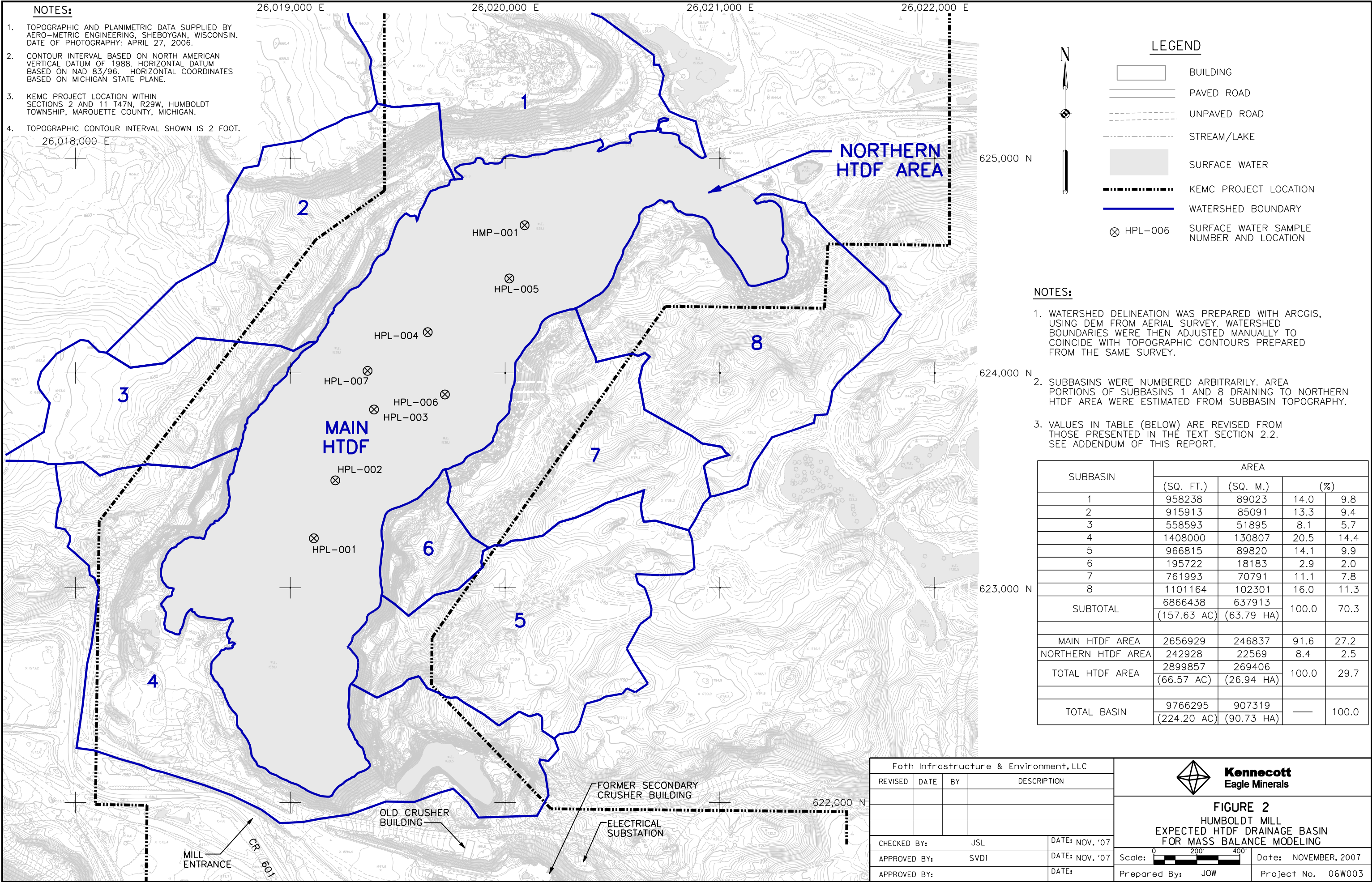
Net water in any month (W) is found by :

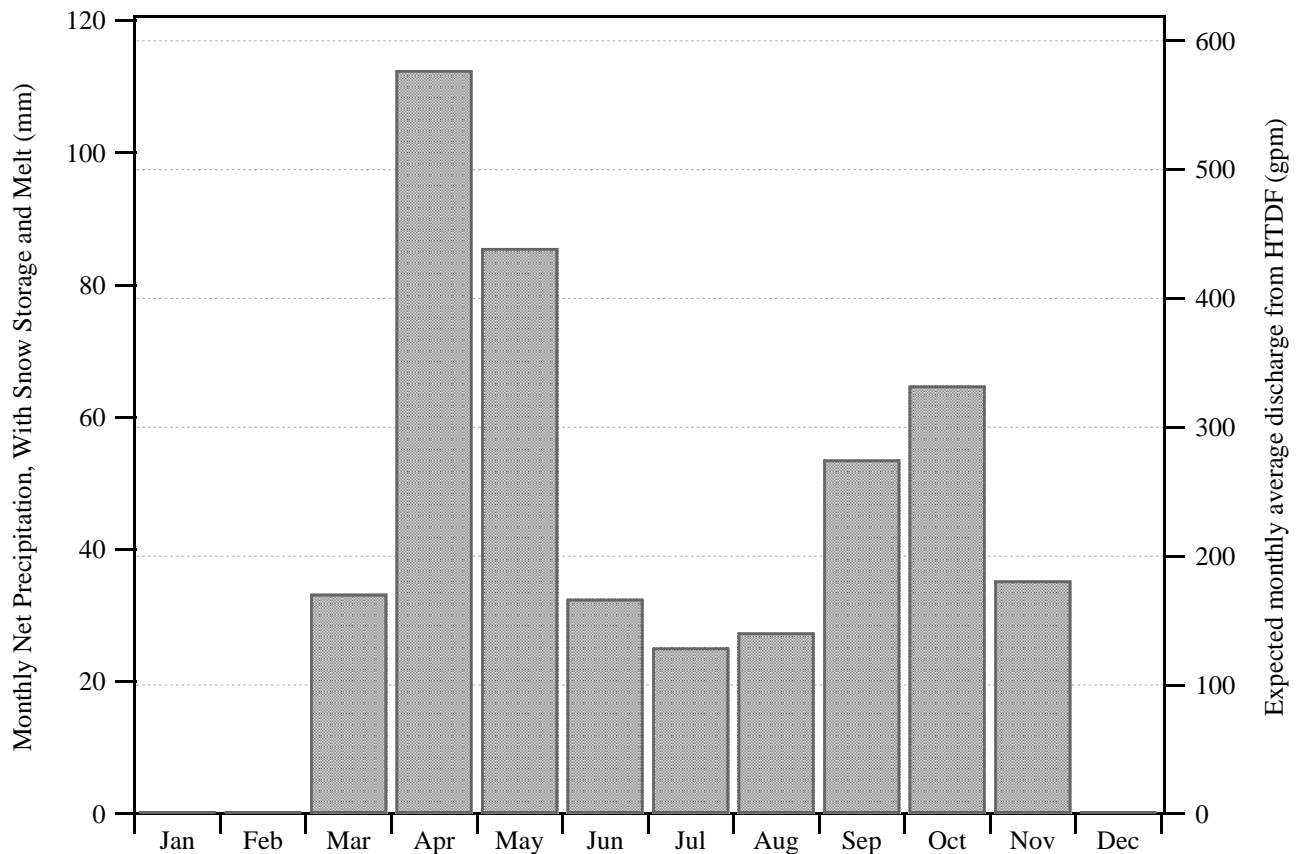
$$W_i = (1 - F_i) \times (P_i - E_i + S_{i-1})$$

where F is the percent storage by snow or ice,
P is the precipitation, E is the evaporation, and S_{i-1} is the storage from the prior month.



Foth Infrastructure & Environment, LLC				 Kennecott Eagle Minerals	
REVISED		BY	DESCRIPTION		
				FIGURE 1 NORMAL MONTHLY CLIMATE FOR HTDF	
CHECKED BY: JBM			DATE: OCT '07	Scale: NA Prepared by: GRE Project No: 06W003	
APPROVED BY: JBM			DATE: OCT '07		
APPROVED BY:			DATE:		





Month	Precip. (in.)	Evap. (in.)	Precip-Evap (in.)	Percent Storage	Storage (in.)	Net (in.) (mm)	
Jan	1.82	0.15	1.67	100%	4.09	0	0
Feb	1.32	0.30	1.02	100%	5.12	0	0
Mar	2.32	0.89	1.43	80%	5.24	1.31	33.3
Apr	2.42	1.33	1.09	30%	1.90	4.43	112.6
May	3.10	1.63	1.47	0%	0.00	3.37	85.7
Jun	3.35	2.07	1.28	0%	0	1.28	32.5
Jul	3.80	2.81	0.99	0%	0	0.99	25.2
Aug	3.74	2.66	1.08	---	0	1.08	27.4
Sep	3.88	1.77	2.11	0%	0	2.11	53.5
Oct	3.29	0.74	2.55	0%	0	2.55	64.8
Nov	2.44	0.30	2.14	35%	0.75	1.39	35.4
Dec	1.82	0.15	1.67	100%	2.42	0	0
Annual	33.3	14.78	18.52			18.52	470.3

Simulated net precipitation from 1971-2000 NCDC monthly normal precipitation at Champion - Van Riper Park, Michigan and NRCS monthly normal evaporation data from Marquette Co., Michigan. Ice and snowpack storage is estimated based on temperatures and typical seasonal snowpack.

Basin flow rate calculated from net precipitation, basin area of 857,628 m², average of 30.67 days per month for 9 month period, and units conversion (5.451 m³/d = 1 gpm). Flow dampening due to lake elevation changes ignored.


Outflow estimate shown in plot (above) does not consider the expected average annual groundwater inflow of 43 gpm.

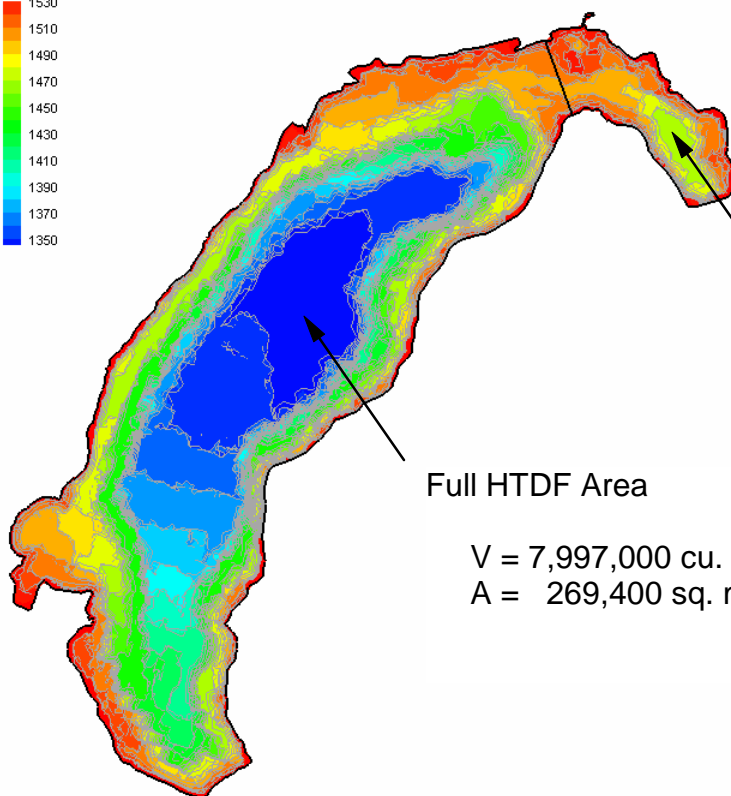
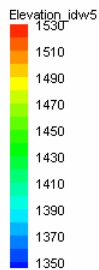
Net water in any month (W) is found by :

$$W_i = (1-F_i) \times (P_i - E_i + S_{i-1})$$

where F is the percent storage by snow or ice, P is the precipitation, E is the evaporation, and S_{i-1} is the storage from the prior month.



Foth Infrastructure & Environment, LLC				 Kennecott Eagle Minerals	
REVISED		BY	DESCRIPTION	FIGURE 3 NET PRECIPITATION AND HTDF BASIN DISCHARGE - EXISTING CONDITIONS	
CHECKED BY: JBM			DATE: OCT '07	Scale: NA	Date: OCTOBER 2007
APPROVED BY: JBM			DATE: OCT '07	Prepared by: GRE	Project No: 06W003
APPROVED BY:			DATE:		

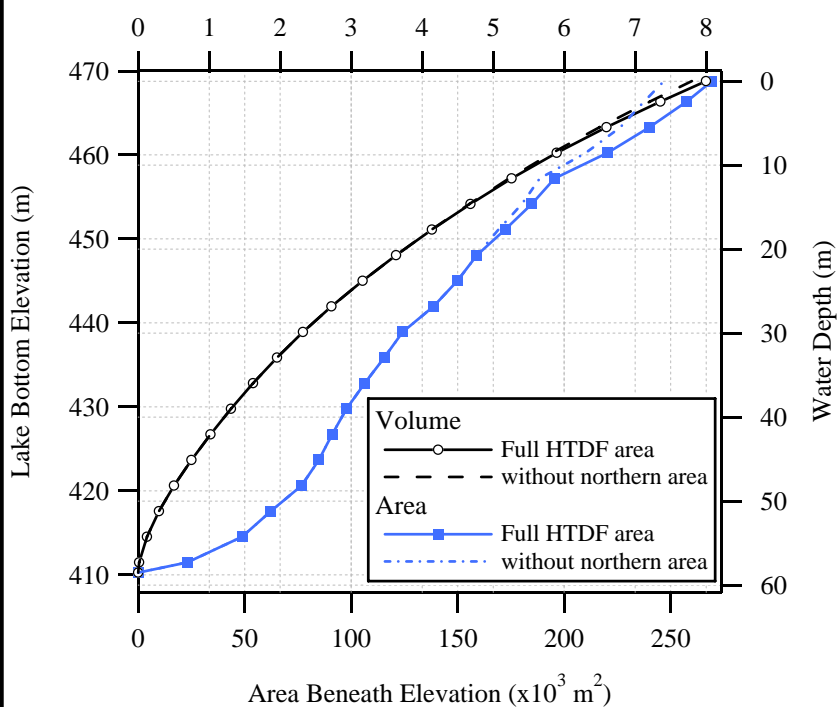


Northern HTDF Area Only

V = 200,000 cu. m
A = 22,600 sq. m

Full HTDF Area

V = 7,997,000 cu. m
A = 269,400 sq. m



Water Depth		Elevation		Full HTDF Area		Without Northern Area	
				Bed Area	Volume	Bed Area	Volume
(ft)	(m)	(ft)	(m)	(m ²)	(m ³)	(m ²)	(m ³)
0	0	1538	468.78	269400	7997216	246831	7797434
8	2.44	1530	466.34	257504	7354816	237529	7206804
18	5.49	1520	463.30	240089	6596485	226432	6499727
28	8.53	1510	460.25	220408	5894689	210189	5834317
38	11.58	1500	457.20	195514	5260824	188546	5226646
48	14.63	1490	454.15	184789	4681243	180144	4664763
58	17.68	1480	451.10	172269	4137087	169185	4132386
68	20.73	1470	448.06	159005	3632225	159005	3632225
78	23.77	1460	445.01	149840	3161544	149840	3161544
88	26.82	1450	441.96	138674	2721849	138674	2721849
98	29.87	1440	438.91	124181	2321258	124181	2321258
108	32.92	1430	435.86	115561	1955892	115561	1955892
118	35.97	1420	432.82	106376	1617661	106376	1617661
128	39.01	1410	429.77	97813	1306477	97813	1306477
138	42.06	1400	426.72	91053	1018646	91053	1018646
148	45.11	1390	423.67	84843	750580	84843	750580
158	48.16	1380	420.62	76693	504399	76693	504399
168	51.21	1370	417.58	62281	292602	62281	292602
178	54.25	1360	414.53	48724	123429	48724	123429
188	57.30	1350	411.48	23047	14050	23047	14050
192	58.52	1346	410.26	0	0	0	0



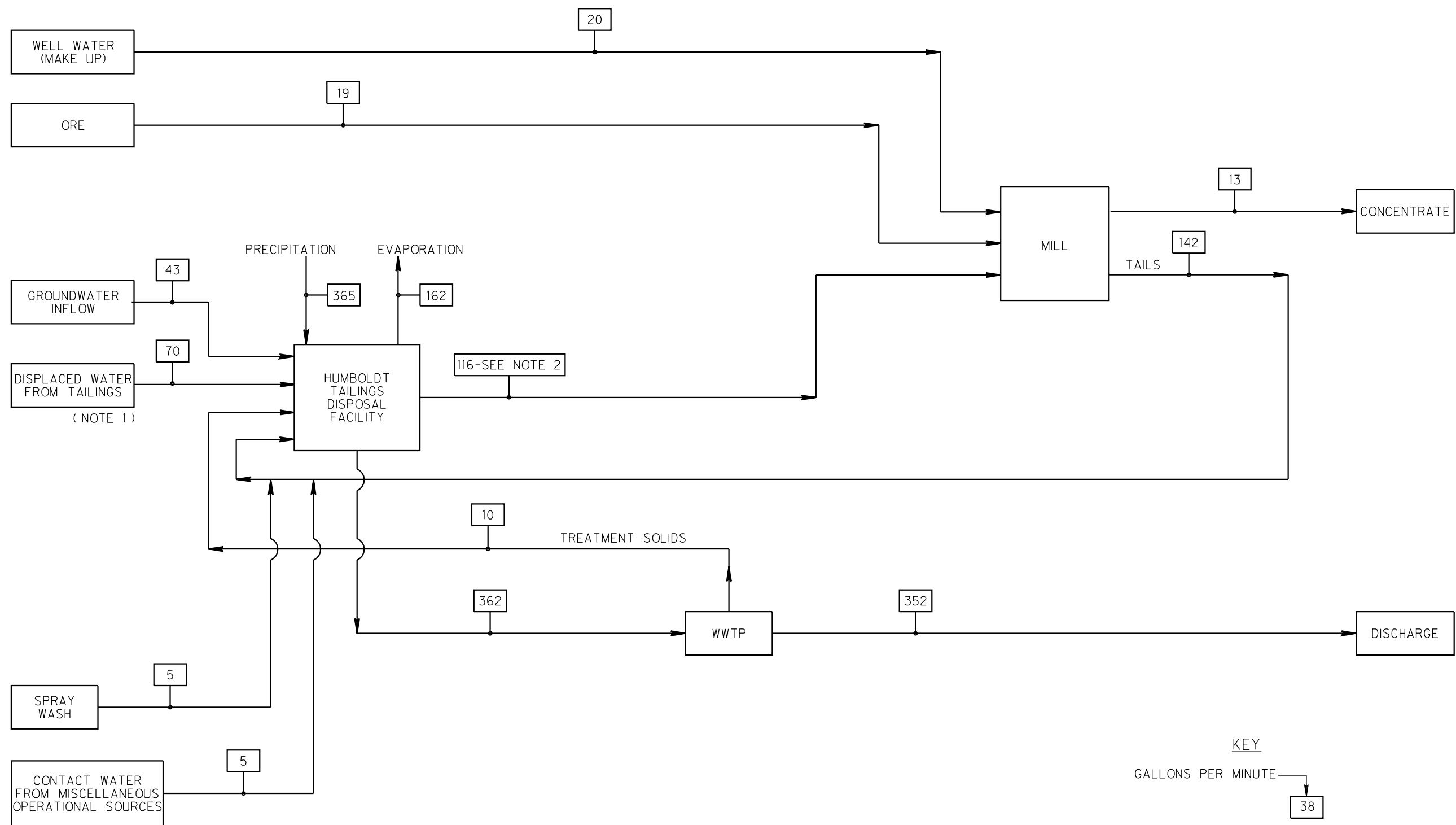
Foth Infrastructure & Environment, LLC			
REVISED		BY	DESCRIPTION
CHECKED BY: JBM		DATE: OCT '07	
APPROVED BY: JBM		DATE: OCT '07	
APPROVED BY:		DATE:	



Kennecott
Eagle Minerals


FIGURE 4
HTDF EXISTING BATHYMETRY AND
VOLUMETRIC RELATIONSHIPS

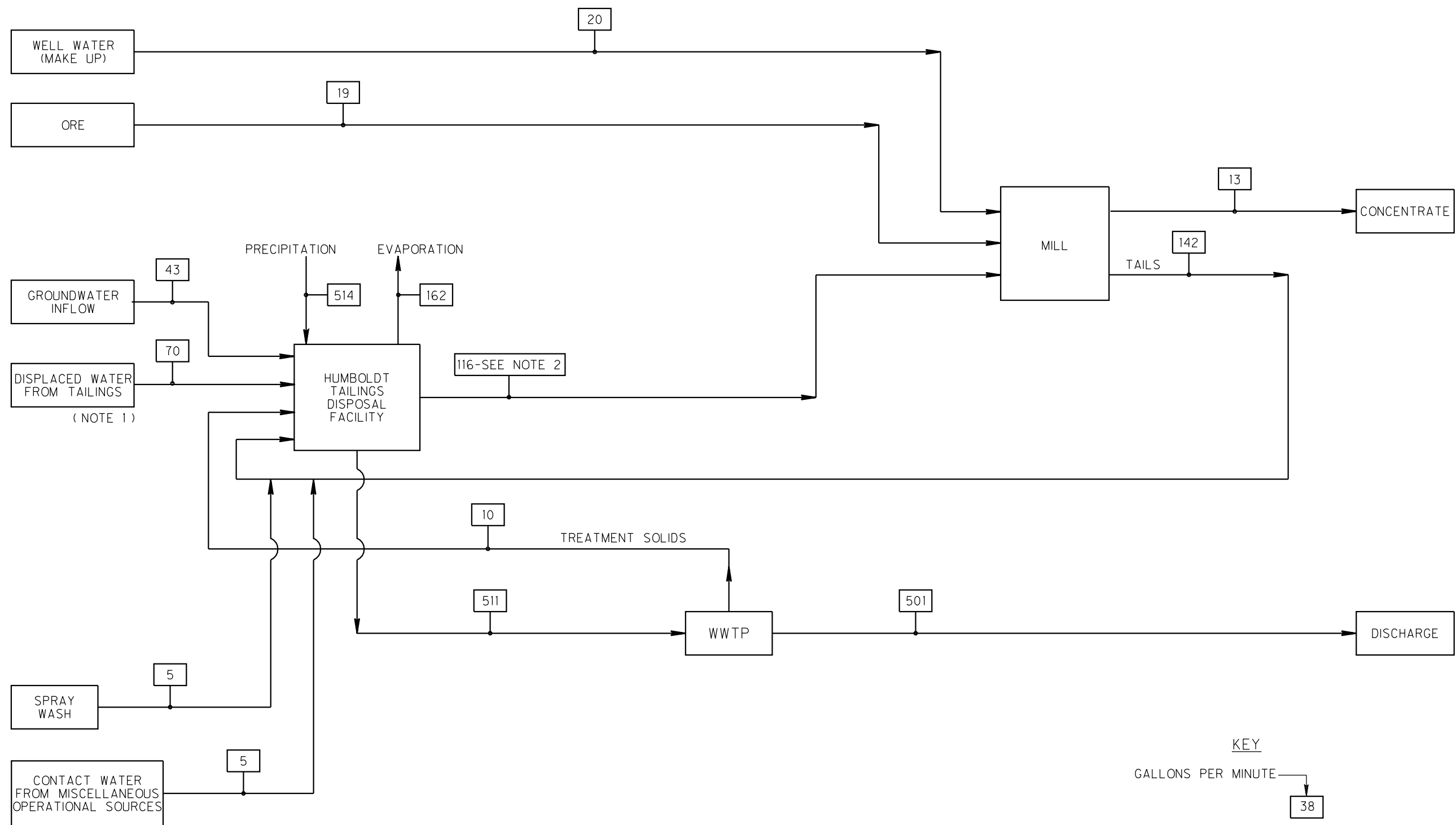
Scale: NA	Date: OCTOBER 2007
Prepared by: GRE	Project No: 06W003



NOTES:


1. THE DISPLACED WATER FROM THE TAILINGS IS THE VOLUME OF TAILINGS SOLIDS WHICH DISPLACES WATER FROM THE TAILINGS DISPOSAL FACILITY.
2. MAY VARY SLIGHTLY BASED ON OPERATIONAL REQUIREMENTS.

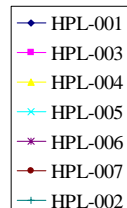
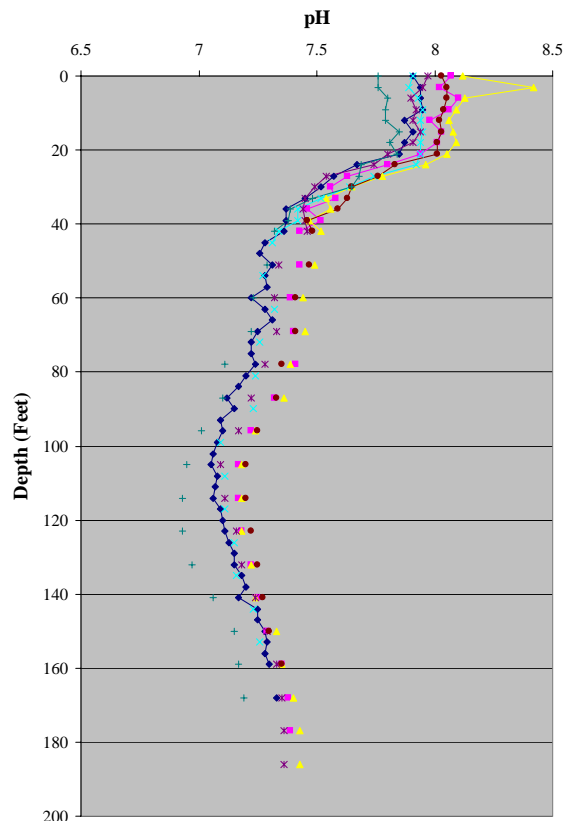
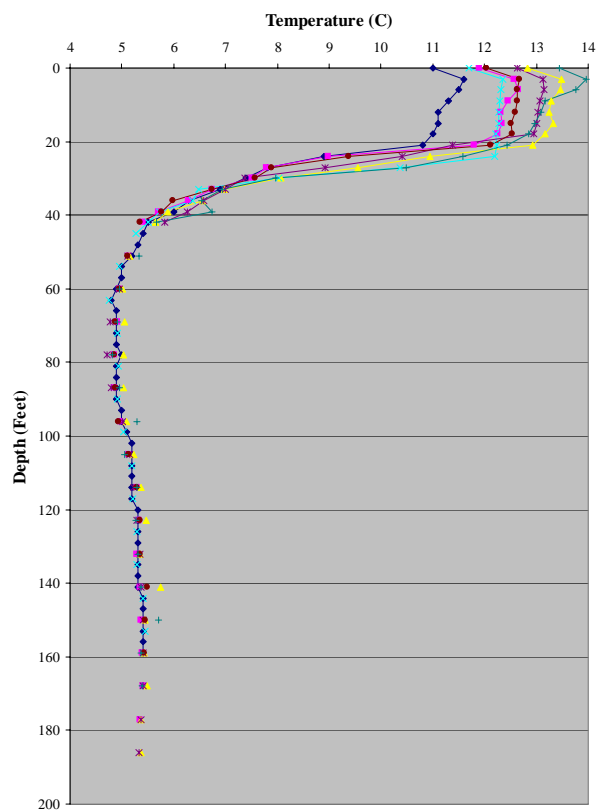
Foth Infrastructure & Environment, LLC				 Kennecott Eagle Minerals	
REVISED	DATE	BY	DESCRIPTION		
				FIGURE 5 WATER BALANCE - HTDF AVERAGE ANNUAL PRECIPITATION HUMBOLDT MILL PROJECT	
CHECKED BY:		JJF1	DATE: NOV. '07	Scale:	NONE
APPROVED BY:		SVD1	DATE: NOV. '07	Date: NOVEMBER, 2007	
APPROVED BY:			DATE:	Prepared By: GJB	Project No. 06W003



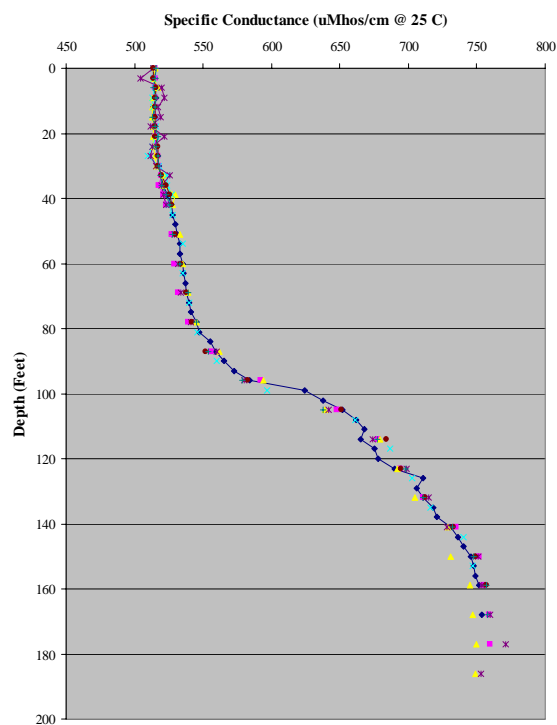
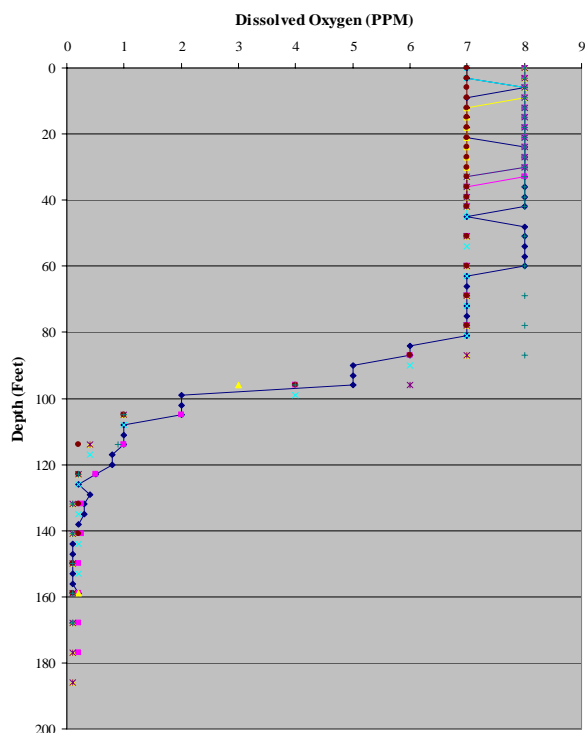
NOTES:


1. THE DISPLACED WATER FROM THE TAILINGS IS THE VOLUME OF TAILINGS SOLIDS WHICH DISPLACES WATER FROM THE TAILINGS DISPOSAL FACILITY.
2. MAY VARY SLIGHTLY BASED ON OPERATIONAL REQUIREMENTS.

Foth Infrastructure & Environment, LLC				 Kennecott Eagle Minerals	
REVISED	DATE	BY	DESCRIPTION		
				FIGURE 6 WATER BALANCE - HTDF MAXIMUM ANNUAL PRECIPITATION HUMBOLDT MILL PROJECT	
CHECKED BY:		JJF1	DATE: NOV. '07	Scale:	NONE
APPROVED BY:		SVD1	DATE: NOV. '07	Date: NOVEMBER, 2007	
APPROVED BY:			DATE:	Prepared By: GJB	Project No. 06W003

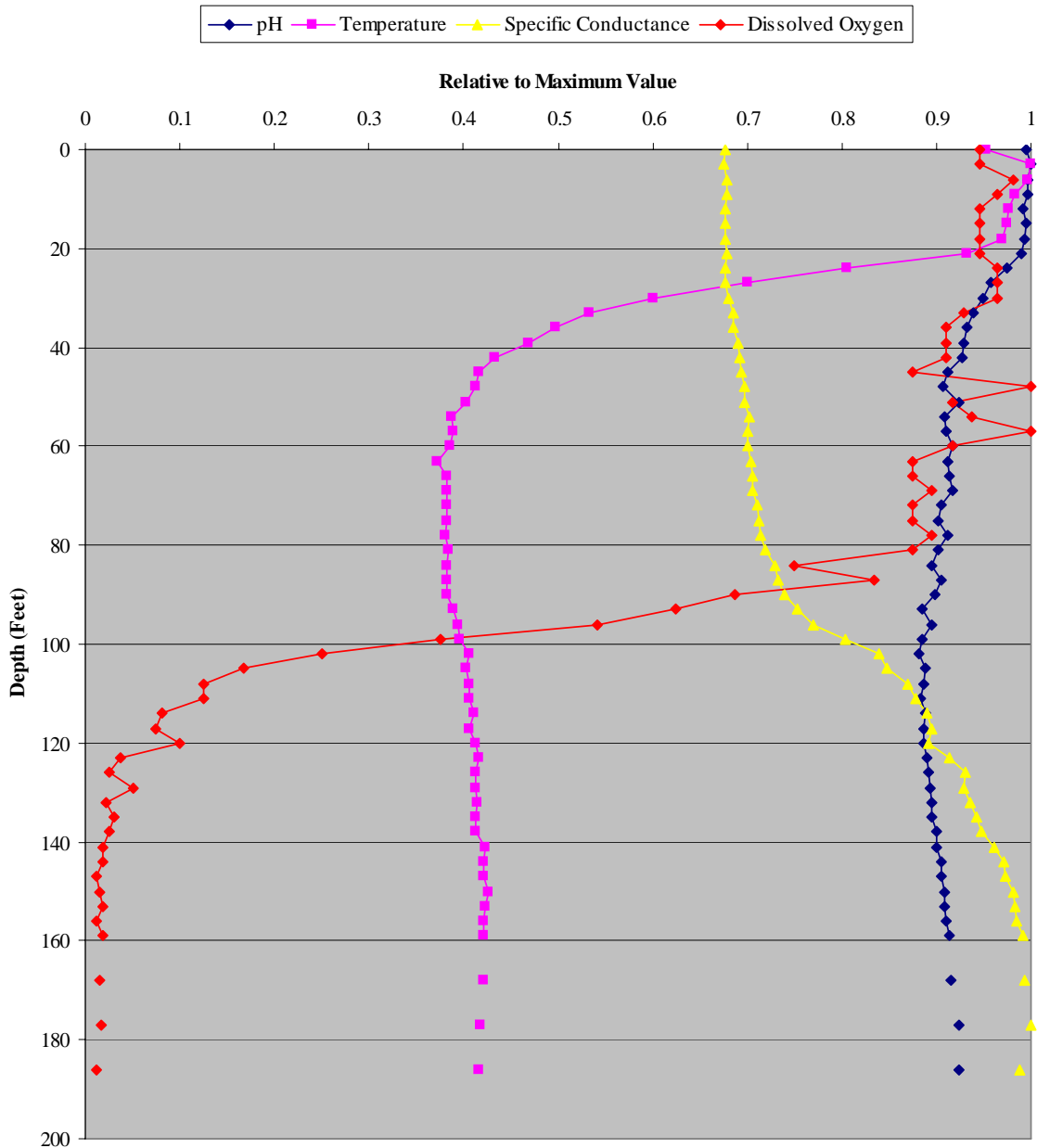


collected
May 25, 2007




Foth Infrastructure & Environment, LLC				 Kennecott Eagle Minerals	
REVISED		BY	DESCRIPTION		
				FIGURE 7 HTDF VERTICAL PROFILE - SELECTED FIELD PARAMETERS	
CHECKED BY: GRE			DATE: OCT '07	Scale: NA	Date: OCTOBER 2007
APPROVED BY: GRE			DATE: OCT '07	Prepared by: JBM	Project No: 06W003
APPROVED BY:			DATE:		

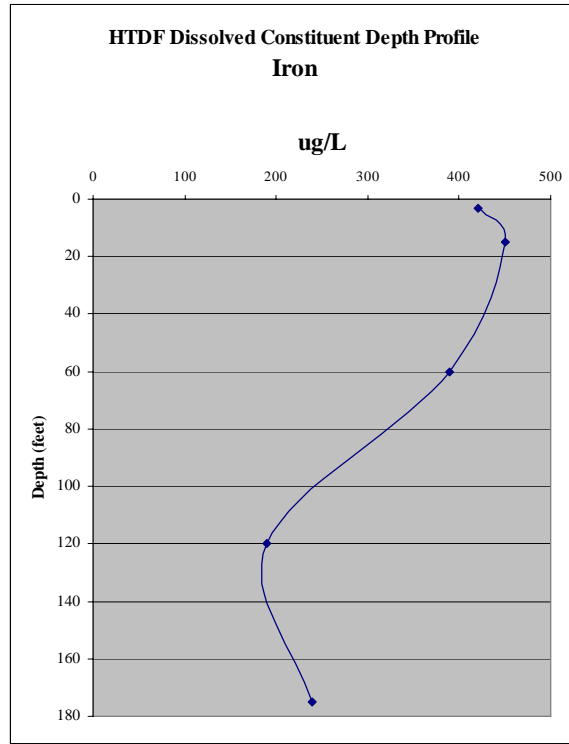
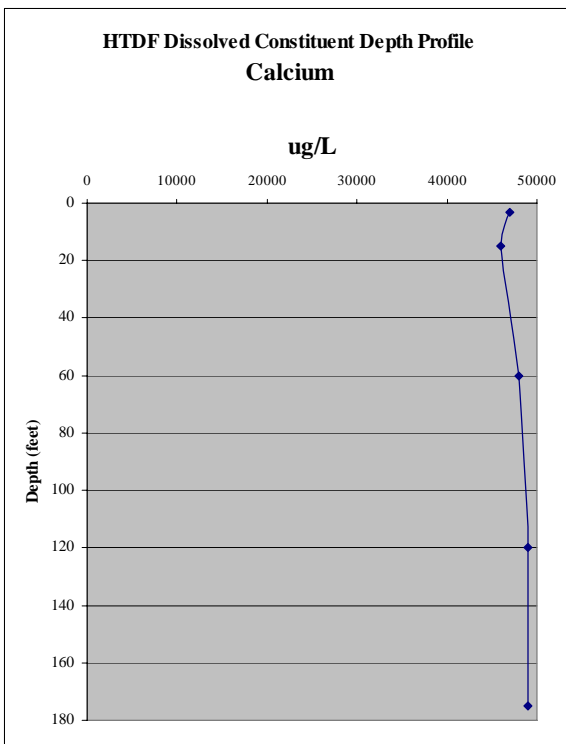
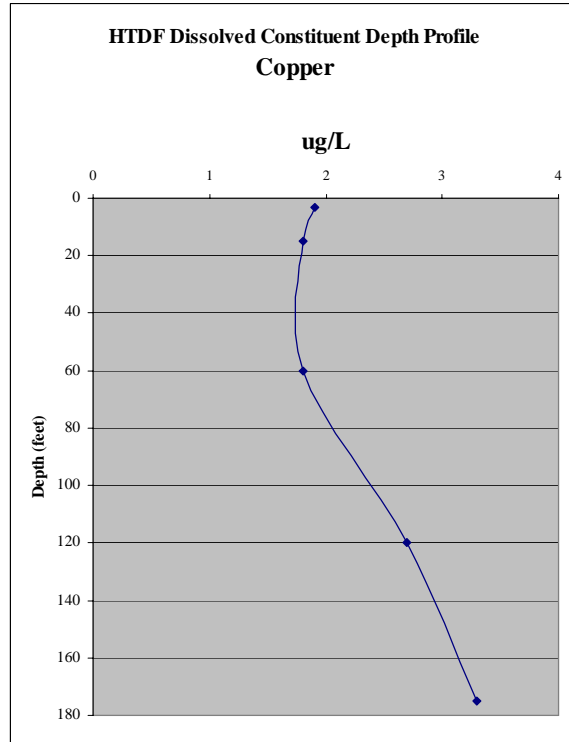
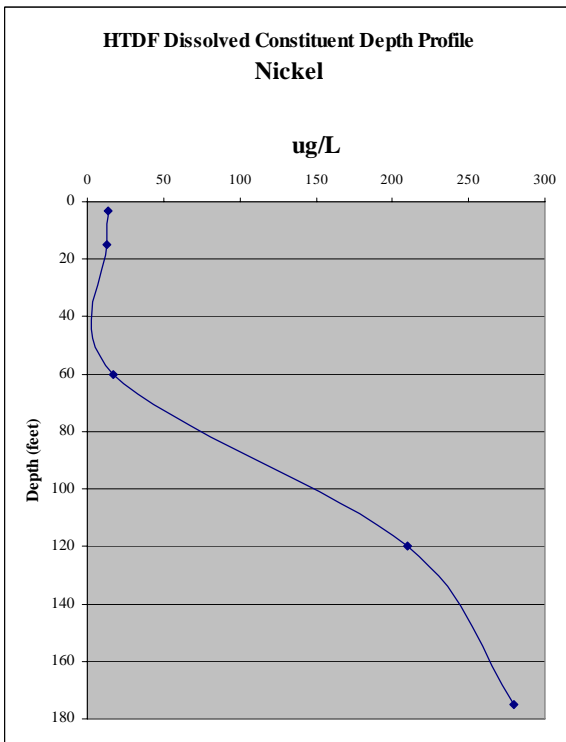
HTDF Field Parameters May 25 2007 **Average of Values from Seven Stations**



Four HTDF field parameters at many water depths. Average at each depth from seven horizontal locations. Parameters are plotted relative to the maximum value for each parameter.



Foth Infrastructure & Environment, LLC				 Kennecott Eagle Minerals	
REVISED		BY	DESCRIPTION	FIGURE 8 HTDF VERTICAL PROFILE - THERMOCLINE AND CHEMOCLINE	
CHECKED BY: GRE		DATE: OCT '07		Scale: NA	Date: OCTOBER 2007
APPROVED BY: GRE		DATE: OCT '07		Prepared by: JBM	Project No: 06W003
APPROVED BY:		DATE:			



Samples collected May 25, 2007




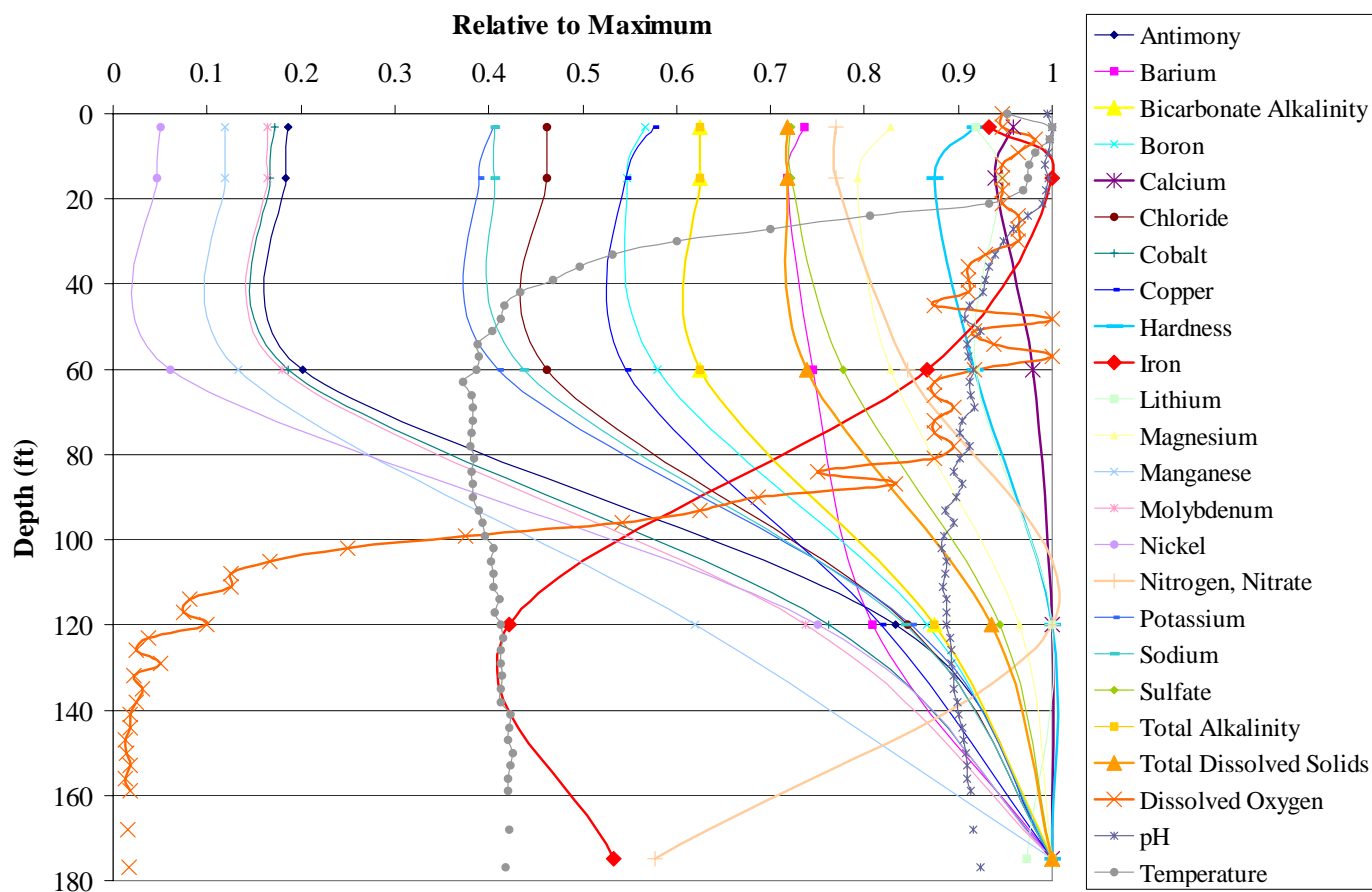
Foth Infrastructure & Environment, LLC				 Kennecott Eagle Minerals	
REVISED		BY	DESCRIPTION		
CHECKED BY: GRE			DATE: OCT '07		
APPROVED BY: GRE			DATE: OCT '07		
APPROVED BY:			DATE:		
				Scale: NA	Date: OCTOBER 2007
				Prepared by: JBM	Project No: 06W003

FIGURE 9
HTDF VERTICAL PROFILE -
SELECTED CHEMICAL CONSTITUENTS

HTDF Chemical Depth Profiles



Depth profiles for twenty-one chemical constituents and three field parameters measured in the HTDF. Parameters are plotted relative to the maximum value for each parameter. Samples collected May 25, 2007.



Foth Infrastructure & Environment, LLC			
REVISED		BY	DESCRIPTION
CHECKED BY: GRE		DATE: OCT '07	
APPROVED BY: GRE		DATE: OCT '07	
APPROVED BY:		DATE:	

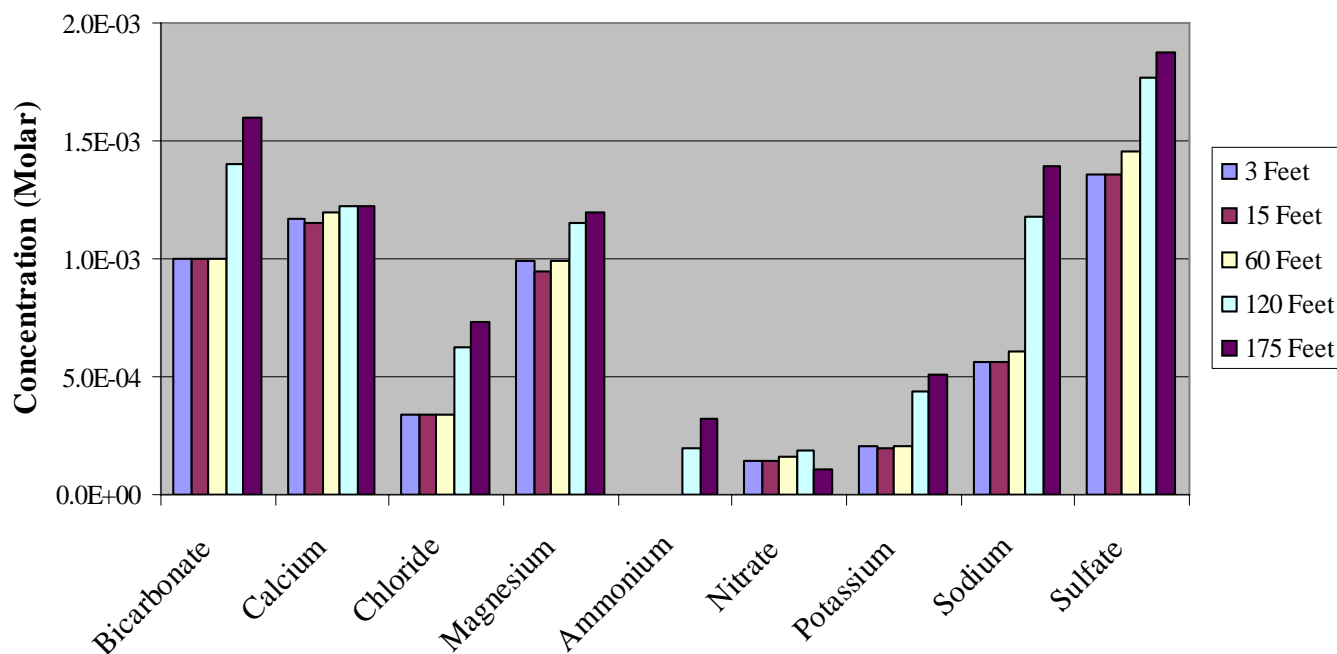


Kennecott
Eagle Minerals

FIGURE 10
HTDF VERTICAL PROFILE -
MULTIPLE CHEMICAL CONSTITUENTS

Scale: NA	Date: OCTOBER 2007
Prepared by: JBM	Project No: 06W003

HTDF Major Chemical Species At Five Depths - May, 2007



HTDF Intensity Parameters, Dissolved Oxygen And Water Temperature Compartment Average July, 2007 (Molar Concentrations)

Compartment	Volume Fraction	pH	p _e (25°C)	Ionic Strength	Dissolved Oxygen	Temperature (°C)
1	0.081	8.30	7.05	8.25x10 ⁻³	2.7x10 ⁻⁴	21.1
2	0.157	8.05	6.40	8.11x10 ⁻³	3.0x10 ⁻⁴	17.3
3	0.457	7.44	6.60	8.54x10 ⁻³	2.7x10 ⁻⁴	5.8
4	0.191	7.28	6.40	1.04x10 ⁻²	1.2x10 ⁻⁵	5.5
5	0.114	7.48	6.03	1.11x10 ⁻²	2.9x10 ⁻⁶	5.6
HTDF ¹	1	7.58	6.88	9.09x10 ⁻³		

HTDF Alkalinity—May, 2007

Compartment	Volume (m ³)	Alkalinity (M)	Total (Tonnes CaCO ₃)
1	646,000	9.97x10 ⁻⁴	64
2	1,256,000	9.98x10 ⁻⁴	125
3	3,657,000	9.99x10 ⁻⁴	365
4	1,524,000	1.40x10 ⁻³	213
5	914,000	1.60x10 ⁻³	146
HTDF ¹	7,997,000	1.14x10 ⁻³	914

¹Values are sums or volume-weighted averages



Foth Infrastructure & Environment, LLC

REVISED	BY	DESCRIPTION
CHECKED BY:	GRE	DATE: OCT '07
APPROVED BY:	GRE	DATE: OCT '07
APPROVED BY:		DATE:

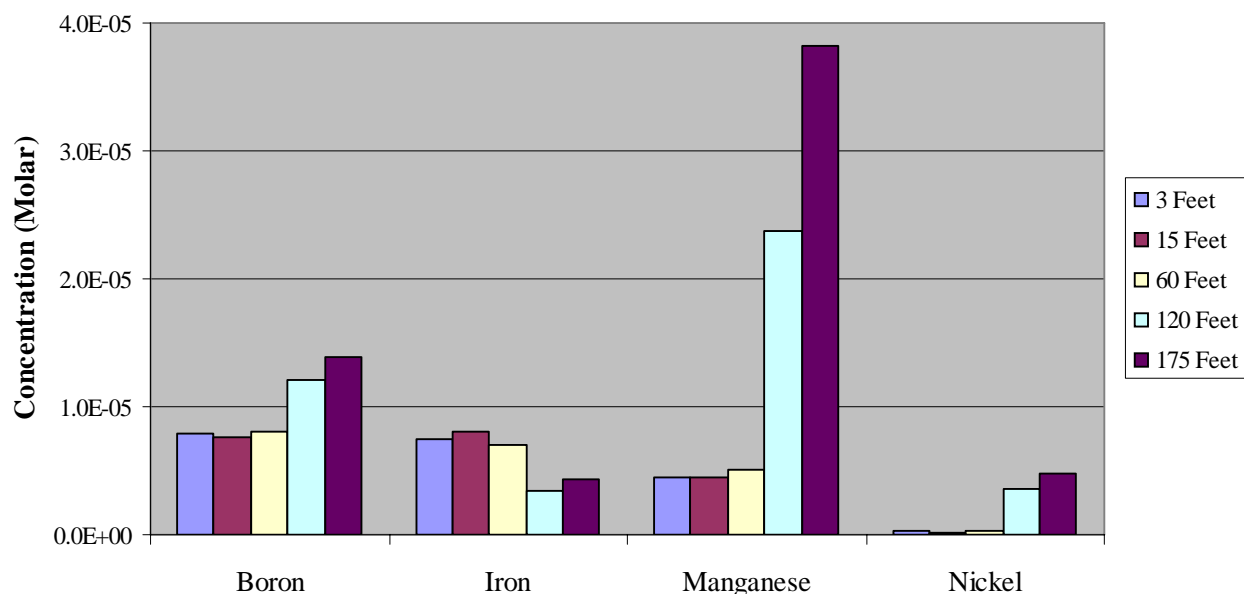


Kennecott
Eagle Minerals

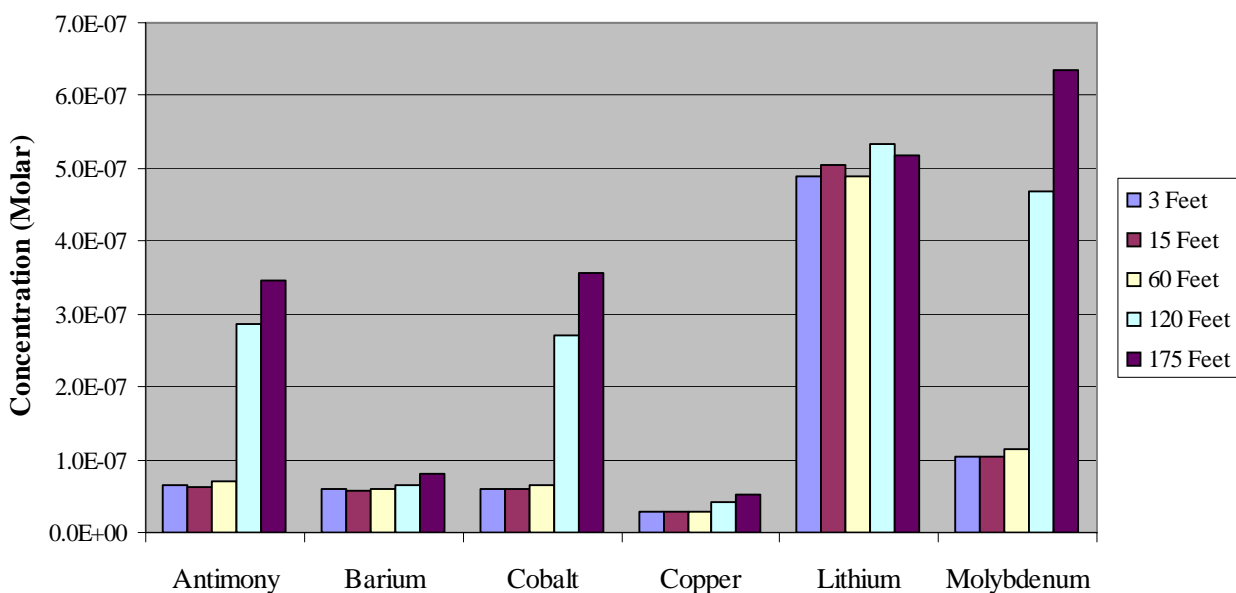
FIGURE 11
HTDF MAJOR ELEMENT CONCENTRATIONS

Scale: NA	Date: SEPTEMBER 2007
Prepared by: JBM	Project No: 06W003

HTDF Minor Chemical Species (I) At Five Depths - May, 2007



HTDF Minor Chemical Species (II) At Five Depths - May, 2007



Foth Infrastructure & Environment, LLC			
REVISED		BY	DESCRIPTION
CHECKED BY: GRE		DATE: OCT '07	
APPROVED BY: GRE		DATE: OCT '07	
APPROVED BY:		DATE:	

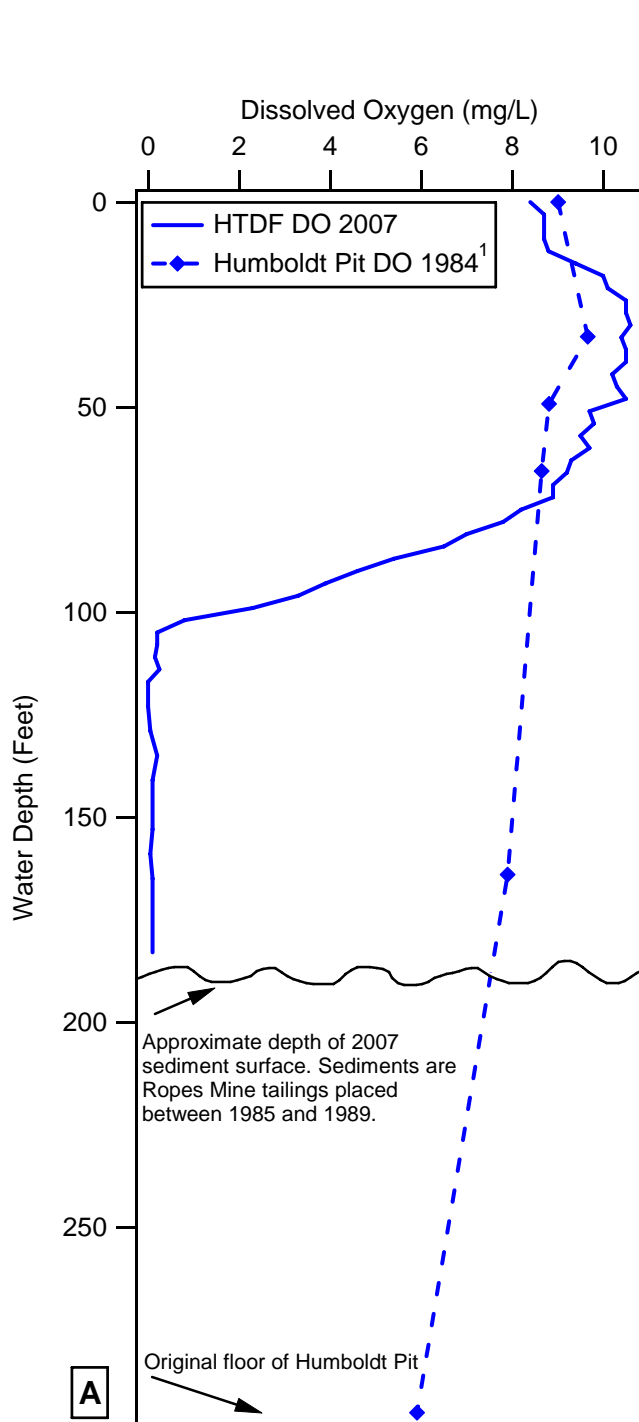


Kennecott
Eagle Minerals

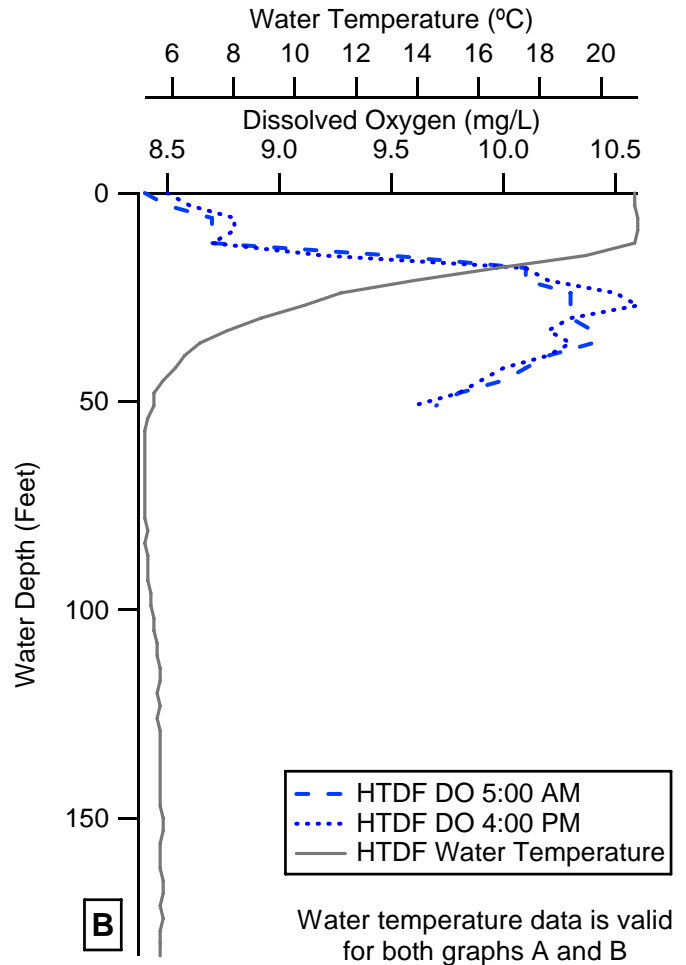
FIGURE 12
HTDF MINOR ELEMENT CONCENTRATIONS

Scale: NA	Date: SEPTEMBER 2007
Prepared by: JBM	Project No: 06W003

Dissolved Oxygen In The HTDF And Humboldt Pit Historical And Diurnal Variation



¹ Traverse Engineering, 1984



A - Concentration of dissolved oxygen in the water column of the HTDF in July, 2007 and Humboldt Pit in 1984. Before tailings from the Ropes Mine were placed in the Pit, dissolved oxygen was present throughout the water column. This indicates that oxygen consumption from substances such as decaying organic matter was limited. After placement of tailings, oxygen is almost completely consumed below 100 feet.

B - Measurements of dissolved oxygen in the HTDF in the early morning and late afternoon of July 12, 2007. The depth profiles are almost identical and indicate that no significant primary production (algal growth) occurred during this time.



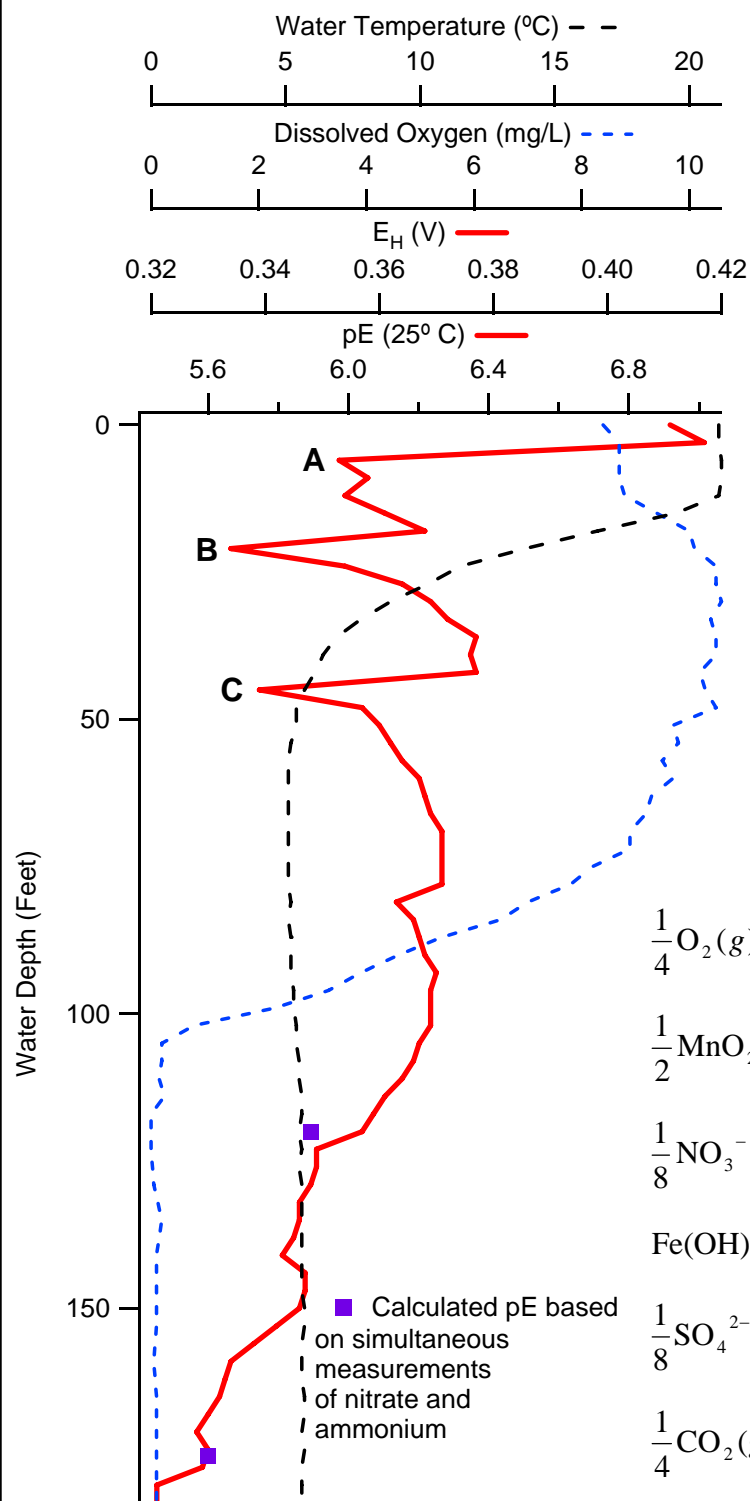
Foth Infrastructure & Environment, LLC			
REVISED		BY	DESCRIPTION
CHECKED BY: GRE		DATE: OCT '07	
APPROVED BY: GRE		DATE: OCT '07	
APPROVED BY:		DATE:	



**Kennecott
Eagle Minerals**

**FIGURE 13
HTDF DISSOLVED OXYGEN**

Scale: NA	Date: OCTOBER 2007
Prepared by: JBM	Project No: 06W003

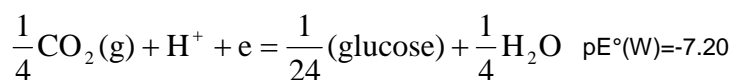
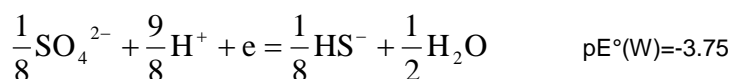
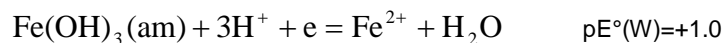
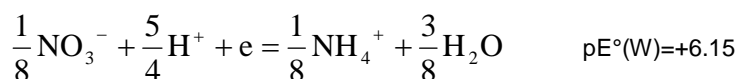
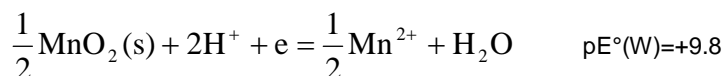



Redox Potential (ORP) In The HTDF

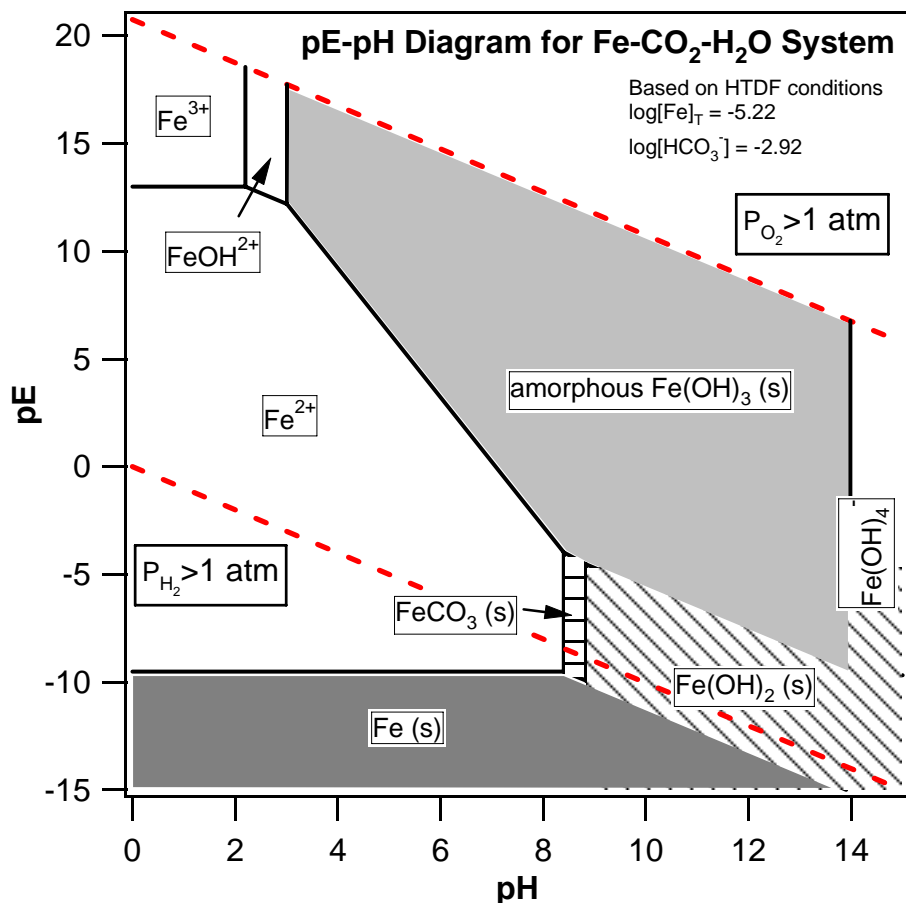
- Redox potential measured in the HTDF (July, 2007).
- Measured with platinum electrode and Ag/AgCl reference electrode, no temperature correction.
- Standard hydrogen electrode (E_H) values calculated from ZoBell calibration.
- pE values calculated from E_H values at 25°C reference temperature.
- Several major (A, B, C) and minor redox boundaries are visible in the profile.
- Calculation of two pE values based on simultaneous measurements of nitrate (NO_3^-) and ammonium (NH_4^+) concentrations are similar to those obtained by direct measurement.

Several common aquatic redox reactions are shown below with their $pE^\circ(W)$ values. These values represent the pE of a solution with equimolar concentrations of reductant and oxidant, and at pH=7. (Fe^{2+} , Mn^{2+} at 10^{-6} M).

Common Aquatic Redox Reactions

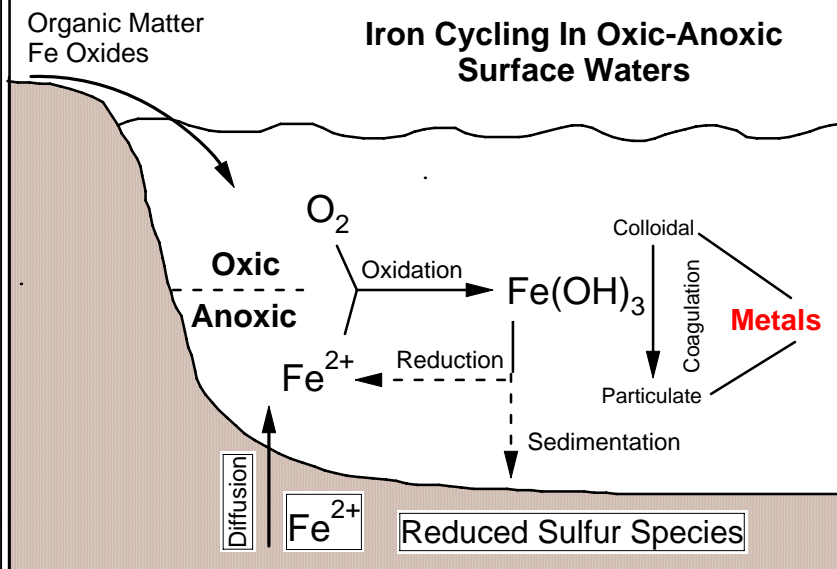


Foth Infrastructure & Environment, LLC				 Kennecott Eagle Minerals	
REVISED		BY	DESCRIPTION		
				FIGURE 14 HTDF REDOX CHEMISTRY	
CHECKED BY: GRE			DATE: OCT '07	Scale: NA	Date: SEPTEMBER 2007
APPROVED BY: GRE			DATE: OCT '07	Prepared by: JBM	Project No: 06W003
APPROVED BY:			DATE:		



Above: The pE-pH diagram for the iron-carbonate-water system shows the thermodynamically-favored chemical species. The system will move towards one species for a given set of pE-pH conditions. However, because of disequilibrium and slow kinetics, several nearby species are often present with the dominant species. Amorphous solid Iron (III) Hydroxide and dissolved Iron (II) are the expected dominant species in the HTDF.

Right: When bottom waters are anoxic, like those in the HTDF, an iron cycle can develop. Dissolved Iron (II) diffuses upward into oxic water and is oxidized to solid Iron (III) hydroxide, forming initially as colloids. As these colloids coagulate, they collect other metals, form particles and settle. Some particles reach the sediment, others are dissolved by reduction and continue the cycle.



Foth Infrastructure & Environment, LLC

REVISED	BY	DESCRIPTION

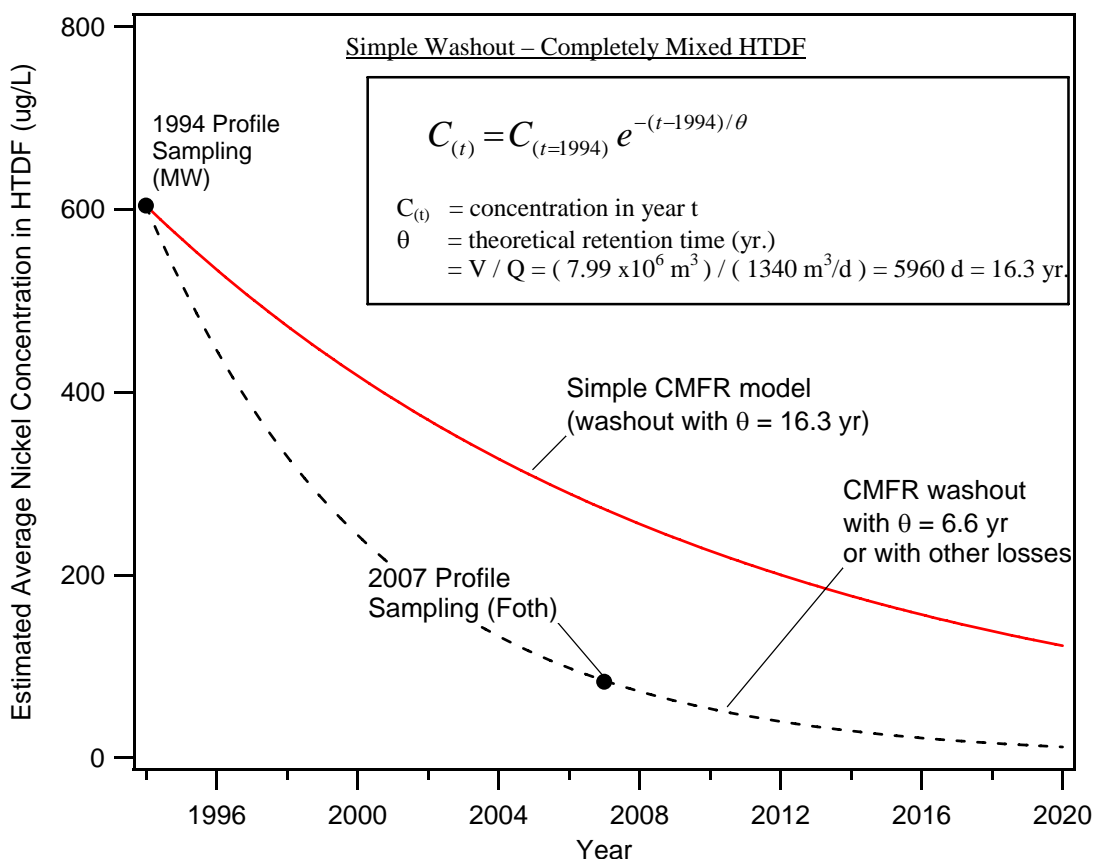


**Kennecott
Eagle Minerals**

**FIGURE 15
AQUATIC IRON CYCLING**

Scale: NA	Date: SEPTEMBER 2007
Prepared by: JBM	Project No: 06W003


			Nickel Concentration and Mass from HTDF Profile Sampling						
			1994		2007		Differences		
HTDF Segmentation			(Montgomery Watson)						
Compartment	Depth Range (ft.)	Volume (x10 ⁶ m ³)	concentration (ug/L)	mass (kg)	concentration (ug/L)	mass (kg)	decrease in concentration (ug/L)	decrease in mass (kg)	Percent decrease (%)
1 + Northern HTDF	0-6	0.64	200	128	14	9	186	119	93
2	6-24	1.26	350	441	13	16	337	425	96
3	24-96	3.66	520	1903	17	62	503	1841	97
4	96-144	1.52	950	1444	210	319	740	1125	78
5	144-192	0.91	1000	910	280	255	720	655	72
Sum		7.99		4826		662		4165	86
Completely Mixed Concentration			604		83		521		

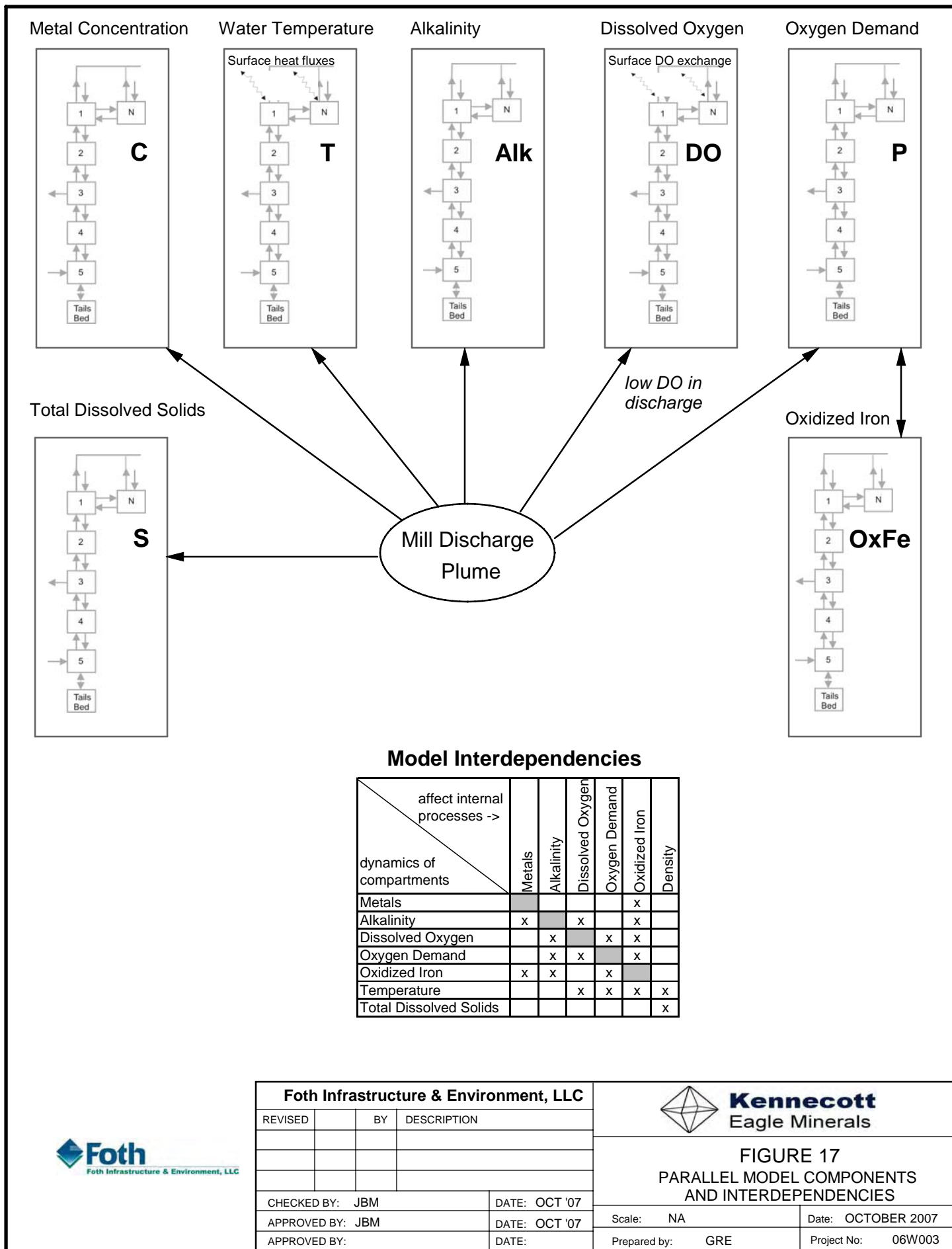


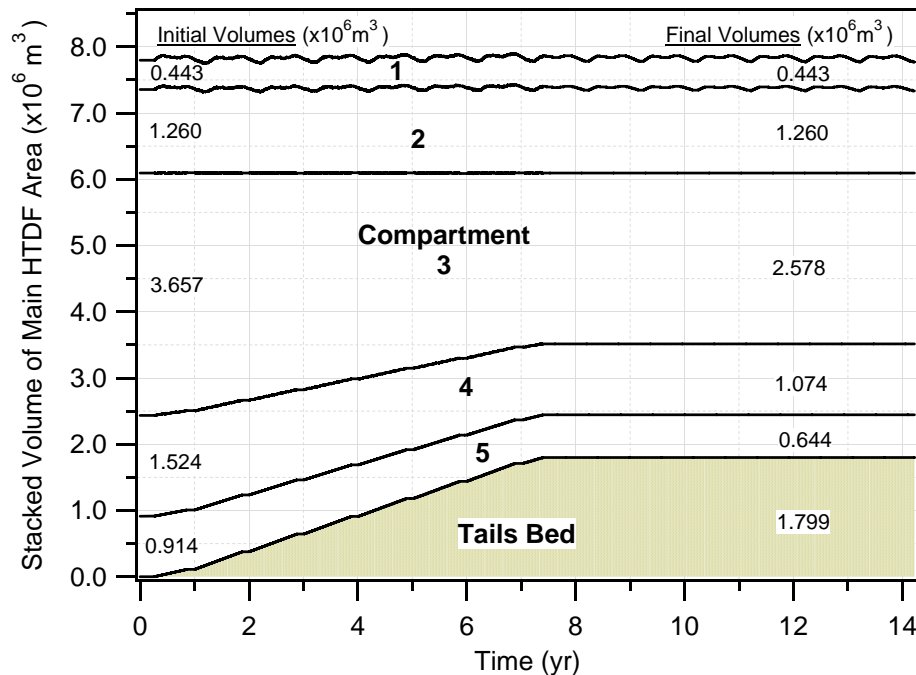
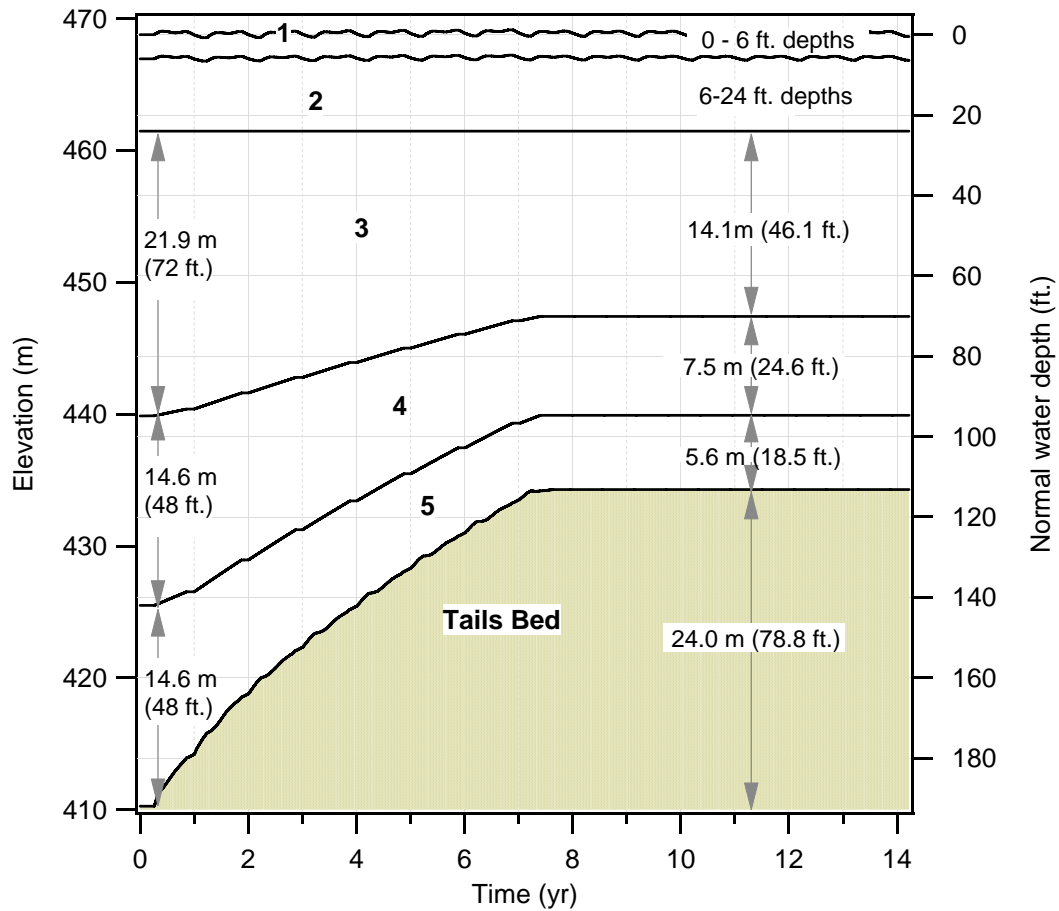
Loss of nickel within system (to sediment) must be active:

- ◆ Complete mix model washout would have to be 2.5 times higher
- ◆ HTDF is stratified, so mass flux due to washout is further constrained by lower surface concentrations
- ◆ Metals are likely scavenged by colloids within HTDF, and settle out to the HTDF bed sediments



Foth Infrastructure & Environment, LLC				 Kennecott Eagle Minerals	
REVISED		BY	DESCRIPTION		
				FIGURE 16 OBSERVED DECREASE IN HTDF NICKEL CONCENTRATIONS	
CHECKED BY: JBM		DATE: OCT '07		Scale: NA	Date: OCTOBER 2007
APPROVED BY: JBM		DATE: OCT '07		Prepared by: GRE	Project No: 06W003
APPROVED BY:		DATE:			





Foth Infrastructure & Environment, LLC			
REVISED		BY	DESCRIPTION
CHECKED BY: JBM		DATE: OCT '07	
APPROVED BY: JBM		DATE: OCT '07	
APPROVED BY:		DATE:	



Kennecott
Eagle Minerals

FIGURE 18
HTDF MODEL COMPARTMENT
DIMENSIONS UPON LOADING

Scale: NA	Date: OCTOBER 2007
Prepared by: GRE	Project No: 06W003

Overall Flow Balance

$$Q_D + Q_{nat} + Q_{gw2} = Q_R + Q_{T,out} + \dot{V}_T \quad (1)$$

$$Q_D = \text{Discharge flow rate, including solids} \quad (2)$$

$$Q_{nat} = \text{Natural, net surface flows} \quad (3)$$

$$Q_{gw2} = \text{Groundwater inflow at southern end} \quad (4)$$

$$Q_R = \text{Return flow rate to mill} \quad (5)$$

$$Q_{T,out} = \text{Total outflow to wastewater treatment plant} \quad (6)$$

$$\dot{V}_T = \text{Total volume rate of change in HTDF from changes in storage and loading of tails} \quad (7)$$

Distribution of discharge to tails bed and main compartments (1-5)

Balance at point of discharge mixing (initiation of discharge plume)

$$Q_D + Q_{5P} = Q_{PTB} + Q_{P5} + Q_{P54} \quad (8)$$

Q_{5P} = Flow from compartment 5 to discharge plume, to provide pore water and brought into discharge plume by hydrodynamic forces.

$$= n \dot{V}_{TB} + (MF_D) Q_D \quad (9)$$

where n = tails bed porosity, \dot{V}_{TB} = volume rate that tails bed increases due to loading, MF_D = mixing factor for discharge

$$Q_{PTB} = \text{Flow from discharge plume to tails bed} \quad (10)$$

$$= n \dot{V}_{TB} + \dot{V}_S \quad (11)$$

where \dot{V}_S = discharge flow rate of solids (without pore volume) = $\dot{M}_{DT} / (G_s \gamma_w)$.

$$Q_{P5} = \text{Flow from discharge plume to compartment 5} \quad (12)$$

= $(1 - MF_{P5}) (Q_D + Q_{5P} - Q_{PTB})$
where MF_{P5} = mixing factor for discharge plume to compartment 5, and MF_{Pi} is a function of fluid densities (and $i = 5$):

$$MF_{Pi} = MF_{min} \quad \text{for } \rho_P \geq \rho_i \quad (13)$$

$$MF_{Pi} = \min \left[1, \frac{\sqrt{\frac{\rho_i - \rho_D}{\rho_i + \rho_D}}}{DF} \right] (MF_{max} - MF_{min}) + MF_{min} \quad (14)$$

where DF = density factor (typically < 0.02) which scales the sensitivity of mixing function to the difference in densities, MF_{max} and MF_{min} are the maximum and minimum portions of the plume flow to bypass compartment i (typically 0.99 to 0.03).

$$Q_{P54} = \text{Flow from discharge plume, bypassing 5 to compartment 4 and above.} \quad (15)$$

$$= (MF_{P5}) (Q_D + Q_{5P} - Q_{PTB})$$

Balance at point of discharge to compartments 4, 3, and 2

Starting with $i = 4$,

$$Q_{P(i+1,i)} = Q_{Pi} + Q_{P(i,i-1)} \quad (16)$$

$$Q_{Pi} = \text{Flow from discharge plume to compartment } i \quad (17)$$

$$= (1 - MF_{Pi}) Q_{P(i+1,i)}$$

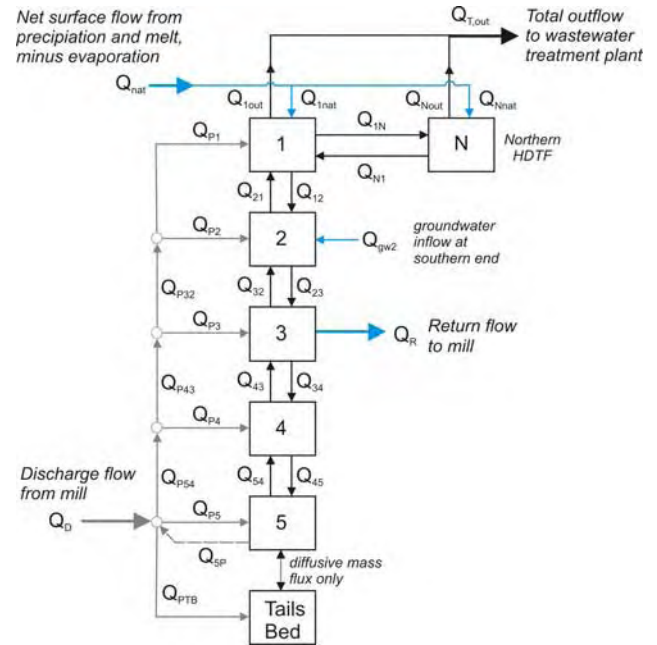
$$Q_{P(i,i-1)} = \text{Flow from discharge plume, bypassing } i \text{ to the compartment } i-1 \text{ and above} \quad (18)$$

$$= (MF_{Pi}) Q_{P(i+1,i)}$$

This set of equations (16-18) are repeated, with $i = 3$ next, then $i = 2$.

Remainder of discharge to compartment 1

$$Q_{P1} = Q_{P21} = Q_{P32} - Q_{P2} \quad (19)$$



Flow Balance

Inter-compartmental Flows (1-5, 1-N)

$$Q_{54} = (Q_{P5} - Q_{5P}) + (Q_{45} - \dot{V}_5) \quad (20)$$

$$Q_{P5} - Q_{5P} = \text{net plume discharge (see Eqns. 9, 12)} \quad (21)$$

$$Q_{45} = \text{mixing flow sensitive to densities} \quad (22)$$

$$= MF_{54} \text{ (see Eqns. 13-14)}$$

$$\dot{V}_5 = \text{volume change in 5} = -VF_5 (\dot{V}_{TB}) \quad (23)$$

$$\text{where } VF_5 = \text{fixed volume fraction (0.15) of lower HTDF volume (= } V_3 + V_4 + V_5 \text{) that decreases with tails loading.}$$

$$Q_{43} = Q_{P4} + Q_{54} + Q_{34} - Q_{45} - \dot{V}_4 \quad (24)$$

$$Q_{34} = MF_{43} Q_{mix} \text{ and } \dot{V}_4 = -VF_4 (\dot{V}_{TB}) = -0.25 (\dot{V}_{TB}) \quad (25)$$

$$Q_{mix} = \text{intercompartmental mixing flow (15,000 m}^3\text{/d)}$$

$$Q_{32} = Q_{P3} + Q_{43} + Q_{23} - Q_R - Q_{34} - \dot{V}_3 \quad (26)$$

$$Q_{34} = MF_{32} Q_{mix} \text{ and } \dot{V}_3 = -VF_3 (\dot{V}_{TB}) = -0.60 (\dot{V}_{TB}) \quad (27)$$

$$Q_{21} = Q_{P2} + Q_{32} + Q_{12} + Q_{gw2} - Q_{23} - \dot{V}_2 \quad (28)$$

$$Q_{12} = \min(MF_{21} Q_{mix}, Q_{wind}) \quad (29)$$

$$Q_{wind} = \text{wind-generated flows during ice-free season (typically 2000 m}^3\text{/d)}$$

$$\dot{V}_2 = -VF_2 (\dot{V}_{US}) = -0.74 (\dot{V}_{US}) \quad (30)$$

$$\dot{V}_{US} = \text{change in upper volume (1+2), from storage} \quad (31)$$

$$Q_{1out} = Q_{P1} + Q_{21} + Q_{1nat} + Q_{N1} - Q_{1N} - Q_{12} - \dot{V}_1 \quad (32)$$

$$Q_{N1} = Q_{1N} = 0.5 Q_{Nnat} \quad (33)$$

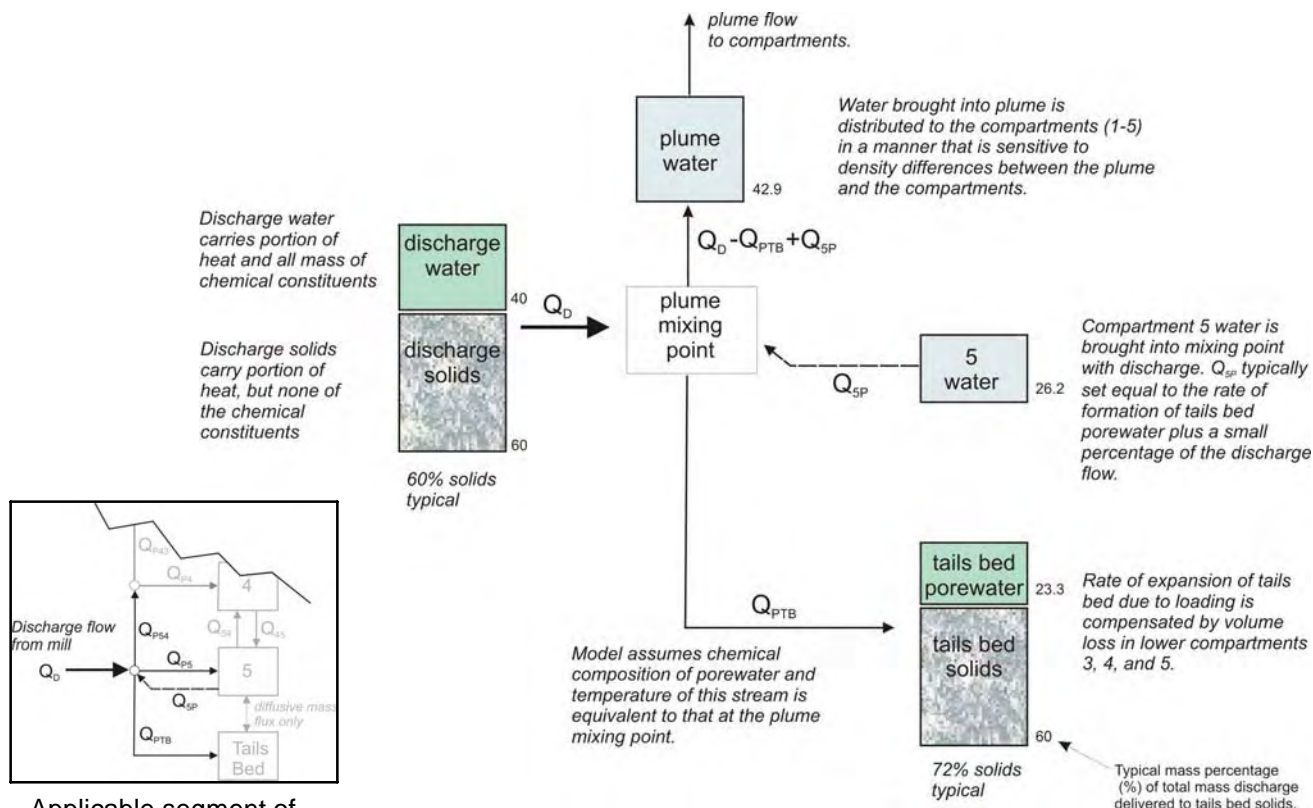
$$\dot{V}_1 = -VF_1 (\dot{V}_{US}) = -0.26 (\dot{V}_{US}) \quad (34)$$

$$Q_{Nout} = Q_{1nat} - \dot{V}_N \quad (35)$$

$$Q_{Nout} = Q_{1nat} - \dot{V}_N \quad (36)$$



Foth Infrastructure & Environment, LLC				Kennecott Eagle Minerals	
REVISED		BY	DESCRIPTION	FIGURE 19 FLUID FLOW BALANCE FOR HTDF MASS BALANCE MODEL	
CHECKED BY: JBM			DATE: OCT '07	Scale: NA	Date: OCTOBER 2007
APPROVED BY: JBM			DATE: OCT '07	Prepared by: GRE	Project No: 06W003
APPROVED BY:			DATE:		



Applicable segment of flow balance diagram

Mass Balance

Balance at point of discharge mixing (initiation of discharge plume)

$$C_P (Q_D - Q_{PTB} + Q_{SP}) = C_D Q_{DW} + Q_{SP} C_5 + (\text{RECYCLE}) Q_R C_3$$

$$C_P = [C_D Q_{DW} + Q_{SP} C_5 + (\text{RECYCLE}) Q_R C_3] / (Q_D - Q_{PTB} + Q_{SP}) \quad (1)$$

$$C_P = \text{Concentration of discharge plume } (\mu\text{g/L}) \quad (2)$$

$$C_D = \text{Concentration in mill tails pore water, without additional contribution from recycle stream } (\mu\text{g/L}) \quad (3)$$

$$Q_{DW} = \text{Flow rate for discharge (pore) water from mill } (\text{m}^3/\text{d}) \quad (4)$$

$$Q_R = \text{Return flow rate to mill (reclaimed, m}^3/\text{d}) \quad (5)$$

$$Q_{SP} C_5 = \text{Mass rate from compartment 5 drawn into mixing point, flows may include pore water and water drawn into plume by hydrodynamic forces of discharge.} \quad (6)$$

$$\text{RECYCLE} = \text{Flag (0 or 1) to include recycle mass as part of mill discharge.} \quad (7)$$

$$Q_R C_3 = \text{Mass rate in return water from compartment 3 if RECYCLE = 1.} \quad (8)$$

Heat Balance

Balance at point of discharge mixing (initiation of discharge plume)

Rate of heat in discharge plume to compartments:

$$T_P (Q_D - Q_{PTB} + Q_{SP}) HF_W = H_D + T_5 Q_{SP} HF_W - T_P \dot{M}_{DT} HF_{DT} - T_P n \dot{V}_{TB} HF_W \quad (9)$$

$$T_P = \text{Temperature of discharge plume } (^\circ\text{C}) \quad (10)$$

$$HF_W = \text{Heat factor for water} = \rho_w C_p = 0.00419 \frac{\text{GJ}}{^\circ\text{C m}^3} \quad (11)$$

(roughly constant with temperature, ignores salinity effect)

$$H_D = \text{Heat rate from discharge (GJ/d)} \\ = T_{DT} \dot{M}_{DT} HF_{DT} + T_{DW} Q_{DW} HF_W \quad (12)$$


T_{DT} = Temperature expected of dry tails ($^\circ\text{C}$), used to set discharge temperature with estimated incoming water temperature (T_{DW}), which is sensitive to supply and return water temperatures. Typically set to 27°C to achieve a discharge temperature of 10°C .

$$HF_{DT} = \text{Heat factor for dry tails, estimated as } 0.00084 \frac{\text{GJ}}{^\circ\text{C tonne}}$$

Rearranging (9) to yield temperature of discharge plume:

$$T_P = \frac{\frac{H_D}{HF_W} + T_5 Q_{SP}}{Q_D - Q_{PTB} + Q_{SP} + \dot{M}_{DT} \frac{H_D}{HF_W} + n \dot{V}_{TB}} \quad (13)$$



Foth Infrastructure & Environment, LLC				 Kennecott Eagle Minerals	
REVISED		BY	DESCRIPTION		
				FIGURE 20 HTDF MODEL MASS AND HEAT BALANCES FOR INITIATION OF DISCHARGE PLUME	
CHECKED BY: JBM			DATE: OCT '07	Scale: NA	Date: OCTOBER 2007
APPROVED BY: JBM			DATE: OCT '07	Prepared by: GRE	Project No: 06W003
APPROVED BY:			DATE:		

Balance of Potential and Kinetic Energy

Potential energy

$$PE_{1,initial} = M_1 g d / 2 \quad (1)$$

$$PE_{1,midpoint} = M_1 g (0) = 0 \quad (2)$$

$$PE_{2,initial} = -M_2 g d / 2 \quad (3)$$

$$PE_{2,midpoint} = M_2 g (0) = 0 \quad (4)$$

$$\Delta PE_1 = PE_{1,midpoint} - PE_{1,initial} = -M_1 g d / 2 \quad (5)$$

$$\Delta PE_2 = PE_{2,midpoint} - PE_{2,initial} = +M_2 g d / 2 \quad (6)$$

$$\Delta PE_{Total} = \Delta PE_1 + \Delta PE_2 = -\frac{gd}{2}(M_1 - M_2) \quad (7)$$

where

M = mass of weights 1 and 2

PE = potential energy of weights M_1 and M_2 at the initial and midpoint positions

g = gravitational constant

d = distance

Kinetic energy

At the midpoint, the energy of the system will be in the form of kinetic energy, and the velocity of the two weights will be equal in magnitude,

$$\Delta KE_1 = \frac{1}{2} M_1 v^2 \quad (8)$$

$$\Delta KE_2 = \frac{1}{2} M_2 v^2 \quad (9)$$

$$\Delta KE_{Total} = \Delta KE_1 + \Delta KE_2 = \frac{1}{2} v^2 (M_1 + M_2) \quad (10)$$

where

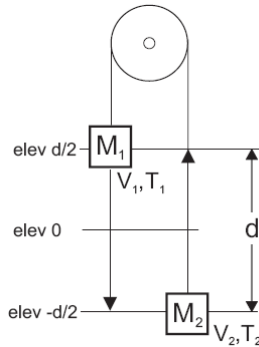
KE = kinetic energy of weights M_1 and M_2

v = velocity

A system energy balance requires that the decrease in potential energy be equal to the increase in kinetic energy,

$$-\Delta PE_{Total} = \Delta KE_{Total} \quad (11)$$

$$\frac{gd}{2}(M_1 - M_2) = \frac{1}{2} v^2 (M_1 + M_2) \quad (12)$$



**Physical analogy for mixing:
Pulley with two weights.**

Interfacial Velocity of Parcels of Water with Same Volume

From the definition of density (ρ),

$$\rho = \frac{M}{V} \quad (13)$$

By substituting density and volume for mass, the system can represent parcels of water crossing an interface (midpoint) rather than weights on a rope. Because water here may be considered incompressible, the volumes of the two parcels must be equal. Substituting into Equation 12, simplifying and solving for velocity,

$$gd(\rho_1 V - \rho_2 V) = v^2(\rho_1 V + \rho_2 V) \quad (14)$$

$$v = \sqrt{gd} \times \sqrt{\frac{(\rho_1 - \rho_2)}{(\rho_1 + \rho_2)}} \quad (15)$$

Mixing Flow at Interface

The magnitude of mixing should be proportional to the velocity of water parcels at the interface, which is proportional only to the density term in Equation 15.

The absolute level of density-dependent mixing flow between compartments is set by proportioning of a maximum mixing flow (Q_{mix} , typically set to 15,000 m³/d),

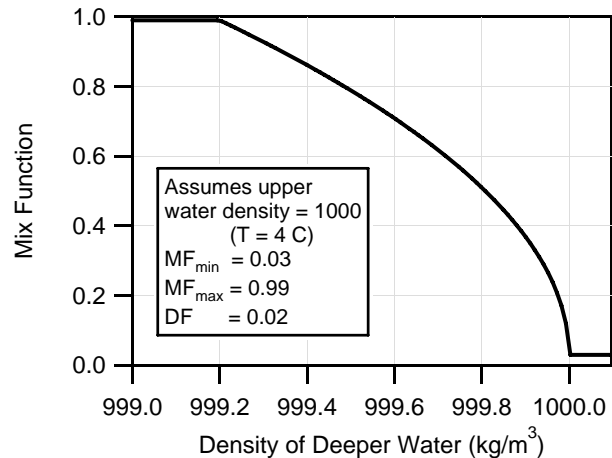
$$Q_{12} = MF_{12}(Q_{mix}) \quad (16)$$

using the following mixing factors (MF):

$$MF_{12} = MF_{min} \quad \text{for } \rho_2 \geq \rho_1 \quad (17)$$

$$MF_{12} = \min \left\{ 1, \frac{\sqrt{\frac{\rho_1 - \rho_2}{\rho_1 + \rho_2}}}{DF} \right\} (MF_{max} - MF_{min}) + MF_{min} \quad \text{for } \rho_2 < \rho_1 \quad (18)$$

where DF = density factor (typically < 0.03) which scales the sensitivity of mixing function to the difference in densities, MF_{max} and MF_{min} are the maximum and minimum portions of the plume flow to bypass compartment i (typically 0.98 to 0.02).



Mixing Function.



Foth Infrastructure & Environment, LLC

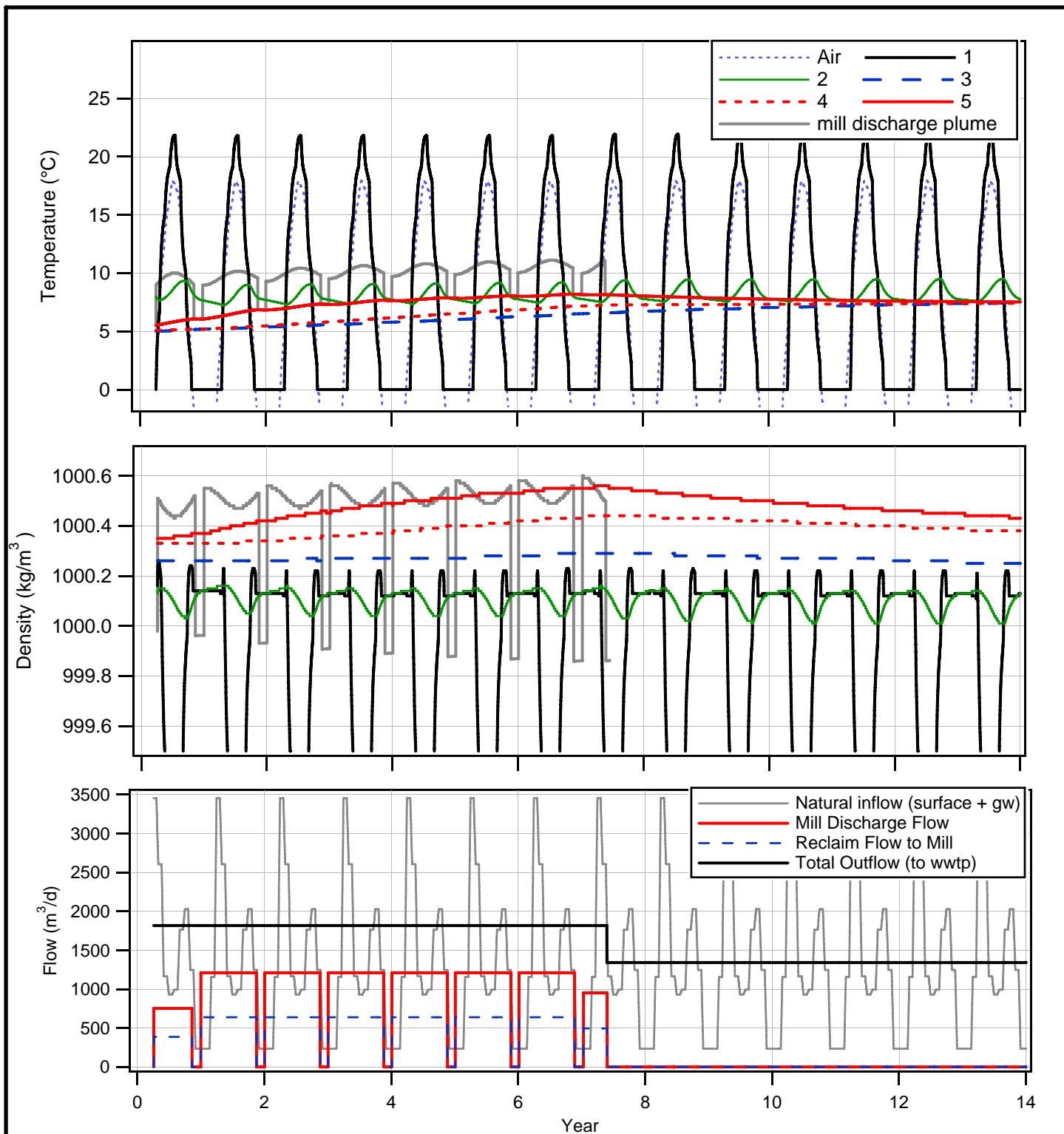
REVISED	BY	DESCRIPTION
CHECKED BY:	JBM	DATE: OCT '07
APPROVED BY:	JBM	DATE: OCT '07
APPROVED BY:		DATE:



**Kennecott
Eagle Minerals**

**FIGURE 21
DERIVATION OF MIXING FLOW
FROM DIFFERENCES IN DENSITY**

Scale:	NA	Date:	OCTOBER 2007
Prepared by:	JBM	Project No:	06W003



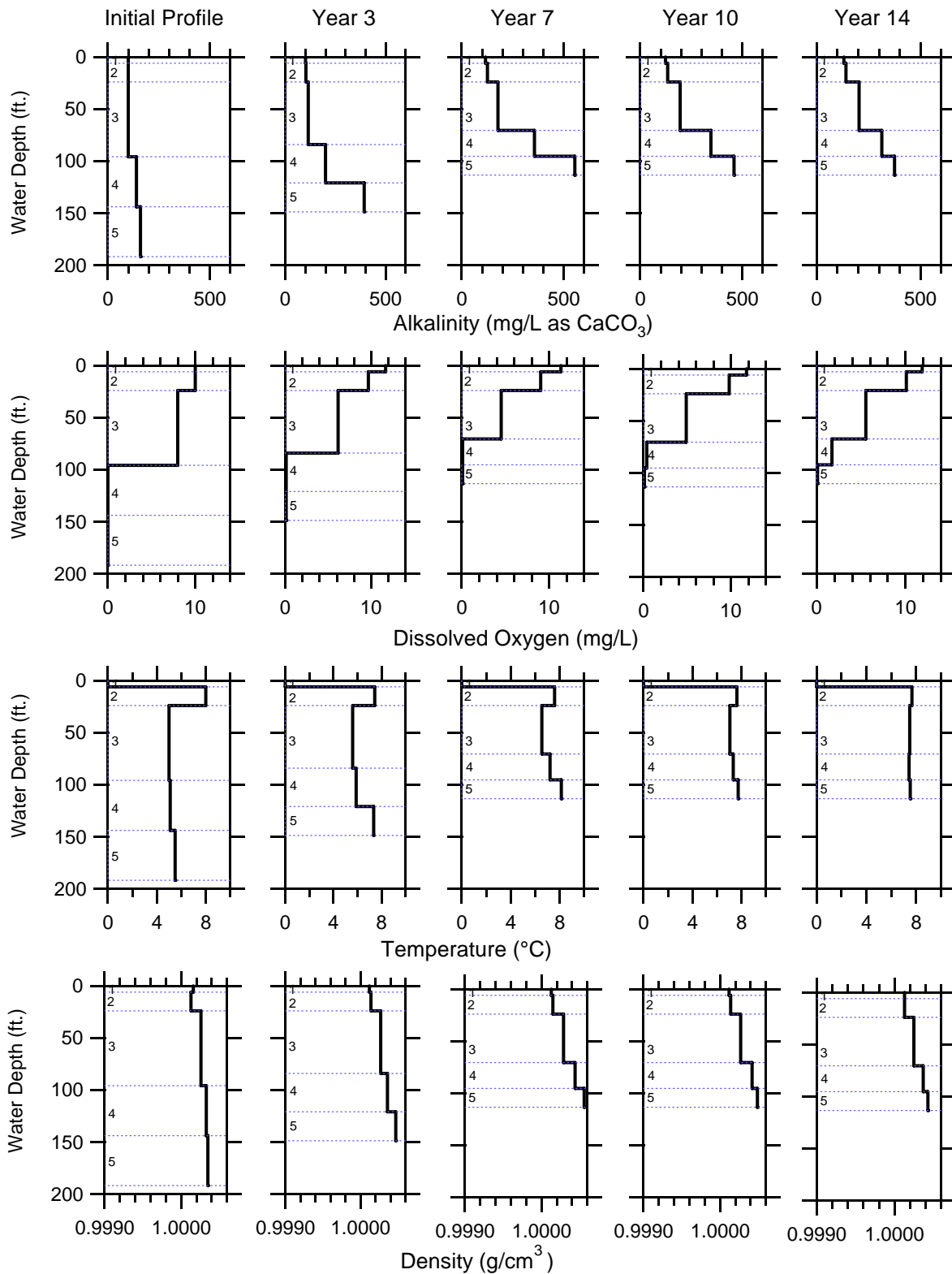
Foth Infrastructure & Environment, LLC			
REVISED		BY	DESCRIPTION
CHECKED BY: JBM		DATE: OCT '07	
APPROVED BY: JBM		DATE: OCT '07	
APPROVED BY:		DATE:	



Kennecott
Eagle Minerals


FIGURE 22
MODELED TRENDS IN TEMPERATURE
DENSITY, AND FLOW

Scale: NA	Date: OCTOBER 2007
Prepared by: GRE	Project No: 06W003



Note: All curves drawn for 94th day of year (First week of April), with some ice cover.



Foth Infrastructure & Environment, LLC				 Kennecott Eagle Minerals	
REVISED		BY	DESCRIPTION		
				FIGURE 23 HTDF MODEL DEPTH PROFILES FOR SYSTEM VARIABLES	
CHECKED BY: JBM			DATE: OCT '07	Scale: NA	Date: OCTOBER 2007
APPROVED BY: JBM			DATE: OCT '07	Prepared by: GRE	Project No: 06W003
APPROVED BY:			DATE:		

mill discharge
reclaimed to mill
precip - evap
to wwtp

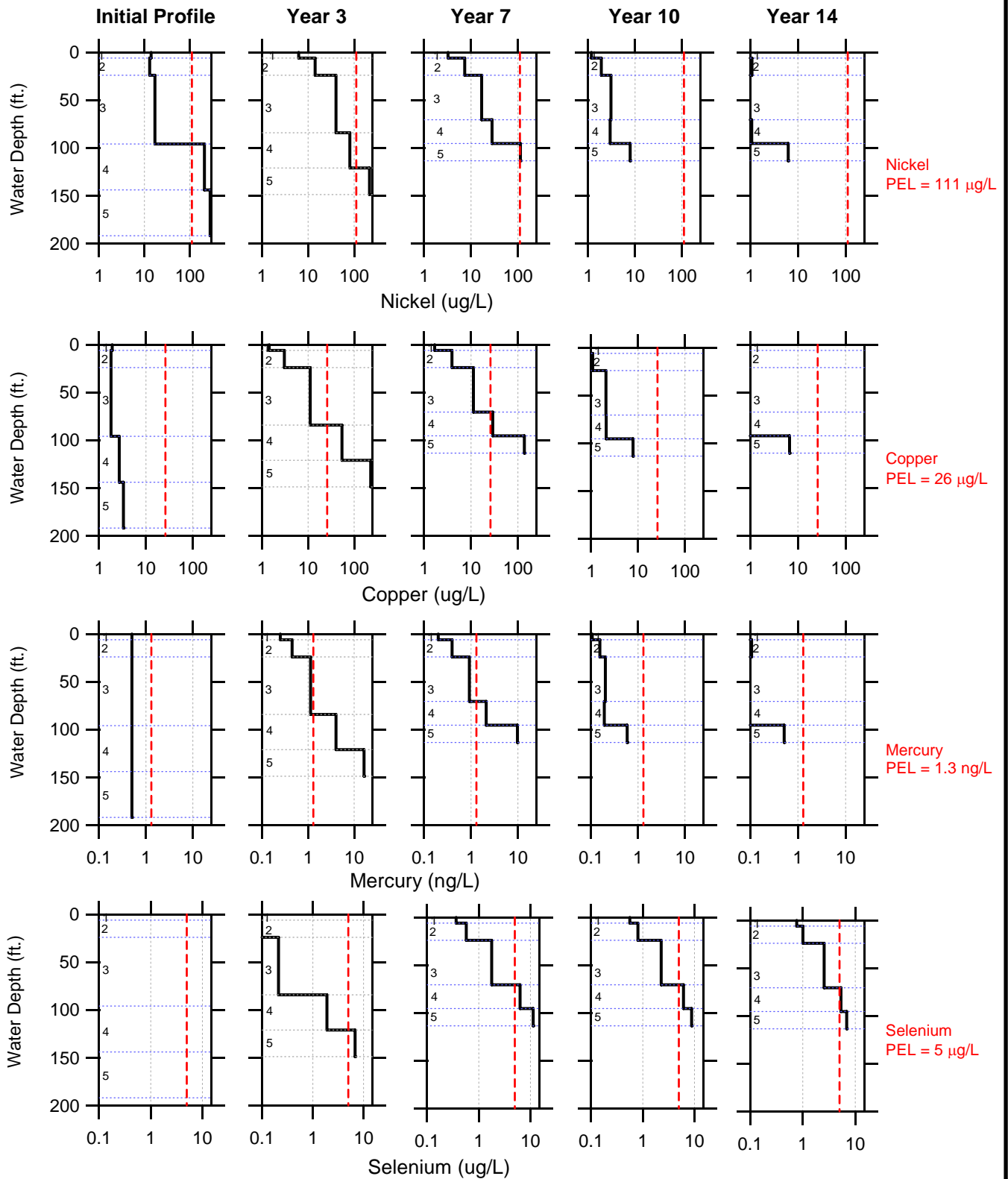
potential chemical profiles in HTDF during loading

DO OxFe P Alk

The diagram shows a cross-section of a settling tank divided into five horizontal layers, numbered 1 to 5 from top to bottom. Arrows indicate 'mill discharge' entering at the top left, 'reclaimed to mill' exiting at the top left, 'precip - evap' occurring within the tank, and 'to wwtp' exiting at the top right. To the right of the tank, four graphs show the potential chemical profiles for DO (Dissolved Oxygen), OxFe (Oxidized Iron), P (Phosphorus), and Alk (Alkalinity) during loading. Each graph has a vertical axis representing depth or layer number, corresponding to the tank layers. The DO profile shows a sharp increase in layer 1, a plateau in layers 2-4, and a sharp drop in layer 5. The OxFe profile shows a sharp increase in layer 1, a plateau in layers 2-4, and a sharp drop in layer 5. The P profile shows a sharp increase in layer 1, a plateau in layers 2-4, and a sharp drop in layer 5. The Alk profile shows a sharp increase in layer 1, a plateau in layers 2-4, and a sharp drop in layer 5.




M: \06W003\igr\MixingFunctionDefn.pxp

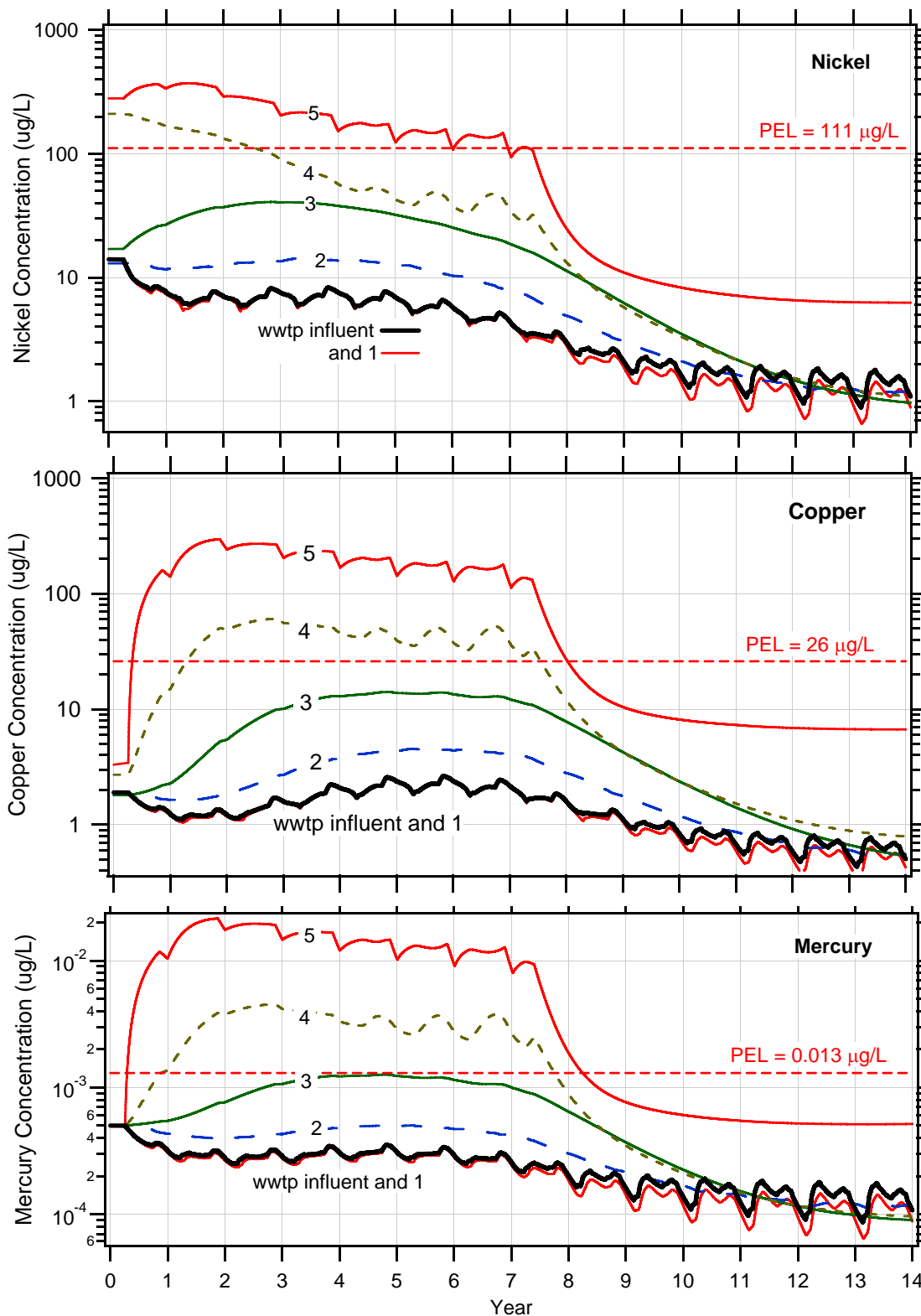


Note: All curves drawn for 94th day of year (First week of April), with some ice cover.

Preliminary Effluent Limits (PEL) calculations shown in Appendix F.



Foth Infrastructure & Environment, LLC				 Kennecott Eagle Minerals	
REVISED		BY	DESCRIPTION		
				FIGURE 25 HTDF MODEL DEPTH PROFILES FOR SELECTED METALS	
CHECKED BY: JBM		DATE: OCT '07		Scale: NA	Date: OCTOBER 2007
APPROVED BY: JBM		DATE: OCT '07		Prepared by: GRE	Project No: 06W003
APPROVED BY:		DATE:			



Preliminary Effluent Limit (PEL)
calculations shown in Appendix F.



Foth Infrastructure & Environment, LLC

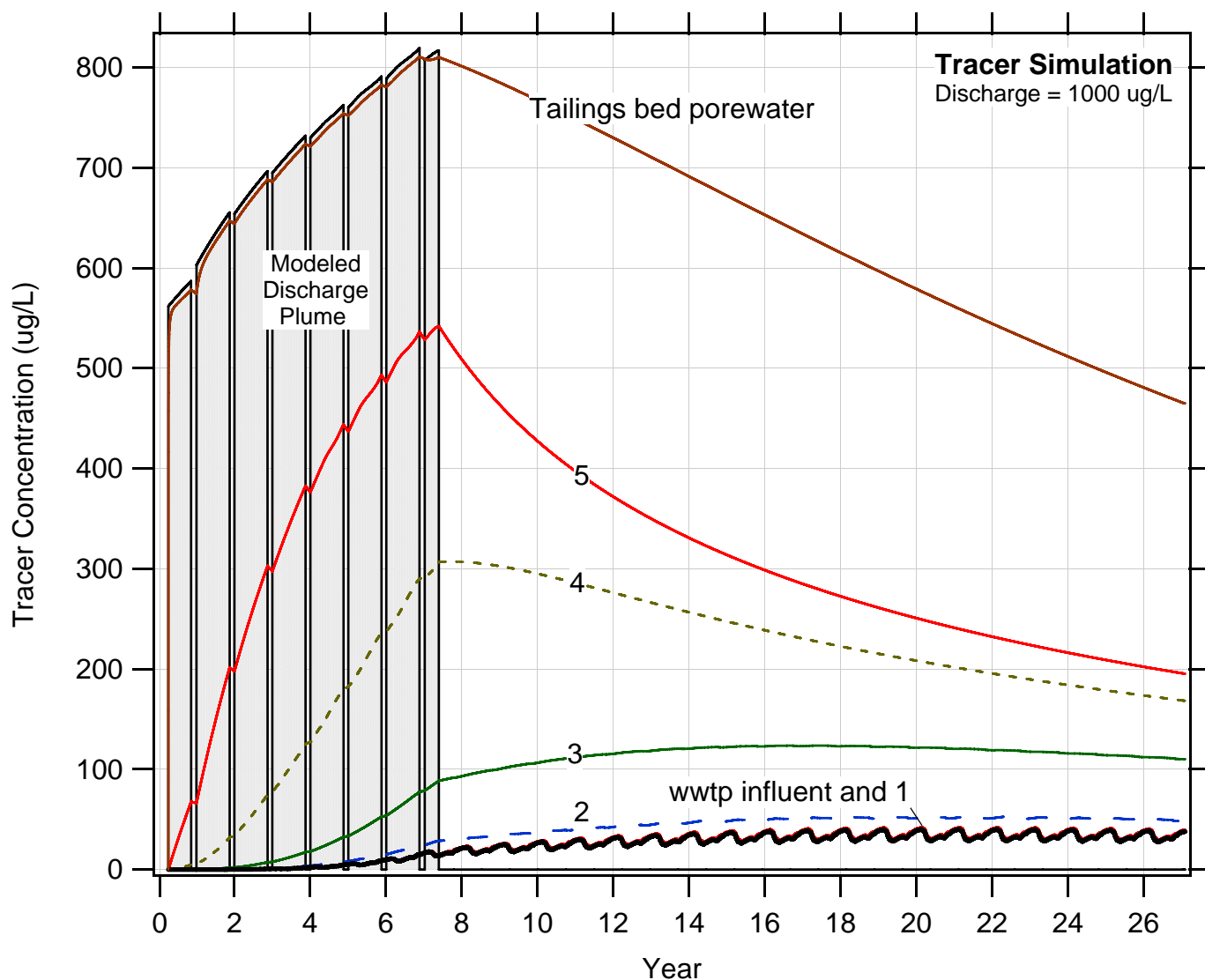
REVISED	BY	DESCRIPTION
CHECKED BY:	JBM	DATE: OCT '07
APPROVED BY:	JBM	DATE: OCT '07
APPROVED BY:		DATE:



Kennecott
Eagle Minerals


FIGURE 26
HTDF MODEL - SIMULATED TRENDS
FOR NICKEL, COPPER, AND MERCURY

Scale: NA	Date: OCTOBER 2007
Prepared by: GRE	Project No: 06W003



- Tracer simulation run for zero initial and background concentrations, and no losses due to scavenging.
- Modeled discharge plume concentrations consider full mass loadings, recycle stream, and mixing at plume mixing point.
- Increase in modeled discharge plume follows from increase in compartment 3 (recycle) and compartment 5 (mixing point).
- Decrease in tailings bed porewater concentrations are due to diffusion to compartment 5. Additional mass stored in buried tailings (beneath active bed).



Foth Infrastructure & Environment, LLC				 Kennecott Eagle Minerals	
REVISED		BY	DESCRIPTION		
				FIGURE 27 HTDF MODEL - SIMULATED TRENDS FOR TRACER INPUT CASE	
CHECKED BY: JBM		DATE: OCT '07		Scale: NA	Date: OCTOBER 2007
APPROVED BY: JBM		DATE: OCT '07		Prepared by: GRE	Project No: 06W003
APPROVED BY:		DATE:			